Extracellular freezing in frost hardy plants and its structural and physical factors

Dissertation

der Mathematisch-Naturwissenschaftlichen Fakultät

der Eberhard Karls Universität Tübingen

zur Erlangung des Grades eines

Doktors der Naturwissenschaften

(Dr.rer.nat.)

Vorgelegt von

MSc. Rena T. Schott

aus Sindelfingen

Tübingen

2019

Extracellular freezing in frost hardy plants and its structural and physical factors

Dissertation

der Mathematisch-Naturwissenschaftlichen Fakultät

der Eberhard Karls Universität Tübingen

zur Erlangung des Grades eines

Doktors der Naturwissenschaften

(Dr.rer.nat.)

Vorgelegt von

MSc. Rena T. Schott

aus Sindelfingen

Tübingen

2019

Gedruckt mit der Genehmigung der Mathematisch-Naturwissenschaftlichen Fakultät der Eberhard Karls Universität Tübingen

Tag der mündlichen Prüfung:	28.05.2019
Dekan:	Prof. Dr. Wolfgang Rosenstiel
1. Berichterstatter:	Prof. Dr. James H. Nebelsick
2. Berichterstatter:	PD Dr. Dr. Wilfried Konrad

Acknowledgments

I gratefully thank my supervisors Anita Roth-Nebelsick and James Nebelsick for accompanying me with knowledge and advice throughout my PhD thesis. During these years, I learned a lot for my future career and life.

Furthermore, I am grateful to Christoph Neinhuis, Dagmar Voigt, Markus Günther and Barbara Ditsch for the opportunity of using the cryoSEM and the Botanical Garden in Dresden. I thank my colleagues at the museum for their advice and all the others helping me and influencing me throughout my PhD thesis.

This work was funded by the German Research Foundation (DFG) as part of the Transregional Collaborative Research Centre (SFB/Transregio) 141 ‘Biological Design and Integrative Structures’/project A01: Transport of heat and mass in natural porous materials with graded structure: from functional properties of plant tissues towards customized construction materials.

Table of content

Abbreviations

AFP: anti-freeze protein

C: Celsius

cryoSEM: cryo scanning electron microscope

DM: digital microscope

ESEM: environmental scanning electron microscope

h: hour

H_2O: water

INA: ice nucleation activity

INT: ice nucleation temperature

LF: laboratory freezer

m: meter

median T_{INT}: median ice nucleation temperature

µCT: micro X-ray computed tomography

X-ray: X radiation

SEM: scanning electron microscope

SMNS: State museum of natural history Stuttgart

TU D: Technical University Dresden

Symbols

°: degree

Glossary

Adaptation: Evolutionary change of a trait due to a selective advantage

Cold acclimation: Acclimation to colder/subzero temperatures

Dehydration mechanism: Cell dehydration with extracellular ice formation at subzero temperatures

Freeze cythorrhysis: Shrinkage of cells during the dehydration mechanism

Structural adaptation: A morphological adjustment

(Deep) super cooling: Prevention or manipulation of internal ice crystal growth

Thesis:

Extracellular freezing in frost hardy plants and its structural and physical factors

Zusammenfassung

In dieser Arbeit wurden die strukturellen Anpassungen von Pflanzen an Frostereignisse anhand verschiedener Arten untersucht (*Betula nana*, *Betula albosinensis*, *Castanea sativa*, *Stachys byzantina* und *Equisetum hyemale)*. Ein physikalisches Modell am Beispiel von *E. hyemale*, welches den Dehydrationsmechanismus erklären kann, wurde erstellt.

Von dem Strauch *B. nana* und den Bäumen *B. albosinensis* und *C. sativa*, welche aus verschiedenen Regionen kommen und unterschiedliche Wuchsformen sowie Frosttoleranzen besitzen, wurden ältere und jüngere Zweige im Hinblick auf die „ice nucleation temperature“ und die Verteilung von Gewebe, Luft und Wasser/Eis innerhalb des Kortex der Rinde ausgewertet. Die „median ice nucleation temperatures“ der jungen und älteren Zweige glichen sich im Winter an. Weniger aktive Eisnuklei wurden im Winter ermittelt, was auf ein organisiertes Gefrieren hindeutet. Eisbildung trat in den Interzellularräumen des Kortex auf. Die zwei *Betula* Arten besaßen eine höhere Porosität als *C. sativa*.

Die kleine, mehrjährige *S. byzantina* zeigte durchgehende Interzellularräume – zwei an der unteren und ein bis zwei an der oberen Seite – entlang der Petiolen und Blattadern. Diese Interzellularräume befinden sich zwischen der Epidermis und dem Kollenchym oder zwischen Kollenchymreihen. Auf jeder Seite der Petiolen und Blattadern und an der unteren Seite konnten entsprechende Verbindungszonen, die sich an der oberen Seite mit wachsendem Eisvolumen lösten, nachgewiesen werden. Das Eiswachstum führte zu einer Deformation des Querschnitts und einer starken Dehydrierung des lebenden Gewebes.

In *E. hyemale* sammelt sich das Eis in Interzellularräumen des Chlorenchyms, im substomatären Raum, in Vallekularkanälen und in der Markhöhle. Eis in den Kanälen zeigt eine typische Trennung von Wasser und gelösten Stoffen. Unterschiedliche Protuberanzen, sowie Wasser in speziellen Regionen wie dem Parenchymmark, welches durch den Gefrierprozess deformiert wird, wurden gefunden. Diese könnten bei der extrazellulären Eisbildung eine Rolle spielen.

Basierend auf den Ergebnissen zu *E. hyemale* wurde ein physikalisches Modell erstellt. Dieses erklärt den Wasserefflux aus den Zellen und das Gefrieren an speziellen Stellen, sowie die weitere Dehydrierung durch das Eis. Die Ergebnisse des Modells wurden mit den Ergebnissen der anderen Arten verglichen, und wahrscheinlich ist das Modell in der Lage, die bei frostharten Arten häufig vorkommende extrazelluläre Eisbildung an bevorzugten Stellen zu erklären.

Summary

In this thesis, the structural adaptations of plants were investigated by studying freezing in different taxa (*Betula nana*, *Betula albosinensis*, *Castanea sativa*, *Stachys byzantina* and *Equisetum hyemale*). A physical model exploring the interrelationship between tissue structure and extracellular freezing is devised based on *E. hyemale*.

Younger and older stems of the shrub *B. nana* and the trees *B. albosinensis* and *C. sativa,* which differ in habitat demands and frost hardiness, were analyzed and evaluated with regard to their ice nucleation temperature and the distribution of tissue, air and water/ice within the cortex of the bark. The median ice nucleation temperature of younger and older *B. nana* stems became similar from summer to winter and the number of active ice nuclei were lower for winter samples, which indicates controlled freezing processes. The ice crystallization occurred within the intercellular spaces of the cortex of the bark. Tissue porosity of the two *Betula* species was larger than for *C. sativa*.

The small, perennial *S. byzantina* revealed continuous intercellular spaces – two on the lower and one or two on the upper side – along the petiole and leaf veins. These intercellular spaces exist between the epidermis and the collenchyma or between collenchyma layers. Connection zones within each side of the petiole or vein and in the middle of the lower side remain open during the freezing event, while the connection zone on the upper part separate. Ice growth leads to a deformation of the cross section and a strong dehydration of the living tissue.

In *E. hyemale*, ice accumulates in the intercellular spaces of the chlorenchyma, substomatal chambers, vallecular canals and pith cavities. Protuberances different in form and size have been found as well as water at specific regions as in the parenchymatous pith. The parenchymatous pith gets deformed during a freezing event and it might play a role during extracellular freezing.

Based on the results of the *E. hyemale*, a model of the physical process was devised which explains the water efflux out of the cells, extracellular freezing and ice accumulation at specific sites. The model is consistent with results from the other species and therefore probably describes the process of extracellular freezing in general.

List of publications

Published manuscripts

1) **Schott, Rena T.** & Roth-Nebelsick, Anita (**2018**) Ice nucleation in stems of trees and shrubs with different frost resistance. IAWA Journal **39,** 177–190.
2) **Schott, Rena T**.; Voigt, Dagmar; Roth-Nebelsick, Anita (**2017**): Extracellular ice management in the frost hardy horsetail *Equisetum hyemale* L. In: Flora 234, S. 207–214. DOI: 10.1016/j.flora.2017.07.018.

Submitted manuscripts

3) Konrad, Wilfried; **Schott, Rena**; Roth-Nebelsick, Anita (**submitted**): A model of frost-resistance based on extracellular freezing, motivated by observations of *Equisetum hyemale*. Submitted to Journal of Theoretical Biology

Manuscripts in preparation

4) **Schott, Rena T.**; Roth-Nebelsick, Anita (**in prep a**): Anatomical adaptations of *Stachys byzantina* C. Koch to extracellular ice formation.
5) **Schott, Rena T.**; Roth-Nebelsick, Anita (**in prep b**): Detailed 2- and 3-dimensional evaluation of the freezing process within important structures of *Equisetum hyemale* L. var. *robustum*.

EBERHARD KARLS
UNIVERSITÄT
TÜBINGEN

Mathematisch-Naturwissenschaftliche Fakultät

Personal contributions

Paper number	Number of authors	Candidates position	Scientific ideas %	Data generation %	Analysis & interpretation %	Paper writing %
3	3	2	35	25	25	25
2	3	1	50	100	25	25
1	2	1	70	100	75	80
5	2	1	75	100	75	90
4	2	1	80	100	75	90

I certify that the above statement is correct

Date, Signature of the candidate

I/We certify that the above statement is correct

Date, Signature of the doctoral committee or at least of one of the supervisor

Introduction

Frost adaptation of plants

During plant evolution, various adaptations to environmental conditions evolved along with different strategies for surviving seasonal changes. Some plant species, for example, overwinter as seeds, while others lose their leaves, or do not undergo any visible seasonal changes at all. Some plants are able to withstand freezing temperatures throughout the whole winter while others are able to deal with freeze-thaw cycles in early spring in order to have a reproduction advantage. One visual adaptation to different climate regimes is plant size and growth form which sometimes enables them to develop their own microclimate (Körner 2016).

Crucial for the survival of these different plants or plant parts is the corresponding acclimation to different seasons triggered over diurnal changes in light availability (photoperiodic control) and temperature (Lenz *et al.* 2013). In general, tropical and subtropical species cannot endure temperatures below 10 °C, while many temperate plants are able to endure chilling temperatures while avoiding injury. Other temperate plants develop species specific frost resistance to freezing process usually triggered by extrinsic or intrinsic ice nucleating substances (Pearce 2001). Plants within boreal and arctic regions have to be able to deal with even lower temperatures throughout the year (Körner 2016).

Cold acclimation

In general, the ability of a plant to undergo acclimation is species and environment specific. Cold acclimation as a preparation for dealing with subzero temperatures is a physiological adaptation in late autumn or early winter within a period of lower non-freezing temperatures during shorter day length (Levitt 1980; Steponkus 1984; Thomashow 1999; Xin and Browse 2000). An important part of cold acclimation is the protection of the primary side for freeze injury (Levitt 1980; Xin and Browse 2000). Xin and Browse (2000) summarize the steps of cold acclimation as follows: reduction of water content, gene regulation, reduced growth, hormone balance, membrane modification, cell wall modification, energy balance, increased antioxidants, and osmotic regulation. In general, necessary

changes in cell biology and cell metabolism as an adaptation to dropping temperatures cannot be ascribed to low and non-freezing temperatures or to cold acclimation.

(Deep) supercooling

Freeze avoidance – the so-called (deep) supercooling - is one adaptation to subzero temperatures. The term supercooling or deep supercooling is mostly an indication of higher or lower subzero ice nucleation temperatures (INT). Part of the (deep) supercooling mechanism are antifreeze proteins (AFPs) - also called ice reconstructing proteins - used to prevent the cell contents from freezing by inhibiting ice crystal growth or reconstructing ice morphology (Sharma and Deswal 2014). For (deep) supercooling, the cell membrane or part of it must be altered for prevention of a cellular water loss due to fast accumulation of extracellular ice. Ice crystal growth into the cell must also be prevented by a reduction in osmotic potential. Within the cells, heterogeneous nucleating agents causing intracellular ice formation at warmer temperatures must be absent (Wisniewski and Davis 1989; Arias *et al.* 2015). Plants, which depend more on the (deep) super cooling mechanism have in general smaller intercellular spaces with a lesser water content within these apoplastic spaces (Arias *et al.* 2015). For example different olive cultivars decrease their INT from summer to winter (Arias *et al.* 2017). Differences in the (deep) supercooling abilities can exist within different tissues as for example Körner (2016) stated that xylem water of certain species can endure temperatures down to -40 °C, while other internal structures freeze at higher subzero temperatures.

Dehydration mechanism

The frost surviving method of interest in this study is the dehydration mechanism including the desiccation of the living tissue and the buildup of extracellular ice bodies (Gusta and Wisniewski 2013).

Many different species are able to protect important internal plant parts and even the cells themselves do this with extracellular ice crystal growth. For example, some moss species can become covered by ice crystals extracted from the living species themselves as a protecting carpet (Lenné *et al.* 2010; Moffett

2015). During higher subzero temperatures (-4 °C) water filled hydroid cells of the moss *Ceratodon purpureus* tend toward embolism and parenchyma cells of the inner cortex can lose ~80 % volume through dehydration at lower temperatures (-20 °C) (Lenné *et al.* 2010).

Other species prefer an intercellular model for ice storage. The French scientist Prillieux (1869) was one of the first to look into this mechanism. He studied various herbaceous species, such as, for example, the greater celandine (*Chelidonium majus*) and a comfrey species (*Symphytum*) which are able to survive night frost in early spring. Herbs react to freezing mainly with an internal accumulation of big ice crystals in intercellular spaces between the epidermis and sometimes a few parenchyma layers and the living tissue which also leads to a visible deformation in cross section (Fig. 1). According to the sketches of Prillieux (1869), the layers around the intercellular spaces could be smooth or partly teared apart. Some of those species can show a reversible wilting as visible optical reaction to internal freezing (Fig. 1). In the past, research interests moved slightly towards the analysis of (deep) supercooling events (*e.g.* Sharma and Deswal 2014), but a few decades ago, mechanisms of dehydration moved back into focus (*e.g.* McCully *et al.* 2004). The results of imaging techniques showing the freezing behavior of the California poppy (*Eschscholzia californica* Cham.)

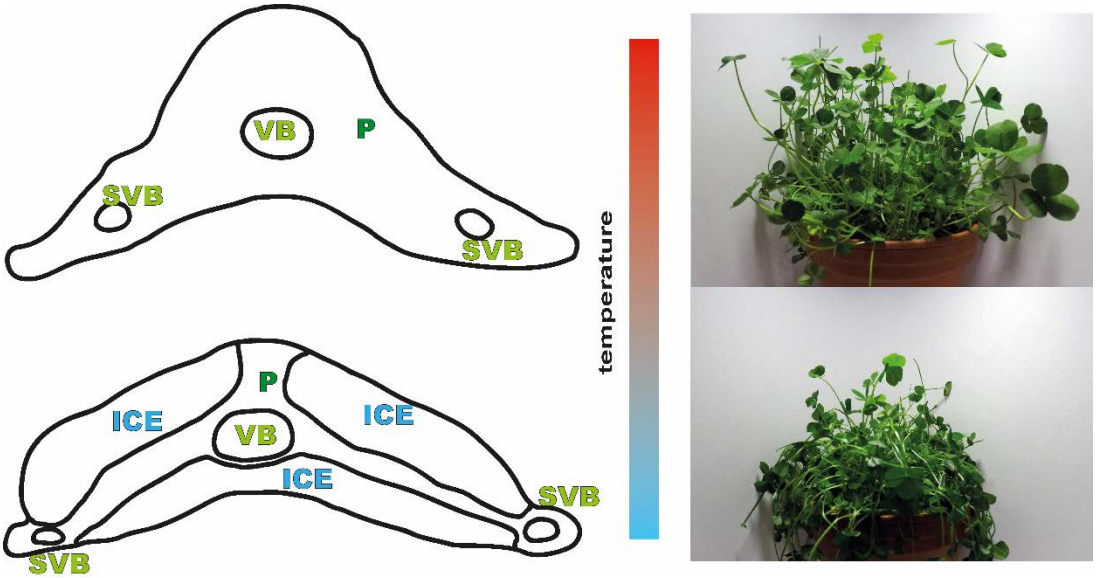

Fig. 1: Left: Schematic description of the reversible dehydration mechanism corresponding to temperature changes of an herb petiole. Above: Fully hydrated cross section of a petiole B: frozen cross section of a petiole with ice lakes and a tissue deformation. P: parenchyma; VB: vascular bundle; SVB: sub-vascular bundle. Right: Images of a potted *Trifolium repens*. Above: Fully hydrated state. Below: Frost induced wilting.

and white clover (*Trifolium repens* L) for example, show comparable results to those of Prillieux (1869). Through freeze cythorrhysis the parenchyma tissue shrunk, while at the same time ice crystals grew under the epidermis and hypodermis. The shrinkage of the parenchyma tissue resulted in a separation of the parenchyma and the epidermis. The connection between the parenchyma and epidermal tissue remained only at some locations (McCully *et al.* 2004). Other species, as for example the snow gum leaves (Eucalyptus pauciflora) (Ball *et al.* 2004; McCully *et al.* 2004) and rough horsetail (*Equisetum hyemale*) (Niklas 1989) do not show wilting during freezing thanks to stabilizing components within their tissues.

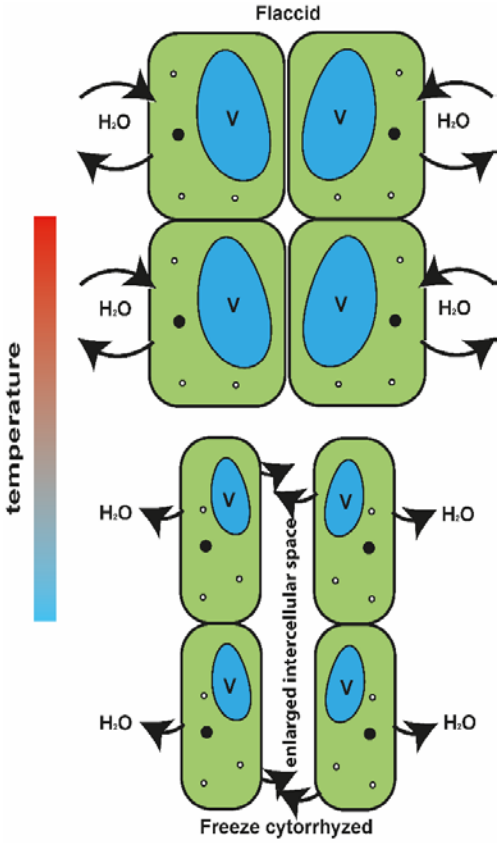

Fig. 2: Schematic description of the reversible dehydration mechanism with intact cell connections. A: fully flaccid cells at above zero temperatures with a normal water exchange. B: enlarged intercellular spaces and corresponding shrunken cells caused by water loss triggered within an acclimated plant with species specific subzero temperature (freeze cytorrhyzed).

Without many molecules within the intercellular spaces the freezing point is higher (Xin and Browse 2000). With decreasing temperature, the water potential of ice decreases reaching substantial differences to the water potential of the liquid cell content (Guy 1990). This leads to a sudden drop of water potential of the frozen intercellular spaces which attract cell water from adjacent cells (Fig. 2) (Mazur 1969; Xin and Browse 2000). Over time, more ice can accumulate within the formerly air filled spaces (Niklas 1989).

The aforementioned cell wall adaptations during cold acclimation are crucial for the prevention of cell wall rupture during the reversible dehydration mechanism. Osmotic regulation by, for example, sugar is crucial for preventing the cells from excessive water loss through dehydration (Steponkus 1984). The dehydration mechanism should be seasonally regulated (Körner 2016) and be organized at specific sites. For blueberry species, for example, this results in a higher freezing temperature with fewer ice nucleation sites *(Kishimoto et al. 2014a;* 2014b). In general, the functionality of cells and some connections between them need to be maintained. Reversible dehydration leads to freeze cythorrhysis (McCully *et al.* 2004; Lenné *et al.* 2010) whereby substantial shrinkage of the living cell is only possible within soft and not within rigid tissues (Beck *et al.* 2007).

Objectives

In many parts of the world, plants exist with different temperatures and seasonal changes. Scientific interest in frost induced dehydration mechanisms started over 150 years ago (*e.g.* Prillieux 1869). The basic research within this field focused on different species or plant parts with only a few interspecific comparisons. Of interest is, for example, the ability of some plants to survive late spring frosts (*e.g.* the petioles of *T. repens* and *E. californica*, McCully *et al.* 2004) or the ability for cold acclimation (*e.g.* Kishimoto *et al.* 2014a) and the presence of deciduous or evergreen species which lack cold acclimation (*e.g.* Hacker and Neuner 2007, 2008). The general dehydration mechanism and coupled extracellular ice build-up can be visualized for acclimated and cold acclimated plants and has been described for various taxa (Prillieux 1869; McCully *et al.* 2004; Roden *et al.* 2009; Neuner *et al.* 2010).

The detailed morphology of the tissues are essential traits which enable the plants to undergo dehydration mechanisms. While various studies have described extracellular freezing and cell deformation, a causal physical understanding of the interrelationships between structure and ice body localization is largely missing. This study therefore addressed the following questions. 1) How is site-specific ice accumulation achieved with respect to physical processes? and 2) Which structural preconditions are necessary to direct large ice bodies within tissues?

The underlying concept for this study is the assumption that there is a general mechanism of dehydration and directed water flow for all plants and plant parts which show site-specific extracellular ice formation. To obtain evidence for this general mechanism, different evergreen species were evaluated. By focusing predominantly on the evaluation of different imaging techniques (DM; SEM, ESEM, cryoSEM and µCT) and by comparing the results among different species, a fundamental understanding of the interrelationships between structure and freezing can be obtained. These results on the structural facts are the basis for the first physical explanation of dehydration mechanisms.

Methods

Types of analysis

Many different methods for analyzing and visualizing ice crystallization in intercellular spaces have been developed and tested for observing the freezing process and its temporal course. These include high-resolution infrared thermography (Wisniewski *et al.* 2015) and infrared differential thermal analysis alone or combined with differential imaging chlorophyll fluorescence (Hacker and Neuner 2007; Hacker *et al.* 2008; Hacker and Neuner 2008; Wisniewski *et al.* 2008; Neuner *et al.* 2010; Kishimoto *et al.* 2014b).

Various imaging techniques, such as light microscopy/digital microscopy (DM) can furthermore provide information on the tissue structure of fresh or freshly frozen states and the distribution of tissue, air, water and/or ice (*e.g.* Kishimoto *et al*. 2014b). Further details on the structure can be gained through scanning electron microscopy (SEM), an environmental scanning electron microscope (ESEM) and cryo-scanning electron microscopy (cryoSEM) (Ball *et al.* 2002; Ball *et al.* 2004; McCully *et al.* 2004; Ball *et al.* 2006). Micro X-ray computed tomography (µCT) has thus far been seldom used in this context despite having the potential to provide more insight into the structure of a given frozen condition (*e.g.* Zhao and Takhar 2017).

At the start of the freezing experiments, knowing the INT and the corresponding ice nucleation activity (INA) for the current seasonal conditions (*e.g.* Kishimoto *et al.* 2014a; 2014b) can help determining the needed temperatures for the different freezing experiments. The course and distribution of INT and INA also allow some insights on the degree of cold acclimation and corresponding dehydration mechanism. The chosen analytic methods within the dissertation presented were DM, SEM, ESEM, cryoSEM and µCT as well as the determination of the INT and INA for selected species. Samples were analyzed from naturally acclimated species during summer and cold acclimated species during winter in fresh, naturally or artificially frozen states. The methods used proved to be convincing and comparable.

Selected species

For the analysis of the dehydration mechanism of the intercellular freezing, various plant parts (Tab. 1) of the chosen species with different features were analyzed. Woody, deciduous species were collected as representatives for freezing within stiffer tissues. As an example for the evergreen herbs, *Stachys byzantina* C. Koch was chosen and another species with a high water content *Equisetum hyemale* var. *robustum* was also sampled. The main experimental phase was during the winter season, while the results generated during summer served for comparison.

Table 1: List of the selected taxa and samples

Taxa	**samples**
Betula nana	Current year and at least 2 years old stems
Betula albosinensis	Current year and at least 2 years old stems
Castanea sativa	Current year and at least 2 years old stems
Stachys byzantina	Petioles and leaves
Equisetum hyemale	Stems

Woody species

The current year stems of three woody species - *Betula nana*, *Betula albosinensis* and *Castanea sativa* – and at least 2-years old stems of *B. nana* and *C. sativa* were sampled. These consisted of different growth forms, distributions and corresponding degrees of frost resistance. They were evaluated and compared in winter in both natural and artificial acclimated states, and in addition during summer for *B. nana*. Next to the DM image evaluation of the different state of the cortex of the bark, an INT and INA determination with an adapted method of Kishimoto *et al.* (2014a; 2014b) was used to determine the optimum temperature for the freezing events and for making interspecific comparisons with the median T_{INT}. The median T_{INT} and the determination of cumulative ice nucleation per gram fresh weight or per water volume at defined temperatures was determined to show additional seasonal differences.

The deciduous and diffuse-porous dwarf birch *B. nana*, a shrub native to northern Europe and the western Asia tundra was selected as a woody species which can endure the lowest range of subzero temperatures. The stiff and dull brown twigs are pubescent and not warty with resin dots on the young twigs. The

height of this shrub up to 1 m is an environmental adaptation to the cold tundra. Older stems grow downwards to the ground resulting mostly in an increase of width and not height again as a response to the cold and wind within their natural habitat (Groot *et al.* 1997).

Fig. 3: Left: *Betula nana* species of the Botanical Garden of Dresden; Middle: *Betula albosinensis* of the Hohenheim Botanical Gardens; Right: *Castanea sativa* of the Hohenheim Botanical Gardens

The deciduous hardwood Chinese red birch *B. albosinensis* with a height up to 30 m is native to mid-high mountains of warm temperate regions in China (Guo *et al.* 2013) and is frost resistant, but does not occur within extreme habitats. The thin papery bark ranges from whitish to orange red or pink violet.

The deciduous and ring-porous sweet Chestnut *C. sativa* with a maximum height of 30 m changes bark color from grey and smooth to grey brown with typical cracks occurring during aging. This frost resistant species occurs in warm temperate climates and is distributed from southern Europe to northern Africa and in the region of the Black Sea (Coombes *et al.* 2012).

***Stachys byzantina* C. Koch**

The perennial plant *S. byzantina* is a small and rosette-like evergreen and naturally located within the Near East and the Caucasus. The herbaceous plant has sterile basal rosettes and the flowering stem can reach a height of up to 1 m. Basal leaves densely covered with trichomes are mostly around 3-8 x 0.5-3.5 cm with a 2-6 cm long petiole (Davis 1982a). This old medical herb is a relative popular ornamental plant.

The leaves and petioles of fresh naturally cold acclimated and artificially frozen *S. byzantina* species were analyzed with different imaging techniques (DM, cryoSEM and µCT) regarding important morphological structures with respect to

the distribution and dimensions of intercellular spaces and their role during freezing events. The visual reaction to frost of *S. byzantina* was also evaluated.

Fig. 4: *S. byzantina* species of a public flowerbed in Kiel

Fig. 5: *Equisetum hyemale* species of the Botanical Garden of Dresden

***Equisetum hyemale* var. *robustum* L.**

Equisetum hyemale L., with the common name “winter scouring rush“, shows a worldwide distribution except for Australia and New Zealand, and reaches a height of 0.5 to 1 m. Preferring wet habitats, this spore-bearing species belongs to the class Equisetopsida, which can be traced back to the Carboniferous (Sporne 1979; Husby 2013) This plant consists of internodes and microphyll-bearing nodes every few centimeters and has rare branches (Ludwigs 1911; Speck *et al.* 1998). Special structures such as the hypodermal sterome and the two-layered endodermis result in the stiffness of the stems (Spatz and Emanns 2004; Speck *et al.* 1998). So far, some observations on the freezing process within the *E. hyemale* have been conducted by Schaffner (1908) and Niklas (1989).

For structural analysis of *E. hyemale* stems, some stained and embedded cross sections were prepared. Stems of *E. hyemale* were analyzed in an acclimated and fresh state during summer and cold acclimated and fresh or frozen state during winter using DM, SEM ESEM, cryoSEM and µCT.

Results and Discussion

Woody species

This study on younger and older stems of *B. nana*, *B. albosinensis* and *C. sativa* generated first new insights into the distribution of tissue, air and water/ice within the cortex of the bark in summer and/or winter in naturally or artificially acclimated or cold acclimated plants or their parts (Schott and Roth-Nebelsick 2018). Sample abbreviations used in the following and some results are displayed in table 2.

Table 2: List of the abbreviations of taxa and samples used and the corresponding results of ice nucleation temperature and median of ice nuclei active at -8 °C (adapted from Schott and Roth-Nebelsick 2018)

Abbreviation	Taxa and sample	Median INT [°C] ± SE (N = 4)	Median of ice nuclei active at -8 °C
CSOW	*Castanea sativa*, stems ≥ 2 years "old" , "winter material" = cold acclimated	-8.14 ± 0.14	9
CSYW	*Castanea sativa*, "young" current-year stems, "winter material" = cold acclimated	-8.43 ± 0.25	7
BAOW	*Betula albosinensis*, stems ≥ 2 years "old", "winter material" = cold acclimated	n.a.	n.a.
BAYW	*Betula albosinensis*, "young" current-year stems, "winter material" = cold acclimated	-8.06 ± 0.20	12
BNOW	*Betula nana*, stems ≥ 2 years "old", "winter material" = cold acclimated	-7.52 ± 0.26	21
BNYW	*Betula nana*, "young" current-year stems, "winter material" = cold acclimated	-7.56 ± 0.19	12
BNOS	*Betula nana*, stems ≥ 2 years "old", "summer material" = acclimated	-8.38 ± 0.20	54
BNYS	*Betula nana*, "young" current-year stems, "summer material" = acclimated	-7.01 ± 0.23	49

The comparison of the median INT for younger and older *B. nana* stems in summer and winter differed (Tab. 2). The results of the summer samples of younger *B. nana* stems might be caused by the growing phase in which current year stems are more sensitive and so differ from the older ones. The almost identical distribution of the results of younger and older *B. nana* stems in winter displayed an seasonal adjustment (Schott and Roth-Nebelsick 2018). The distribution of the frozen samples within the INT test of *B. nana* (Schott and Roth-Nebelsick 2018) indicated in a shift towards higher sub-zero temperatures in winter (start: BNYW: -4 °C; BNOW: -3 °C) than in summer (start: BNYs: -5 °C; BNOs: -5 °C) (Schott and Roth-Nebelsick 2018). Together with the fewer INA (Tab. 2) and the higher median T_{INT} they, indicated an earlier and controlled freezing within specific places (Kishimoto *et al.* 2014a). The first samples in the INT test of the *B. albosinensis* froze at -6 °C for the BNYS (Schott and Roth-Nebelsick 2018). Lacking the pronounced peak for younger stems in the course of the INT test (Schott and Roth-Nebelsick 2018), *C. sativa* stems initiated the ice crystal growth nearly at the same temperature (CSYW: -5 °C; CSOW: -6 °C). A slightly lower median T_{INT} with fewer active ice nuclei at -8 °C were calculated for CSYW. The results described in Schott and Roth-Nebelsick (2018) for *C. sativa* are largely consistent with the results of Neuner *et al.* (2010) using IDTA. Taking into account the smaller water amount available for the present study by regarding the “volume effect” on the results (Kishimoto *et al.* 2014a; Schott and Roth-Nebelsick 2018), the small differences of the INT to that achieved by Neuner *et al.* (2010) can be explained.

By comparing the results of the median INT and the distribution of the ice nucleation activity of the different species (Tab. 2 and Fig. 2 in Schott and Roth-Nebelsick 2018) an earlier start of the ice nucleation within *B. nana* samples in winter could be detected. The course of the INT test of the *B. nana* samples (Schott and Roth-Nebelsick 2018) with a tendency to a slightly higher median T_{INT} in comparison to the other species might indicate the need of a faster reaction of *B. nana* to lower temperatures of preparing for colder freezing event at their original distribution. *C. sativa* tended to the lowest INA values, but all in all a very similar ice nucleation activity in winter despite the different frost hardiness could be found (see also Kishimoto *et al*. 2014a). In general a shift of INT towards zero during the cold acclimation indicated the dehydration mechanism as the major

freeze protection (Körner 2016). This avoids possible internal damage by ice crystals during excessive supercooling (Kishimoto *et al.* 2014b).

The intercellular spaces within the bark, and especially those in the cortex of all species (Schott and Roth-Nebelsick 2018), are visible during summer (*B. nana* Fig. 6D, E) and winter (all species: Fig. 6A, B, G, I, K, M). They become enlarged and filled with ice during cold acclimation and after a freezing event at -10 °C (Fig. 6C, F, H, J, L, N). The enlargement might be a result of the cell dehydration during the cold acclimation (Xin and Browse 2000). The approximate percentage of intercellular spaces in the cortex of older stems in summer was determined as followed: *C. sativa*: 1.24 % ± 0.49 (SD); *B. albosinensis*: 8.22 % ± 3.08 and *B. nana*: 16.15 % ± 6.24. The approximate porosity for the current year stems was the following: *C. sativa*: 2.04 % ± 1.11; *B. albosinensis* 9.26 % ± 2.43 and *B. nana* 7.19 % ± 2.44 (Schott and Roth-Nebelsick 2018). Despite all species having visible intercellular spaces in the fresh state in winter, *Betula* species show the largest ones (Fig. 6). This indicates a better structural adaptation to lower temperatures for the genus *Betula* compared to *Castanea*. Older *B. nana* stems which existed through more freeze and thaw cycles showed the best structural adaptation.

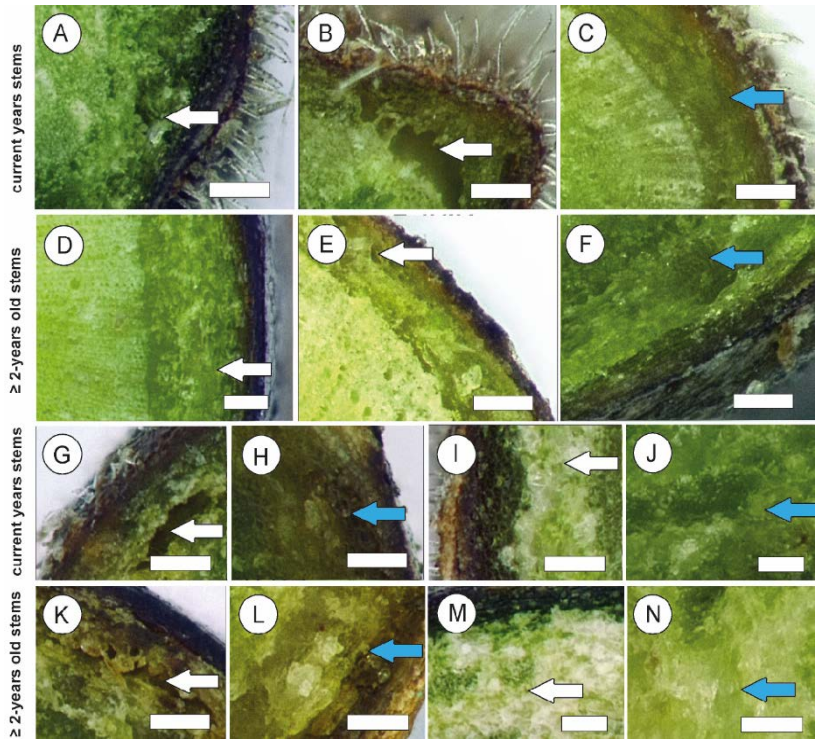

Fig. 6: Detailed view of intercellular spaces of the bark. The arrows point again at intercellular spaces filled with air (white) or ice (blue). A: fresh BNYS. B: fresh BNYW. C: frozen BNYW. D: fresh BNOS. E: fresh BNOW. F: frozen BNOW G: fresh BAYW. H: frozen BAYW. I: fresh CSYW. J: frozen CSYW. K: fresh BAOW. L: frozen BAOW. M: fresh CSOW. N: frozen CSOW. Scale bars = 100 µm (from Schott and Roth-Nebelsick 2018)

The low solute content in the intercellular spaces triggers the ice crystallization within and water from adjacent cells gets drawn out as described in the introduction. Additionally, Kishimoto *et al.* (2014b) reported intrinsic INA within the bark which might result in a promotion of extracellular ice crystal growth. Expected continuous growth of extracellular ice over time (Niklas 1989) makes bigger intercellular spaces for the *Betula* species, especially *B. nana*, a necessary survival adaptation.

Stachys byzantina C. Koch

In this contribution, *S. byzantina* was visually evaluated during an artificial freezing event and the focus was especially on the cold acclimated and fresh or frozen state during winter. This was done in order to identify the sites and dimensions of the intercellular spaces as storage for ice crystals and the surrounding tissue (Schott and Roth-Nebelsick in prep a).

Gaps, such as intercellular spaces underneath the epidermis, can be found within the petiole on three or four sides – two on the lower and one to two on the upper side depending on the dimensions of the included ice (Fig. 3 in Schott and Roth-Nebelsick in prep a). On the lower side the intercellular spaces are clearly separated by a connection zone in the middle (Fig. 7C) and on the upper side the inwards bended cell connections can loosen by growing ice on both sides (Fig. 7D, E). The lower and upper intercellular spaces are separated by continuous connections zones in the right and left side of the petiole which contain small intercellular spaces for ice crystallization for the cells close by (Fig. 9 in Schott and Roth-Nebelsick in prep a). This indicates a limitation of water movement from the dehydrating cells to the sites of ice crystallization within the prepared intercellular spaces. The gaps, which were already observed by (Prillieux 1869) for petioles of some herbaceous species, are situated just underneath the epidermis or separate the epidermis and the collenchyma from the parenchyma (Fig. 4 in Schott and Roth-Nebelsick in prep a). The first collenchyma row can be ruptured with seemingly no signs of force (Fig. 8C, D in Schott and Roth-Nebelsick in prep a). Differences in the position of the gaps in species or between species were also observed by Prillieux (1869). McCully *et al.* (2004) highlighted the differences of poppies (*E.* c*alifornica*) gaps after a single epidermal row and

clovers (*T. repens*) gaps after two rows without any “broken” rows. During the freezing process the main vascular and sometimes the two sub vascular bundles will not lose much volume while the surrounding parenchyma and the 3-4 layers

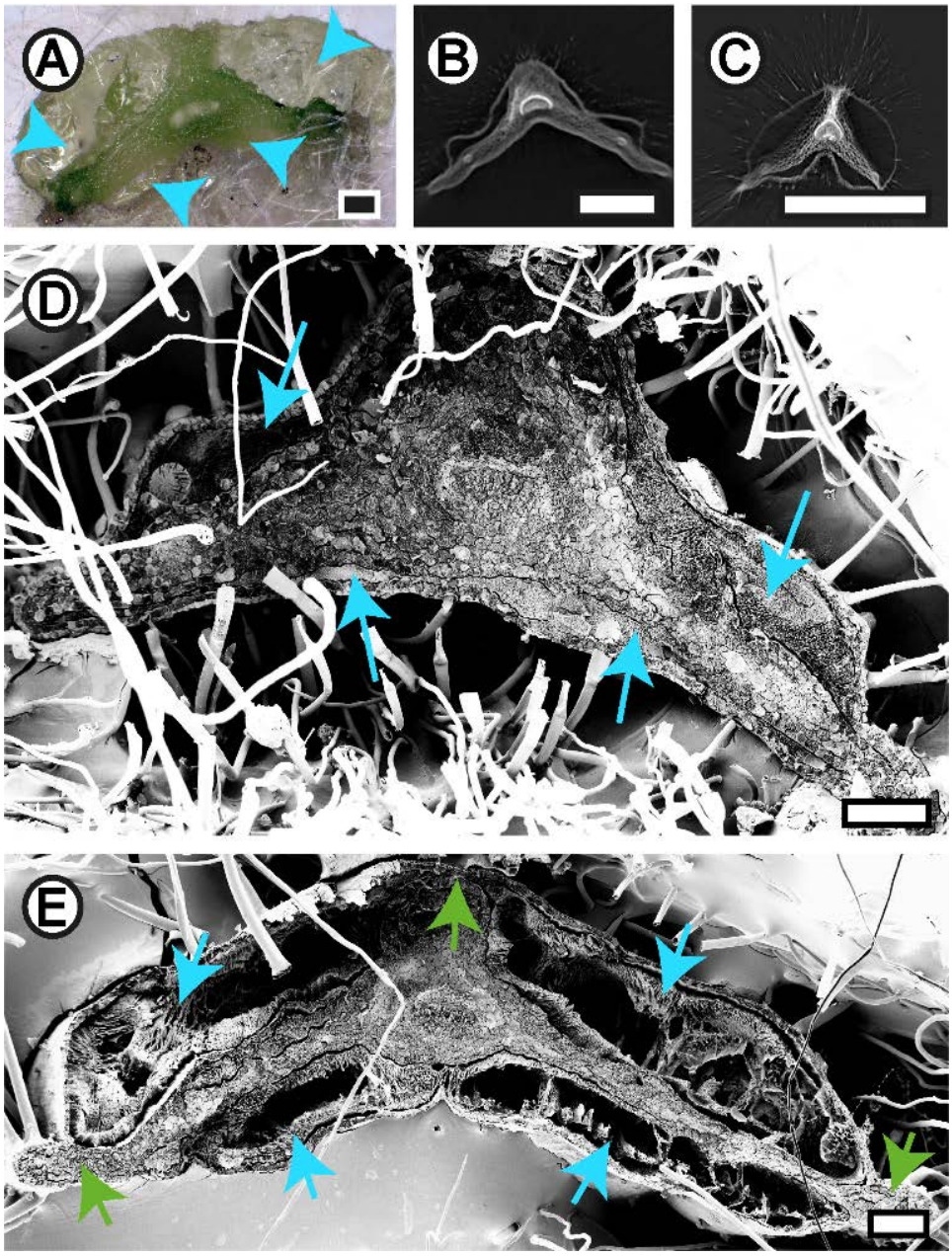

Fig. 7: Cross sections of acclimated and frozen or thawed *S. byzantina* petioles in winter. A: Enlarged intercellular spaces partly filled with ice in a frozen petiole. B: Fresh and naturally in the morning thawed petiole in methanol/ethanol dehydrated and critical point dried (microCT-scan). C: Photo displaying the formerly frozen petiole in methanol/ethanol dehydrated and critical point dried (microCT-scan). D: A frozen petiole showing ice in the intercellular spaces on the abaxial and adaxial side and connection zones at the left and right side. E: A frozen petiole highlighting the dimensions of the intercellular spaces still with ice at the borders and some contact sides at the left and right side of the petiole and at the abaxial and adaxial half. Blue arrows indicate some places of ice crystal growth and green ones indicate contact sides. Scale bars: 200 µm (from Schott and Roth-Nebelsick in prep a).

of chollenchyma lose a great amount of water and deform while the epidermis and collenchyma sometimes bend outwards (Salmaki *et al.* 2011; Schott and Roth-Nebelsick in prep a). Cell connections in the connection zones are quite dense (Fig. 4A, B, D in Schott and Roth-Nebelsick in prep a). These mentioned connection zones are areas where cells are not separated by any larger gaps and maintain the supply of the separated parts.

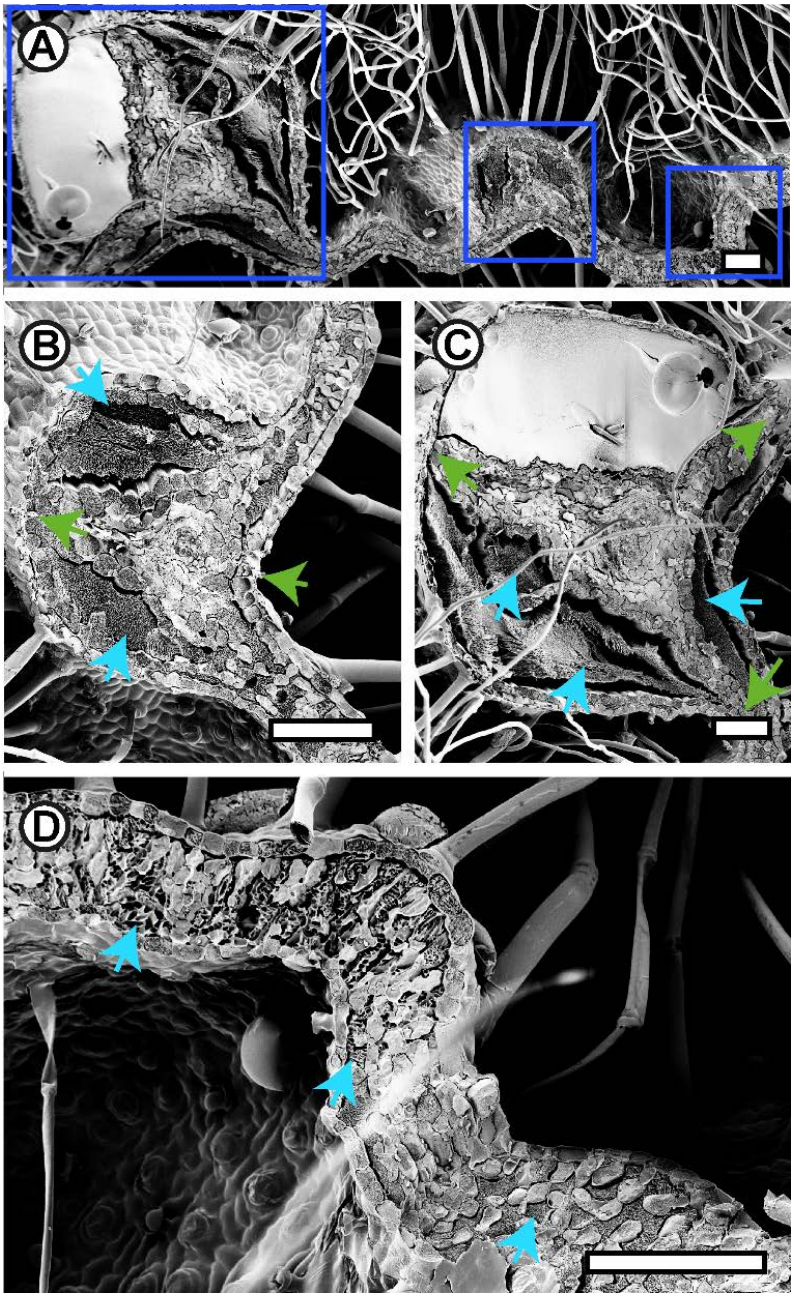

Fig. 8: Frozen CryoSEM images of cross sections of a *S. byzantina* leaf in winter. The ice has a flaky pastry like structure. The white area is tissue tec. A: Showing a larger part of the leaf with mostly ice in the enlarged intercellular spaces. Blue boxes highlight the enlarge parts in B-D. B: Detailed image of the midvein with mostly ice in the expanded intercellular spaces. C: Detailed image of a vein with ice at similar places than the midvein. D: Detailed part of the leaf showing ice between the cells in the leaves. Blue arrows indicate the ice and green ones indicate connection zones. Position in figure 1: 1. Scale bars: 100 µm (from Schott and Roth-Nebelsick in prep a).

Leaves with the typical dense hair cover are structured in palisade and spongy parenchyma and an epidermis and one layer of collenchyma around the parenchyma in the midvein (Salmaki *et al.* 2011). During the freezing event, ice

can be found between the spongy parenchyma cells and even between the two layered palisade parenchyma cells (Fig. 8A, D) which do not have such dense cell connections (Fig. 6 in Schott and Roth-Nebelsick in prep a). The veins follow the same freezing pattern as the petioles with a huge cell dehydration within the parenchyma around the nearly unaffected vascular bundle with 2 main intercellular spaces underneath the epidermis or epidermis and collenchyma on the lower side. A connection zone in the middle and on both sides and 1 or 2 smaller intercellular spaces on the upper side (Fig. 8A - C) exists. Denser cell connections can be found within the parenchyma.

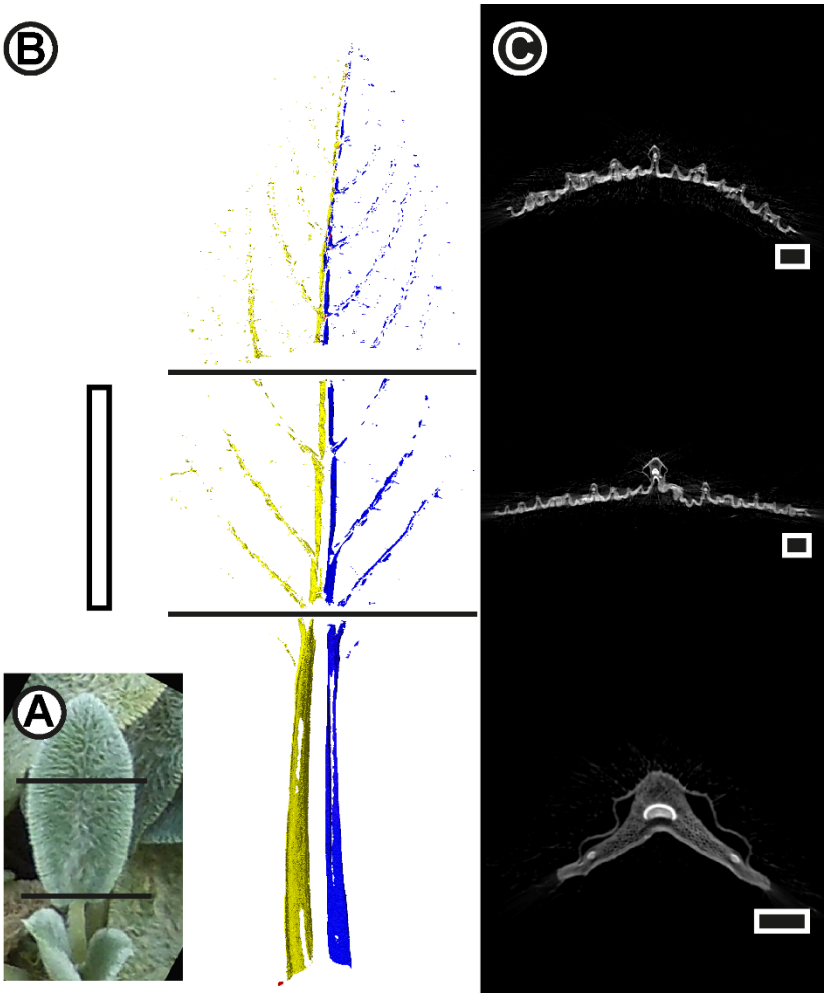

Fig. 9: A: Image of the upper part of a fresh *S. byzantina* leaf with petiole showing the orientation of the segmented parts and the cuts. B: Segmentation of µCT scans of methanol/ethanol dehydrated and CPD dried fresh *S. byzantina* leaf with petiole cut in 3 parts. The intercellular spaces on the left side of the lower part of the leaf and petiole are colored yellow and on the right side blue. The small red areas are the intercellular spaces of the upper part. Scale bars: 1 cm. C: one cross section of each part as an example. Scale bars: B: 1 cm; C: 0.1 cm (from Schott and Roth-Nebelsick in prep a).

Large intercellular spaces can always be found the same locations. They can be found on the upper and lower side going through the whole leaves and petioles as mentioned above (Fig. 7, 8A – C, 9B, C,) and even partly through the stem (Fig. 1A in Schott and Roth-Nebelsick in prep a). This allows for an unhindered ice accumulation along the plant and is probably the result of the similar structure

and the arrangement of the vascular bundle (Salmaki *et al.* 2011). The evaluation of the formerly thawed and methanol/ethanol dehydrated (Talbot and White 2013; Schott *et al.* 2017) critical point dried and scanned plant parts revealed a slight visibility of intercellular spaces within the upper part of the petiole and midvein of the leaf (Fig. 9B (red segmentation), C). Secondly, a strict nearly symmetrical deviation of the lower part in two (Fig. 9B (blue and yellow), C) with intercellular spaces reaching from the petiole through the veins of one leaf half could be detected.

The ability of surviving the partly separation of the parenchyma and the epidermis could be explained through the existence of the corresponding connection zones (anchorages), which keeps the connection of the epidermis and the parenchyma at some places (McCully *et al.* 2004). Those connection zones are mostly visible in the unfrozen and completely visible in the frozen state of the petioles and leaves of *S. byzantina*. Three to four ice impermeable and continuous connection zones do exist. One on each side of the petiole or vein, one in the middle of the lower side and sometimes one on the upper side (Fig. 7 and 8). The fault, including the living tissue as an important part of the freezing process, defined by McCully *et al.* (2004) for poppy and clover and already visible within the other species of Prillieux (1869) is “a particular region of compact tissue arranged so that by expansion it can accommodate large masses of extracellular ice, and by contraction on thawing can restore its form with no apparent damage”. Previous studies of ice growth within other species throughout the whole plant or plant parts also indicated this feature (*e.g.* Hacker and Neuner 2008; Wisniewski *et al.* 2015) and it can also be applied to *S. byzantina* analyzed here.

The differences of cell form and dimensions on both sides of the gaps in the petioles and leaves can be recognized (Fig. 7, 8 and Fig. 4 in Schott and Roth-Nebelsick in prep a). Compared with the larger and rounder cells of the parenchyma epidermis, these cells are smaller and more square-like with straight radial walls, allowing for a larger contact area and maybe stronger connection between one another (Fig. 4, 6C in Schott and Roth-Nebelsick in prep a). A detailed analysis of the petioles and leaves highlighted the for herbs typical dehydration mechanism during a freezing event with larger intercellular spaces under or near the epidermis and a strong dehydration of the living tissue (Prillieux

1869; McCully *et al.* 2004). The extensive structural deformation, however, reported for various annual herbaceous species, such as the taller and more slender *T. repens* and *E. californica* (McCully *et al.* 2004) could not be found in this perennial species. Instead, the freezing behavior could be better compared with that of the leaves of *E. pauciflora* (Ball *et al.* 2004). Also, only minimal deformation by wilting could be recognized by continuous monitoring (Schott and Roth-Nebelsick in prep a). This leads to the assumption of a prevention of wilting through internal stabilizing structures – probably collenchyma and midvein – as *e.g.* within *E. hyemale* (Schott *et al.* 2017). The rosette-like form of the densely growing *S. byzantina* seems also to serve as protection, together with its low height and the carpet of older leaves covering the fresh leaves. Considering the growth form of *S. byzantina* with its petioles closer to the stem, the available place for deformation is in general bigger on the lower side (Fig. 1B in Schott and Roth-Nebelsick in prep a).

Equisetum hyemale var. *robustum* L.

The focus in these studies (Schott *et al.* 2017; Schott and Roth-Nebelsick in prep b) was on the evergreen and moisture loving species *E. hyemale*. This species has some interesting structural features, such as an air-filled canal system, a hypodermal sterome and a two-layered endodermis. Next to some studies with respect to biomechanical aspects (*e.g.* Zajączkowska *et al.* 2017), previous studies on the freezing behavior of *E. hyemale* were conducted by

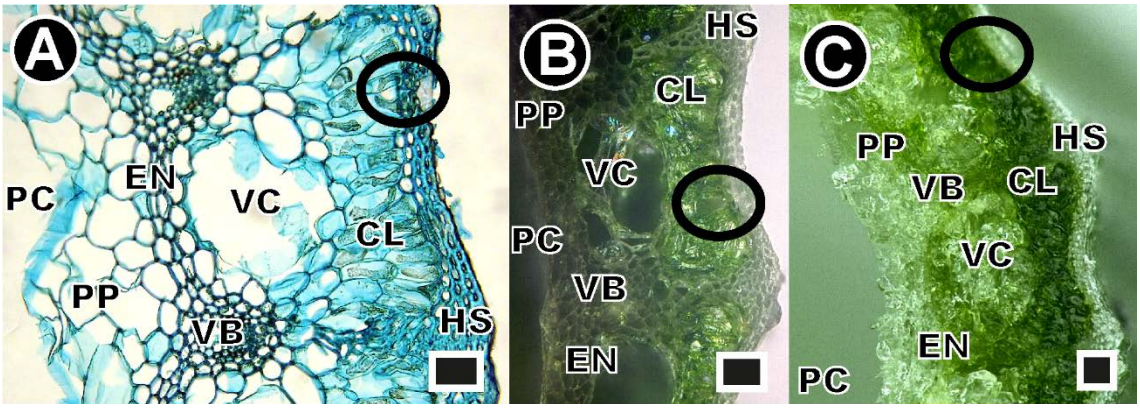

Fig. 10: Detailed parts of cross sections of *Equisetum hyemale* var. *robustum* stems. A: embedded and stained stem. B: fresh stem. C: frozen stem (15 hours at -15 °C). The circles are around a stomata. HS = hypodermal sterome; CL = chlorenchyma; VC = vallecular canal; VB = vascular bundle; EN = endodermis; PP = parenchymatous pith; PC = pith cavity. Scale bars: 100 µm (from Schott and Roth-Nebelsick in prep b).

Schaffner (1908) and Niklas (1989). Various questions, however, were not addressed and are thus considered in the presented work.

The essential morphological structure of *E. hyemale* stems was analyzed in embedded and stained, fresh and frozen cross sections (Fig. 10). From the outside to the inside the hypodermal sterome with stomata (encircled in Fig. 10), the chlorenchyma, the vallecular canal, the vascular bundle, the endodermis and the parenchymatous pith followed by the pith cavity can be seen in Figure 10. Important structural traits for the ice crystal storage are the stomata, the vallecular canals integrated in the cortex, the intercellular spaces within the chlorenchyma and the pith cavity in the middle surrounded by the parenchymatous pith. The two layered endodermis as well as the hypermal sterome stabilize the stems of *E. hyemale* and prevent them from wilting during the freezing process. Moisture stress results in a reduction in cell size and an increase in cell wall thickness (Cutler *et al.* 1977). The small cells with a thick cell wall of the hypodermal sterome and the endodermis might be the main reason for the stem stiffness.

The outer part of the stoma, the ante chamber, is covered with waxes which are probably water repellent (Brune and Haas 2011; Fig. 6B, C in Schott *et al.* 2017; Schott and Roth-Nebelsick in prep b). These waxes are also present between the contact zones of the guard cells growing a little bit further inside (Fig. 2C, G, 6B-D in Schott and Roth-Nebelsick in prep b). Within the sub-stomatal chamber in the plant interior some protuberances could be found on the surface of the cells (Fig. 2A-D in Schott and Roth-Nebelsick in prep b). During the freezing process, ice did not form on these rough surfaces, probably due to the water-repellent waxes of the ante chamber. In contrast, the sub-stomatal chamber became completely filled with ice (Fig. 6B, C in Schott *et al.* 2017; Schott and Roth-Nebelsick in prep b). This provides evidence that extrinsic ice nucleation did not take place (Pearce 2001; Gusta and Wisniewski 2013; Wisniewski *et al.* 2014). This indicates that freezing of *E. hyemale* cannot be triggered by external ice, as it is known to occur in some mosses (Lenné *et al.* 2010; Moffett 2015). This would highlight the importance of the waxes covering the contact zones of the guard cells, reaching even further into the plant interior.

The vallecular canal is partly divided with `sheets´, which partially also line the borders of the vallecular canals (Fig. 5 in Schott and Roth-Nebelsick in prep b).

Protuberances of various sizes and forms are present within the vallecular canals and in the intercellular spaces of the chlorenchyma (Fig. 10A; Fig. 8 in Schott and Roth-Nebelsick in prep b). These are more diverse than reported by Potgieter and van Wyk (1992) for *E. hyemale*. Protuberances within the vallecular canals can grow from underneath the `sheets´. As already described in Kisser (1928) protuberances are regarded as remnants of tissue expansion and formation of intercellular spaces, and suggested functions are purely conjectural (Potgieter and van Wyk 1992). Water droplets around some protuberances or on the `sheets´ can potentially influence ice growth (Fig. 9C-H in Schott and Roth-Nebelsick in prep b). Water adhesion might be improved by a possible rougher surface of the protuberances and `sheets´ (Fig. 9C, D, G in Schott and Roth-Nebelsick in prep b). On some parts of the border - the surrounding membrane - of the vallecular canals were holes between the cells connecting the vallecular canal with the cortex (Fig, 2B in Schott *et al.* 2017; Fig. 5A in Schott and Roth-Nebelsick in prep b). The vallecular canals deform during freezing events while become filled with ice mainly derived from the parenchyma (Fig. 10C, 11) leading to an oval deformation. Despite this deformation, ice can be found within the intercellular spaces along the whole stem (Fig. 12; Fig. 7 in Schott and Roth-Nebelsick, in prep b). The air filled vallecular canals were sealed by a node every

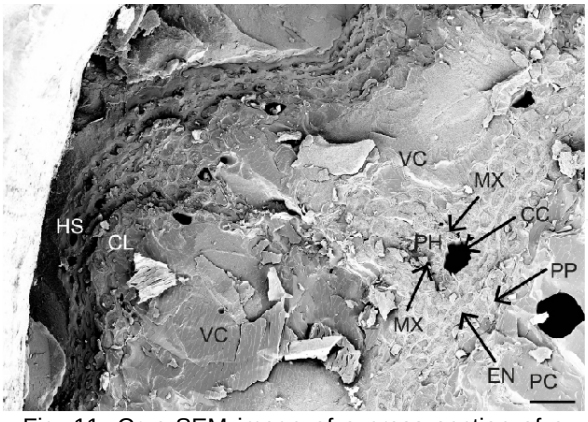

Fig. 11: Cryo-SEM image of a cross section of a naturally acclimated *E. hyemale* shoot, frozen for 72 hours at -20 °C. The vallecular canals (VC), the pith cavity (PC) and the intercellular spaces of the chlorenchyma (CL) are filled with ice. The carinal canal (CC) is empty. EN = endodermis; HS = hypodermal sterome; MX = metaxylem tracheid; PH = phloem; PP = parenchymatous pith. Scale bar = 50 µm (from Schott *et al.* 2017).

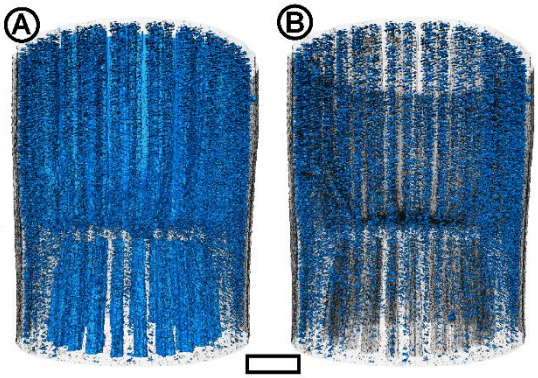

Fig. 12: Segmented (blue) µCT scan of a fresh *E. hyemale* stem, sealed with nail polish, placed inside a small plastic tube with a drop of water. The isosurface is shown in grey. A: upper pith cavity as well as the vallecular canals and the intercellular spaces between the chlorenchyma cells are segmented. B: only the segmented intercellular spaces between the chlorenchyma cells are displayed. Scale bar: 1 mm (from Schott and Roth-Nebelsick in prep b).

few cm (Fig. 12; Speck *et al.* 1998). In some cryoSEM images, the typical separation of solute and water can be seen on the ice within some formerly air-filled vallecular canals (Fig. 11). The freezing within the stems is time dependent. It begins within seconds within the intercellular spaces of the chlorenchyma and in the vallecular canal.

The pith cavity is the central and largest canal of the *E. hyemale* stem which is divided into nodes and internodes (Fig. 12, 13; Fig. 12 in Schott and Roth-Nebelsick in prep b). The pith cavity is lined by the parenchymatous pith. The layers of the parenchymatous pith consist of large, thin cells with a thin cell wall (Fig. 13A, B) which are strongly dehydrated (Fig. 3C, D, 4C, 9A in Schott and Roth-Nebelsick in prep b). This leads to the fact that during a freezing event, most or all cells layers of the parechymatous pith irreversibly collapse (Fig. 1 in Schott *et al.* 2017; Fig. 9H in Schott and Roth-Nebelsick in prep b). Inducing the freezing event in an ESEM, some tissue deformation was observed. Before ice crystall formation on the surface, some “moving shadows” under the thin, compressed parenchymatous pith were detected. The different ice crystals merged in a single cryslat (Fig 12 in Schott and Roth-Nebelsick in prep b).

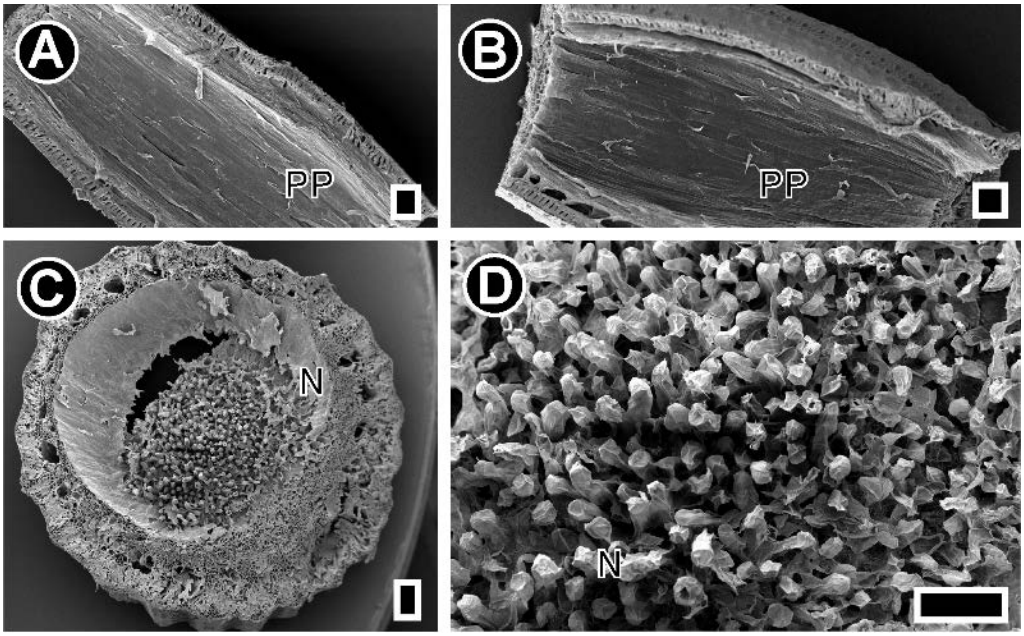

Fig. 13: SEM images of *Equisetum hyemale* var. *robustum* internodes and nodes. A & B: longitudinal sections showing the paper like structure of parenchymatous pith (PP) with a few holes. C: cross section showing the top view of a node (N) with its typical bobble like structure. D: enlargement of the bobbles of the diaphragma (N) in C. Scale bars: 200 µm (from Schott and Roth-Nebelsick in prep b).

The upwards bulged diaphragma is covered by many protuberanes (Fig. 13C, D). During the artificial freezing event in the ESEM the ice crystals grew out of the spaces between the protuberanes of the diaphragma on the upper side as well as on the lower side (Fig. 14). Some ice growth extended to the border of the pith cavity (Supp. 6 in Schott and Roth-Nebelsick in prep b). Upon deacclimation, ice formation diminished especially on the lower part of the diaphragma. The growing ice crystals decreased in size and eventually vanished. Capillary tubes within the node, especially the diaphragma, might influence the water transport between the internodes and they might have an influence on the extracellular ice formation (Niklas 1992). In general the ice grew faster at the borders of the pith cavity.

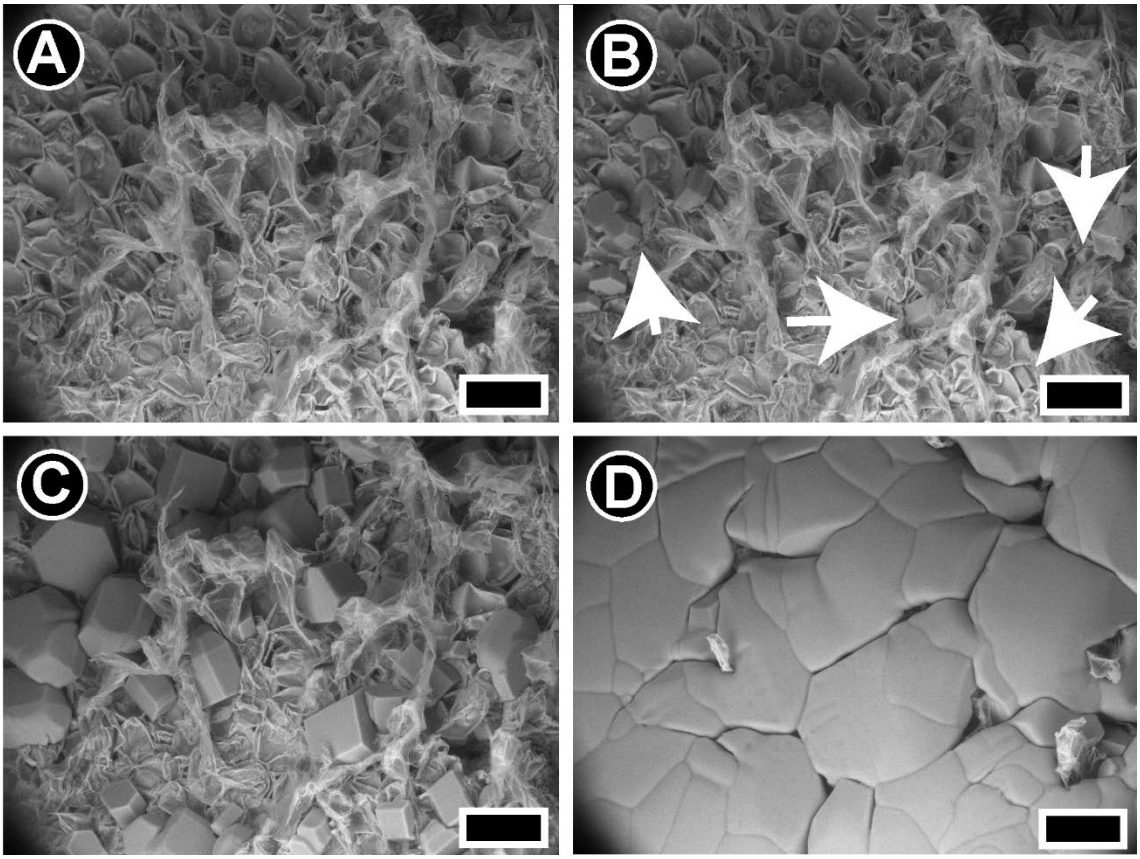

Fig. 14: Selected ESEM images of a diaphragma top of an *Equisetum hyemale* var. *robustum* pith cavity stem (humidity: ~95 %; pressure: 273 Pa; temperature: -10 °C) of continuous recordings. White arrows point at small ice crystals. Scale bars: 100 µm (from Schott and Roth-Nebelsick in prep b).

The ice within the pith cavity accumulated over time (minutes to days, Niklas 1989). During a freezing event, the ice within the pith cavity grew with height along the stem (Fig. 5 in Schott *et al.* 2017). This indicated the existance of more water and /or a greater need of cell protection through dehydration (Speck *et al.*

1998; Schott *et al.* 2017; Schott and Roth-Nebelsick in prep b).Extracellular ice was so far mainly detected within larger intercellular spaces (Ball *et al.* 2004) but other species, for example *E. hyemale*, also show the existence of smaller and larger intercellular spaces (Schott *et al.* 2017; Schott and Roth-Nebelsick in prep b). It seems that stiffer tissue as some leaves (Ball *et al.* 2004) and woody species (Kishimoto *et al.* 2014; Schott and Roth-Nebelsick 2018) prefer smaller intercellular spaces and that softer and slender tissue would result in larger intercellular spaces in ice crystal growth occurs. Some species, as for example *E. hyemale* and *S. byzantina* (Schott and Roth-Nebelsick in prep a), might use both smaller and bigger intercellular spaces combined within the living tissue for freezing events.

Models of the physical process

Finite Element Model

Within the TRR141-A01 cooperation, a TPM (Theory of Porous Media) model was generated to describe cooling and ice formation within *E. hyemale (Eurich et al.* 2016a; 2016b). The axisymmetric model simulates the cooling front within a porous cylinder showing the same canal system as *E. hyemale*. Although informative with respect to the cooling behavior of the system, the structural facts are strongly simplified and cannot simulate the processes on the cellular level occurring in the plant tissues. The model and its behavior is described in detail in Eurich *et al.* (2016a, 2016b).

Analytical model of extracellular freezing

Furthermore, based on all results of *E. hyemale* a theoretical model explaining the physico-chemical process of the water movement during the dehydration mechanism under falling subzero temperatures and the corresponding osmotic-mechanic system was devised (Konrad *et al.* submitted). A mechanism, triggered by temperature changes and initiating and continuing extracellular ice formation, is suggested, based on gradients of volumetric elastic cell wall modulus and related gradients of solute concentration generating a water potential gradient. This gradient attracts the cell water and causes a flow in the wanted direction. The exact derivation of the final equation is explained in (Konrad *et al.* submitted).

To summarize, this model leads to the following five important results: 1) For subzero temperatures, decreasing temperature leads to water efflux out of the cells. 2) This water efflux rises with decreasing cell wall stiffness and increasing cell volume. 3) This extracellular water freezes readily due to its low solute content. 4) Under high air humidity conditions (as granted within plant tissues), a large ice body can develop which grows further by attracting water from adjacent cells. 5) Due to 2), a gradient in cell stiffness and volume is able to direct water towards preferred sites. These results are further explained in the following.

1) **For subzero temperatures, decreasing temperature leads to water efflux out of the cells**

Before building a model, the basics of cell water relations based on cell water potential (Eqn (1)), which is the sum of the turgor pressure and the osmotic pressure (Nobel 2005) has to be evaluated. The changes of cell volume is assumed to be proportional to changes in turgor pressure and related to changes in solute concentration and an approximately constant elastic modulus was assumed (Philip 1958; Steudle *et al*. 1977; Nobel 2005). As described in Konrad *et al.* (submitted), from basic descriptions of the osmotic system, such as eqn (1), it can be concluded that for subzero temperatures, water potential increases when temperature decreases (Konrad *et al.* submitted).

$$\psi_{cell} = \epsilon \left[\frac{c_0 - c}{c} \right] + \frac{\mathcal{R} T}{V_m} \log (1 - c)$$

Eqn (1): Calculation for the cell water potential. a_w: (1-c): activity of the cell sap; mole fractions: c: solute concentration, c_0: cell sap concentration; ϵ: volumetric elastic modulus of the cell; R: ~8.314 J/mol; T: (absolute) temperature; V_m: ~18 x 10^{-6} m^3/mol; (from Konrad *et al.* submitted).

2) **This water efflux rises with decreasing cell wall stiffness and increasing cell volume**

Eqn (2) allows for calculating interrelationships between temperature, solute concentration and cell wall stiffness, shown in Fig. 15. Briefly described, falling subzero temperatures lead to cell water loss, depending on solute concentration, cell wall stiffness and turgor loss point (the solute concentration at which turgor vanishes).

$$\frac{dV}{dt} = \begin{cases} \dfrac{\mathcal{R}V}{\epsilon V_m}\left[\dfrac{c\,(1-c)\left[\log\left(\frac{\varphi}{1-c}\right)\right]^2}{c\,(c_0-c)+c_0\,(1-c)\log\left(\frac{\varphi}{1-c}\right)}\right] & \text{if } t > t_\varphi \\ \dfrac{Vc\,(1-c)\left[H_{fus}-\mathcal{R}T_f\log(1-c)\right]^2}{\epsilon V_m T_f\left\{c_0\,(1-c)\left[H_{fus}-\mathcal{R}T_f\log(1-c)\right]+\mathcal{R}T_f\,c\,(c_0-c)\right\}+H_{fus}\mathcal{R}T_f c^2} & \text{if } t < t_\varphi \end{cases}$$

Eqn (2): Final equation calculating the cell volume change caused by a temperature change. c: solute concentration; c_0: cell sap concentration; dt: temperature change; dV: cell change volume; ϵ: elastic modulus; H_{fus}: fusion enthalpy of ice; R: gas constant:; T: (absolute) temperature; T_f: 0 °C; V: cell volume; V_m: molar volume of (liquid) water; φ: relative humidity (from Konrad *et al.* submitted).

3) This extracellular water freezes readily due to its low solute content

The water potential in the intercellular spaces depends on the physical state (liquid, frozen or vaporous) of the nearly solute-free water which would freeze at around 0 °C with a little decrease through the solutes (Atkins 1997).

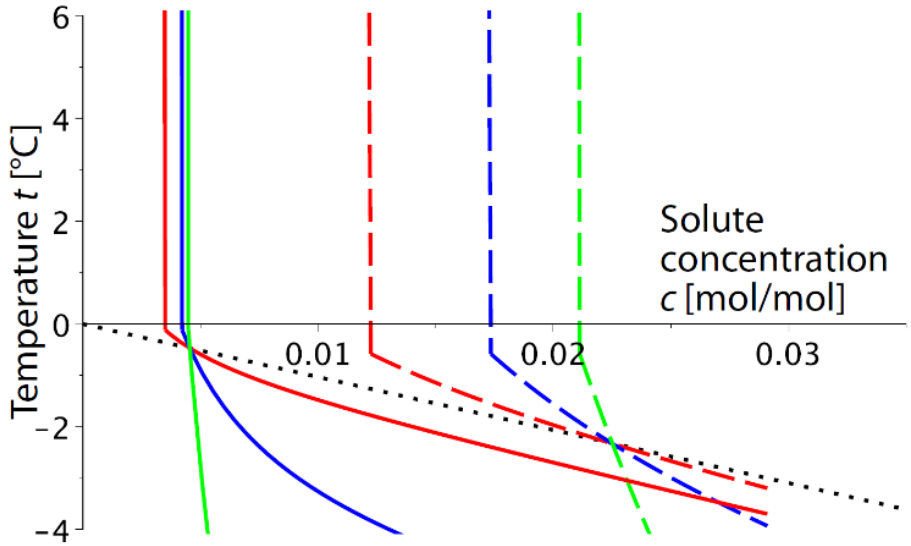

Fig. 15: Visualization of the relation between Celsius temperatures t (ordinate axis) and cell solute concentration c (abscissa) according to equations (17 and 18 (in Konrad *et al.* (submitted))). Black, dotted line: Freezing point depression (according to equation (12 (in Konrad *et al.* (submitted)))). If a plant cell contains a solute of mole fraction c cell water remains liquid for all Celsius temperatures t (ordinate axis) between the c-axis (abscissa) and the black, dotted line. Colored lines (solid or dashed) represent equilibrium of the water potentials in a cell and in intercellular air spaces containing water vapor (for $t > t_\varphi$) or ice (for $t < t_\varphi$). Elastic modulus ϵ of the cell wall is indicated by the colors (red, blue, green) = (1 MPa, 5 MPa, 30 MPa) while the line styles represent the mole fraction c_0 for which the turgor pressure p_{tu} vanishes: (solid, dashed) = (0.0045 mol/mol, 0.0225 mol/mol). The t_φ have been calculated via (19 (in Konrad *et al*. (submitted))) with φ = 0.998 (for the curves related to c_0 = 0.0045 mol/mol) and φ = 0.994 (for the curves related to c_0 = 0.0225 mol/mol). (from Konrad *et al.* submitted).

The relation between the temperature and the cell solute concentration is explained in figure 15. The freezing point depression is marked with the black dotted line in. Above this line for all combinations of cell solute concentrations and temperature the water remains liquid. The different elastic modulus of the cell wall is indicated with color. Turgor loss point c_0 (mole fraction at which the turgor pressure vanishes) is shown by the line style. A longer freeze protection requires a higher solute concentration (Fig. 15). Temperatures above zero have no influence (Fig. 15).

4) **Under high air humidity conditions (as granted within plant tissues), a large ice body can develop which attracts further ice from adjacent cells.**

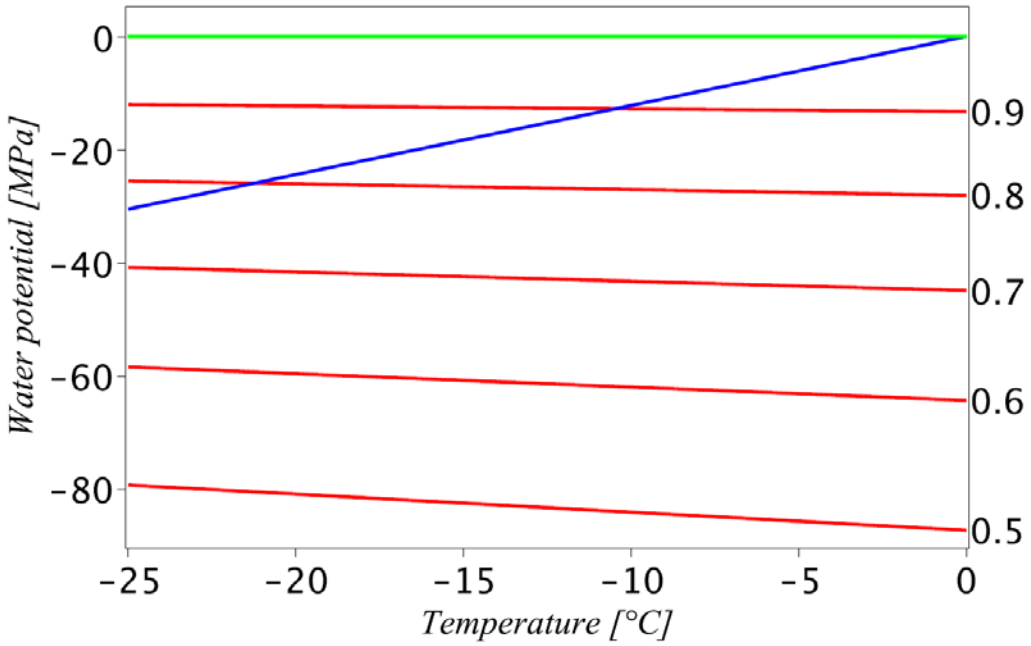

Fig. 16: Water potential of liquid water (green line), ice (blue line) and water vapor (family of red lines), according to expressions (9), (10) and (11) (in Konrad *et al.* (submitted)), as a function of Celsius temperature t. The different red lines represent different relative humidities, from φ = 0.5 (lowermost line) up to φ = 0.9 (uppermost line). (from Konrad *et al.* submitted).

Being in equilibrium, the water potential within the cells and intercellular spaces would have the same value. Every time cells loose nearly solute-free water through the semi-permeable membrane a new equilibrium would be adjusted. Below the freezing point adjacent cells loose water and the water potential of the water vapor and the ice compete. Figure 16 described the water potential of the liquid (green line), solid (blue line) and different gaseous states

(red lines) with different relative humidities. According to the figure 16, ice can form if the combination of the temperature and relative humidity combines above the blue line. So the drawn out water from the adjacent cells vaporizes or freezes within the intercellular spaces with relative humidity depending on the temperature. This means that with decreasing temperature the disturbed equilibrium forms a temporary water potential gradient which attracts cell water until the equilibrium is reestablished.

5) **Due to 2), a gradient in cell stiffness and volume is able to direct water towards preferred sites.**

As shown and explained in an earlier chapter between many *E. hyemale* cells and the corresponding ice storage place is a small distance but no direct connection (Fig. 10) which results in the question: How does the former cell water reaches its destination during a freezing process? In general, if equilibrium of water potential in the cells and the intercellular spaces exists water will not move. Second the variation of cell volume and cell wall thickness in *E. hyemale* (Fig. 10) leads to a variation of the elasto-mechanical properties of the cell wall in some way (Steudle *et al.* 1977). These are confirmed for example by some studies of Speck *et al.* (1998) , with results for Young´s modulus (which are proportional to those of the volumetric elastic modulus (Saito *et al.* 2006)). Considering the results of Speck *et al.* (1998) for different axis heights, this could also explain the observation of more water accumulating within the pith cavity in *E. hyemale* stems with height (Schott *et al.* 2017): ice accumulation increases with decreasing Young´s modulus along the axis. Variation in solute concentration in different cell types at an equilibrium with a given temperature is inevitable, following from the model described in Konrad *et al.* (submitted).

In *E. hyemale,* various cross-sectional gradients in cell wall thickness and cell size can be observed in endodermis cells having a thicker cell wall and smaller size than adjacent cells. The parenchymatous pith cells seemingly become larger towards the pith cavity. Cortex cells close to the vallecular canal are larger than the next layer of cells (schematic in Fig. 5 in Konrad *et al.* submitted; Schott *et al.* 2017). The gradient of the volumetric elastic moduli leads to a gradient of the solute concentration leading in the same direction from the endodermis through

the layers of the parenchymatous pith towards the pith cavity. The same applies for the cells around the vallecular canal. Thereby, it is essential that the stiffer endodermis and the smaller layers of cortex cells around the vallecular canal with the highest solute concentration experience the strongest increase in water potential by decreasing temperatures.

In short, according to the model described in Konrad *et al.* (submitted), the observed gradients in cell wall thickness and cell size explain directed water flow towards the canals and therefore the observed ice accumulation in the canal system. Thereby, a temperature decrease leads to different amounts of water loss and corresponding cell solute concentration. The leaked water generates a loss in cell volume which finally results in cell collapse of the parenchymatous pith layers in *E. hyemale* (Schott *et al.* 2017). The deformation of the vallecular canals, from a circular to an elliptic shape, (Fig. 11) can be explained with the deformation of the surrounding cells (Schott *et al.* 2017). On the outside and inside there are stiffer cells (chlorenchyma followed by the stiff hypodermal sterome (Speck *et al.* 1998) or smaller cells (followed by the endodermis, (Speck *et al.* 1998), while the parenchyma cells between the vallecular canals seem to be softer (Fig. 10).

Appendix of Konrad *et al.* (submitted)

In the appendix of Konrad *et al.* (submitted), ice crystal formation and disappearance, as observed by ESEM studies with *E. hyemale* are described. Two mechanisms operating on different time scales can explain the results. First the sample has to cool down from room temperature and movement of solute-free water from the cells to the intercellular places is triggered. This extracellular water freezes due to its low solute content. Reaching the final temperature, no more water will flow from the adjacent cells. Secondly, sublimation exceeds condensation at a temperature of -10 °C and a relative humidity of 80 %, leading to a steady sublimation of ice to water vapor. Therefore, ice vanishes when cells stop to dehydrate

Conclusion

The results of the model are not related to specific activities of the living cells. Only tissue structure, conductivity, solute concentration and thermodynamics are important (Konrad *et al. submitted)*. The described processes are therefore expected to occur generally if the necessary conditions are met. Therefore, the model could explain the described dehydration mechanism in other plants than *E. hyemale*. As explained in detail before, there is a constant exchange of water between the living cells and the intercellular spaces depending on the temperature changes, and relative humidity is adjusted accordingly (Fig. 19). The cell sizes and cell wall thickness of different tissue layers can form a gradient which directs the leaked water to its destination (Fig. 17; Konrad *et al.* submitted).

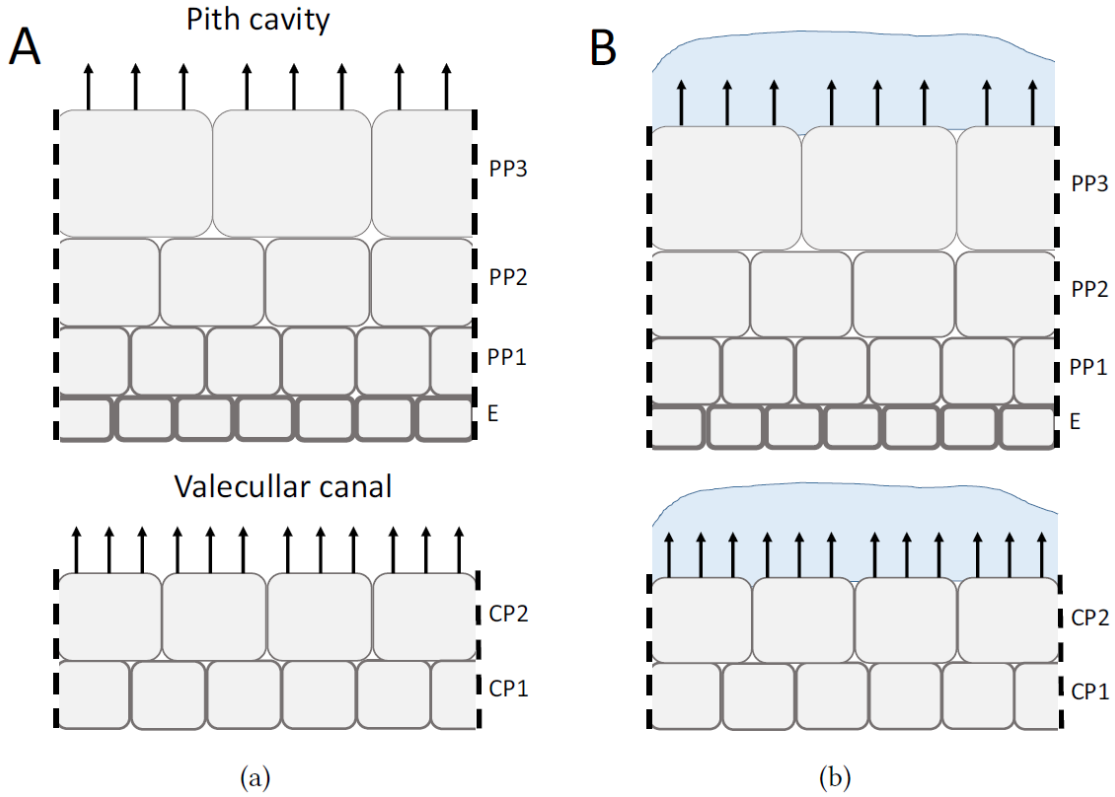

Fig. 17: Schematic representation of tissue showing gradients in cell size and cell wall thickness (indicating differences in cell volumetric elastic modulus ϵ. A temperature decrease triggers water flow, shown as arrows. (a) A temperature drop causes the cell water potential ψ_{cell} to increase. The "softest" and largest cells experience the highest increase; this gradient generates a flow of liquid water with low solute content towards pith cavity and vallecular canal in *E. hyemale*. If the temperature is higher than t_φ extracellular water vapourizes into pith cavity and vallecular canal. (b) If temperature falls below the temperature t_φ extracellular water freezes whereas intracellular sap remains liquid because of freezing point depression due to increased solute concentration. Water flows out of cells until water potential of cells and extracellular ice is equilibrated. Cell layers E: endodermis, (also representing a flow barrier), PP1: parenchymatous pith layer 1, PP2 parenchymatous pith layer 2, PP3: parenchymatous pith layer 3, CP1 cortex parenchyma layer 1, CP2: cortex parenchyma layer 2 (from Konrad *et al.* submitted).

In *S. byzantina* and *E. hyemale*, differences in cell size and wall thickness have been identified which are consistent with the suggested model. By a visual comparison of cortex cells of *Betula* species with those of *C. sativa* possible form differences became visible. All the selected species (*B. nana*, *B. albosinensis*, *C. sativa*, *E. hyemale*, *S. byzantina*) show a cell volume reduction during the frost event and a corresponding volume increase in intercellular spaces or canals. They also seem to have structures for stabilization. An adaptation the moisture stress (Cutler *et al.* 1977) is a reduction in cell size and an increase in cell wall thickness. Taking that into account, the structural cell type adaptations are a necessary protection mechanism.

In general, cells should be quite close to the main place for ice crystal growth otherwise ice will accumulate in smaller intercellular spaces (Schott *et al.* 2017; Schott and Roth-Nebelsick in prep a, in prep b). Connections as pores between different cell types or cells and intercellular spaces of any kind are useful. Despite the circumstance that the suggested model is based on the special structure of *E. hyemale*, the basic dehydration process driven by the cellular osmotic system appears to be applicable in general when cell water loss starts, and rigid cells lose less water than cells with a softer and thinner cell wall. During dehydration triggered by dropping subzero temperatures, specialized surface structures possibly support ice formation, but this requires future work.

References

Arias, N. S.; Bucci, S. J.; Scholz, F. G.; Goldstein, G. (2015): Freezing avoidance by supercooling in Olea europaea cultivars: the role of apoplastic water, solute content and cell wall rigidity. In: *Plant, cell & environment* 38 (10), S. 2061–2070. DOI: 10.1111/pce.12529.

Arias, N. S.; Scholz, F. G.; Goldstein, G.; Bucci, S. J. (2017): The cost of avoiding freezing in stems: trade-off between xylem resistance to cavitation and supercooling capacity in woody plants. In: *Tree physiology* 37 (9), S. 1251–1262. DOI: 10.1093/treephys/tpx071.

Atkins, P. W. (1997): Physical chemistry. New York: W H Freeman & Co.

Ball, M. C.; Canny, M. J.; Huang, C. X.; Egerton, J. J. G.; Wolfe J. (2006): Freeze/thaw-induced embolism depends on nadir temperature. The heterogeneous hydration hypothesis. In: *Plant Cell Environ* 29 (5), S. 729–745. DOI: 10.1111/j.1365-3040.2005.01426.x.

Ball, M. C.; Canny, M. J.; Huang, C. X.; Heady, R. D. (2004): Structural changes in acclimated and unacclimated leaves duriung freezing and thawing. In: *Functional Plant Biology* (31), S. 29–40.

Ball, M. C.; Wolfe, J.; Canny, M.; Hofmann, M.; Nicotra, A. B.; Hughes, D. (2002): Space and time dependence of temperature and freezing in evergreen leaves. In: *Functional Plant Biol.* 29 (11), S. 1259. DOI: 10.1071/FP02037.

Beck, E. H.; Fettig, S.; Knake, C.; Hartig, K.; Bhattarai, T. (2007): Specific and unspecific responses of plants to cold and drought stress. In: *J Biosci* 32 (3), S. 501–510. DOI: 10.1007/s12038-007-0049-5.

Brune, T.; Haas, K. (2011): Equisetum species show uniform epicuticular wax structures but diverse composition patterns. In: *AoB PLANTS* 2011, S. plr009. DOI: 10.1093/aobpla/plr009.

Coombes, A. J.; Debreczy, Z.; Wink, C. (eds.) (2012): Blätter und ihre Bäume. 600 Porträts. Bern: Haupt-Verl. (Haupt Natur).

Cutler, J. M.; Rains, D. W.; Loomis, R. S. (1977): The Importance of Cell Size in the Water Relations of Plants. In: *Physiol Plant* 40 (4), S. 255–260. DOI: 10.1111/j.1399-3054.1977.tb04068.x.

Davis, P. H. (eds.) (1982): Flora of Turkey and the East Aegean Islands. Unter Mitarbeit von J. R. Edmondson, R. R. Mill und Kit Tan. Edinburgh: Edinburgh University Press.

Eurich, L.; Schott, R.; Wagner, A.; Roth-Nebelsick, A.; Ehlers, W. (2016a): From functional properties of frost-resistant plant tissues towards customised construction materials - A continuum-mechanical approach. In: *Proc. Appl. Math. Mech.* 16 (1), S. 81–82. DOI: 10.1002/pamm.201610029.

Eurich, L.; Schott, R. Wagner, A.; Roth-Nebelsick, A.; Ehlers, W. (2016b): Fundamentals of Heat and Mass Transport in Frost-Resistant Plant Tissues. In: Knippers, J. Nickel, K. G. und T. Speck (eds.): Biomimetic Research for

Architecture and Building Construction: Biological Design and Integrative Structures: Cham: Springer International Publishing, S. 97–108.

Groot, W. J. de; Thomas, P. A.; Wein, R. W. (1997): Betula Nana L. and Betula Glandulosa Michx. In: *Journal of Ecology* (85), S. 241–264.

Guo, Y.; Li, G.; Hu, Y.; Di K.; Wang, D.; Yang, G. (2013): Regeneration of Betula albosinensis in strip clearcut and uncut forests of the Qinling Mountains in China. In: *PloS one* 8 (3), S. e59375. DOI: 10.1371/journal.pone.0059375.

Gusta, L. V.; Wisniewski, M. (2013): Understanding plant cold hardiness: an opinion. In: *Physiologia plantarum* 147 (1), S. 4–14. DOI: 10.1111/j.1399-3054.2012.01611.x.

Guy, C. L. (1990): Cold Acclimation and Freezing Stress Tolerance: Role of Protein Metabolism. In: *Annual Review of Plant Physiology and Plant Molecular Biology* (41), S. 187–223.

Hacker, J.; Neuner, G. (2007): Ice propagation in plants visualized at the tisuue level by infrared differential thermal analysis (IDTA). In: *Tree physiology* (27), S. 1661–1670.

Hacker, J.; Neuner, G. (2008): Ice Propagation in Dehardened Alpine Plant Species Studied by Infrared Differential Thermal Analysis (IDTA). In: *Arctic, Antarctic, and Alpine Research* 40 (4), S. 660–670. DOI: 10.1657/1523-0430(07-077)[HACKER]2.0.CO;2.

Hacker, J.; Spindelböck, J. P.; Neuner, G. (2008): Mesophyll freezing and effects of freeze dehydration visualized by simultaneous measurement of IDTA and differential imaging chlorophyll fluorescence. In: *Plant, cell & environment* 31 (11), S. 1725–1733. DOI: 10.1111/j.1365-3040.2008.01881.x.

Husby, C. (2013): Biology and Functional Ecology of Equisetum with Emphasis on the Giant Horsetails. In: *Bot. Rev.* 79 (2), S. 147–177. DOI: 10.1007/s12229-012-9113-4.

Kishimoto, T.; Sekozawa, Y.; Yamazaki, H.; Murakawa, H.; Kuchitsu, K.; Ishikawa, M. (2014a): Seasonal changes in ice nucleation activity in blueberry stems and effects of cold treatments in vitro. In: *Environmental and Experimental Botany* 106, S. 13–23. DOI: 10.1016/j.envexpbot.2014.02.010.

Kishimoto, T.; Yamazaki, H.; Saruwatari, A.; Murakawa, H.; Sekozawa, Y.; Kuchitsu, K. et al. (2014b): High ice nucleation activity located in blueberry stem bark is linked to primary freeze initiation and adaptive freezing behaviour of the bark. In: *AoB PLANTS* 6. DOI: 10.1093/aobpla/plu044.

Kisser J. (1928): Untersuchungen über das Vorkommen und die Verbreitung von Pektinwarzen. In: Jahrbücher für wissenschaftliche Botanik. - Berlin : Borntraeger, Bd. 68, S. 206–232.

Konrad, W.; Schott, R.; Roth-Nebelsick, A. (submitted): A model of frost-resistance based on extracellular freezing, motivated by observations of Equisetum hyemale.

Körner, C. (2016): Plant adaptation to cold climates. In: *F1000Research* 5. DOI: 10.12688/f1000research.9107.1.

Lenné, T.; Bryant, G.; Hocart, C. H.; Huang, C. X.; Ball, M. C. (2010): Freeze avoidance: a dehydrating moss gathers no ice. In: *Plant, cell & environment* 33 (10), S. 1731–1741. DOI: 10.1111/j.1365-3040.2010.02178.x.

Lenz, A.; Hoch, G.; Vitasse, Y.; Körner, C. (2013): European deciduous trees exhibit similar safety margins against damage by spring freeze events along elevational gradients. In: *The New phytologist* 200 (4), S. 1166–1175. DOI: 10.1111/nph.12452.

Levitt, J. (1980): Responses of plants to environmental stresses. Vol. 1. Chilling, freezing, and high temperature stresses. 2. ed. New York - London etc: Academic P XII (Physiological Ecology).

Ludwigs, K. (1911): Untersuchungen zur Biologie der Equiseten. In: *Flora* (103), S. 385–440.

Mazur, Peter (1969): Freezing Injury in Plants. In: *Annu. Rev. Plant. Physiol.* (20), S. 419–448.

McCully, M. E.; Canny, M. J.; Huang, C. X. (2004): The management of extracellular ice by petioles of frost-resistant herbaceous plants. In: *Annals of botany* 94 (5), S. 665–674. DOI: 10.1093/aob/mch191.

Moffett, B. F. (2015): Ice nucleation in mosses and liverworts. In: *Lindbergia* 3 (1), S. 14–16. DOI: 10.25227/linbg.01035.

Neuner, G.; Xu, B.; Hacker, J. (2010): Velocity and pattern of ice propagation and deep supercooling in woody stems of Castanea sativa, Morus nigra and Quercus robur measured by IDTA. In: *Tree physiology* 30 (8), S. 1037–1045. DOI: 10.1093/treephys/tpq059.

Niklas, K. J. (1989): Extracellular freezing in Equisetum hyemale. In: *American Journal of Botany* 76 (4), S. 627–631.

Niklas, K. J. (1992): Plant biomechanics. An engineering approach to plant form and function. Chicago, Ill: Univ. of Chicago Press. Online verfügbar unter http://www.loc.gov/catdir/description/uchi052/91026312.html.

Nobel, P. S. (2005): Physicochemical and environmental plant physiology. 3rd ed. Amsterdam, Boston: Elsevier Academic Press. Online verfügbar unter http://site.ebrary.com/lib/alltitles/docDetail.action?docID=10138275.

Pearce, R. (2001): Plant Freezing and Damage. In: *Annals of botany* 87 (4), S. 417–424. DOI: 10.1006/anbo.2000.1352.

Philip, J. R. (1958): The osmotic cell, solute diffusibility, and the plant water economy. In: *Plant Physiol.* (33), S. 264–271.

Potgieter, M. J.; van Wyk, A. E. (1992a): Intercellular pectic protuberance in plants: their strcuture and taxonomic significance. In: *Bot. Bull. Acad. Sin.* (33), S. 295–316.

Prillieux, M. éd. (1869): Effet De La Gelée Sur Les Plantes. Formation De Glaçons Dans Les Tissus Des Plantes. In: *Bulletin de la Société Botanique de France* 16 (4), S. 140–152. DOI: 10.1080/00378941.1869.10825248.

Roden, J. S.; Canny, M. J.; Huang, C. X.; Ball, M. C. (2009): Frost tolerance and ice formation in Pinus radiata needles: ice management by the endodermis and transfusion tissues. In: *Functional Plant Biology* (36), S. 180–189.

Saito, T.; Soga, K.; Hoson, T.; Terashima, I. (2006): The bulk elastic modulus and the reversible properties of cell walls in developing Quercus leaves. In: *Plant & cell physiology* 47 (6), S. 715–725. DOI: 10.1093/pcp/pcj042.

Salmaki, Y.; Zarre, S.; Lindqvist, C.; Heubl, G.; Bräuchler, C. (2011): Comparative leaf anatomy of Stachys (Lamiaceae. Lamioideae) in Iran with a discussion on its subgeneric classification. In: *Plant Syst Evol* 294 (1-2), S. 109–125. DOI: 10.1007/s00606-011-0450-2.

Schaffner, J. H. (1908): The Air Cavities of Equisetum as Water Reservoirs. In: *The Ohio Naturalist* IX (1), S. 393–394.

Schott, R. T.; Roth-Nebelsick, A. (in prep a): Anatomical adaptations of Stachys byzantina C. Koch to extracellular ice formation.

Schott, R. T.; Roth-Nebelsick, A. (in prep b): Detailed 2- and 3- dimensional evaluation of the freezing process within important structures of Equisetum hyemale L. var. robustum.

Schott, R. T.; Roth-Nebelsick, A. (2018): Ice nucleation in stems of trees and shrubs with different frost resistance. In: *IAWA Journal* 39 (2), S. 177–190. DOI: 10.1163/22941932-20180201.

Schott, R. T.; Voigt, D.; Roth-Nebelsick, A. (2017): Extracellular ice management in the frost hardy horsetail Equisetum hyemale L. In: *Flora* 234, S. 207–214. DOI: 10.1016/j.flora.2017.07.018.

Sharma, B.; Deswal, R. (2014): Antifreeze Proteins in Plants: An overview with an insight into the detection techniques including nanobiotechnology. In: *Journal of Proteins and Proteomics* 52 (2), S. 89–107.

Spatz, H.-C.; Emanns, A. (2004): The mechanical role of the endodermis in Equisetum plant stems. In: *American Journal of Botany* 91 (11), S. 1936–1938.

Speck, T.; Speck, O.; Emanns, A.; Spatz, H.-C. (1998): Biomechanics and Functional Anatomy of Hollow Stemmed Sphenopsids: III. Equisetum hyemale. In: *Bot. Acta* 111, S. 366–376.

Sporne, K. R. (1979a): The Morphology of pteridophytes. London: Hutchinson & Co (Publishers) Ltd.

Steponkus, P. (1984): Role of the Plasma Membrane in Freezing Injury and Cold Acclimation. In: *Annual Review of Plant Physiology and Plant Molecular Biology* 35 (1), S. 543–584. DOI: 10.1146/annurev.arplant.35.1.543.

Steudle, E.; Zimmermann, U.; Lüttge, U. (1977): Effect of turgor pressure and cell size on the wall elasticity of plant cells. In: *Plant Physiol.* 59, S. 285–289.

Talbot, M. J.; White, R. G. (2013): Methanol fixation of plant tissue for Scanning Electron Microscopy improves preservation of tissue morphology and dimensions. In: *Plant methods* 9 (1), S. 36. DOI: 10.1186/1746-4811-9-36.

Thomashow, M. F. (1999): PLANT COLD ACCLIMATION: Freezing Tolerance Genes and Regulatory Mechanisms. In: *Annual Review of Plant Physiology and Plant Molecular Biology* 50, S. 571–599. DOI: 10.1146/annurev.arplant.50.1.571.

Wisniewski, M.; Davis, G. (1989): Evidence for the Involvement of a Specific Cell Wall Layer in Regulation of Deep Supercooling of Xylem Parenchyma. In: *PLANT PHYSIOLOGY* 91 (1), S. 151–156. DOI: 10.1104/pp.91.1.151.

Wisniewski, M.; Glenn, D. M.; Gusta, L. V.; Fuller, M. P. (2008): Using Infrared Thermography to Study Freezing in Plants. In: *Hort Science* 43 (6), S. 1648–1651.

Wisniewski, M.; Gusta, L.; Neuner, G. (2014): Adaptive mechanisms of freeze avoidance in plants. A brief update. In: *Environmental and Experimental Botany* 99, S. 133–140. DOI: 10.1016/j.envexpbot.2013.11.011.

Wisniewski, M.; Neuner, G.; Gusta, L. V. (2015): The use of high-resolution infrared thermography (HRIT) for the study of ice nucleation and ice propagation in plants. In: *Journal of visualized experiments: JoVE* (99), S. e52703. DOI: 10.3791/52703.

Xin, Z.; Browse, J. (2000): Cold comfort farm. The acclimation of plants to freezing temperatures. In: *Plant Cell Environ* 23 (9), S. 893–902. DOI: 10.1046/j.1365-3040.2000.00611.x.

Zajączkowska, U.; Kucharski, S.; Nowak, Z.; Grabowska, K. (2017): Morphometric and mechanical characteristics of Equisetum hyemale stem enhance its vibration. In: *Planta* 245 (4), S. 835–848. DOI: 10.1007/s00425-017-2648-1.

Zhao, Y.; Takhar, P. S. (2017): Micro X-ray computed tomography and image analysis of frozen potatoes subjected to freeze-thaw cycles. In: *LWT - Food Science and Technology* 79, S. 278–286. DOI: 10.1016/j.lwt.2017.01.051.

Appendix I: Further contributions during the time of the PhD project

Conference contributions

Oral presentations

R.T. Schott, W. Konrad, A. Roth-Nebelsick: What can we learn from Equisetum hyemale var. robustum cells dealing with subzero temperatures? **9th International Plant Biomechanics Conference**, 09.-14.08.2018

R.T. Schott, A. Roth-Nebelsick: How important is the distribution, number and size of intercellular spaces during freezing in frost hardy plants? **SEB (Society of Experimental Biology) Florence 2018**, 03.-06.07.2018

Poster presentations

R.T. Schott, A. Roth-Nebelsick: How do *Equisetum hyemale* var. *robustum* and *Stachys byzantina* deal with subzero temperature? **Plant Biology 2018**, 14.-18.07.2018

R.T. Schott, A. Roth-Nebelsick: Freezing behavior of some different frost hardy plants: *Equisetum hyemale* var. *robustum* and the three woody species *Betula nana, Betula albosinensis* and *Castanea sativa.* **Botanikertagung Kiel 2017**, 17.-21.09.2017

R.T. Schott, D. Voigt und A. Roth-Nebelsick: Distribution of ice during subzero conditions within the horsetail *Equisetum hyemale* L.; Poster auf der **SEB (Society of Experimental Biology) Gothenburg 2017**, 03.-06.07.2017

Conference proceedings

Eurich, Lukas; **Schott, Rena**; Wagner, Arndt; Roth-Nebelsick, Anita; Ehlers, Wolfgang (**2016**)**:** From functional properties of frost-resistant plant tissues towards customised construction materials – A continuum-mechanical Approach. – Proceedings in Applied Mathematics and Mechanics, PAMM · Special Issue: Joint 87th Annual Meeting of the International Association of Applied Mathematics and Mechanics (GAMM) and Deutsche Mathematiker-Vereinigung

(DMV), Braunschweig 2016; Editors: V. Bach and H. Fassbender / DOI 10.1002/pamm.201610029

Bookchapter

Eurich, Lukas; **Schott, Rena**; Wagner, Arndt; Roth-Nebelsick, Anita; Ehlers, Wolfgang (**2016**): Fundamentals of Heat and Mass Transport in Frost-Resistant Plant Tissues. In: Jan Knippers, Klaus G. Nickel und Thomas Speck (Hg.): Biomimetic Research for Architecture and Building Construction: Biological Design and Integrative Structures. Cham: Springer International Publishing, S. 97–108.

Public outreach

Museum exhibition

Baubionik – Biologie beflügelt Architektur. Rosensteinmuseum, Staatliches Museum für Naturkunde Stuttgart. October 19th, 2017 – May 6th, **2018**.

Companion volume for the exhibition

Schott, Rena T.; Eurich, Lukas; Wagner, Arndt; Roth-Nebelsick, Anita; Ehlers, Wolfgang: Gefrieren – aber richtig. In: Stuttgarter Beiträge zur Naturkunde 82 (**2017**), Naturkundemuseum Stuttgart, Knippers, Schmid, Speck, S. 62–71.

Eine englische und deutsche Neuauflage ist für 2019 geplant.

Further publications – not project related

Schulz, Dietmar F.; **Schott, Rena T**.; Voorrips, Roeland E.; Smulders, Marinus J. M.; Linde, Marcus; Debener, Thomas (**2016**): Genome-Wide Association Analysis of the Anthocyanin and Carotenoid Contents of Rose Petals. In: Frontiers in plant science 7, S. 1798. DOI: 10.3389/fpls.2016.01798.

Appendix II: Manuscripts

Published manuscript 1: Extracellular ice management in the frost hardy horsetail *Equisetum hyemale* L.

Schott, Rena T.; Voigt, Dagmar; Roth-Nebelsick, Anita (**2017**): Extracellular ice management in the frost hardy horsetail Equisetum hyemale L. In: Flora 234, 207–214. DOI: 10.1016/j.flora.2017.07.018.

Flora 234 (2017) 207–214

Contents lists available at ScienceDirect

Flora

journal homepage: www.elsevier.com/locate/flora

Original Research

Extracellular ice management in the frost hardy horsetail *Equisetum hyemale* L.

Rena T. Schott[a,*], Dagmar Voigt[b], Anita Roth-Nebelsick[a]

[a] State Museum of Natural History Stuttgart, Rosenstein 1, 70191 Stuttgart, Germany
[b] Technical University of Dresden, Institute for Botany, Zellescher Weg 20b, 01062 Dresden, Germany

ARTICLE INFO

Article history:
Received 14 March 2017
Received in revised form 24 July 2017
Accepted 26 July 2017
Edited by Hermann Heilmeier
Available online 31 July 2017

Keywords:
Cold hardiness
Cryo-SEM
Extracellular freezing
Freezing avoidance
Vallecular canals
Winter scouring rush

ABSTRACT

Formation of extracellular ice at specific positions in the plant interior is a common and probably essential component of plant cold hardiness. Studies on extracellular freezing in spore-bearing plants are, however, scarce. In this study, extracellular ice formation in the cold hardy horsetail *Equisetum hyemale* L. is analyzed. Horsetails show an extensive system of intercellular air spaces which are probably crucial for internal ice storage during winter. Previous studies emphasized the spacious pith cavity as the main place for ice crystal growth. Shoots were studied during summer and in the frozen state in winter, after natural acclimatization, by using digital (incident light) microscopy, Scanning Electron Microscopy and Cryo Scanning Electron Microscopy. It was shown that the vallecular canals also contain a large share of ice bodies under freezing conditions. The vallecular canals, which are directly seated within the cortex and whose interior is directly connected to the cortex via gaps in the canal wall, were often and rapidly filled with ice. The pith cavity also contained ice, depending on the position along the shoot and the internode. The carinal canals contained almost no ice crystals. Furthermore, some ice crystals were detected in the intercellular spaces of the chlorenchyma and the substomatal chamber. The stomatal antechamber, however, was always ice-free, probably due to the presence of water-repellent wax crystals. The results of this study support available evidence for the crucial role of pre-existing extensive lacunae for extracellular ice formation in *E. hyemale*. Furthermore, the findings indicate that anatomical details of canal structure and position are important for the pattern of extracellular ice accumulation.

1. Introduction

Cold hardiness is a crucial asset for plants to survive subzero conditions, and various mechanisms are involved. The formation of extracellular ice has long been recognized as a common process during plant freezing (Gusta and Wisniewski, 2013; Levitt, 1980; Molisch, 1897; Pearce, 2001; Prillieux, 1869). Buildup of extracellular ice bodies is placed into the category of freezing avoidance which sums up all physical mechanisms which control the formation of ice in the plant interior (Gusta and Wisniewski, 2013). Whereas freezing tolerance means processes of physiological adaptation, such as changes of membrane composition, the role of freezing avoidance mechanisms is to prevent harmful ice crystal formation within living cells (Gusta and Wisniewski, 2013). Other aspects of freezing avoidance are, for example, the presence of ice nucleators/anti-nucleators and ice barriers, or deep supercooling.

Extracellular ice formation was observed in various plant tissues and organs. A common event is freezing of the xylem content (Utsumi et al., 1998) which occurs quite rapidly (Hacker and Neuner, 2007; Neuner et al., 2010). Extracellular ice formation was also observed in leaves, including conifer needles (Ball et al., 2004; Hacker and Neuner, 2007; Roden et al., 2009), petioles of herbaceous plants (McCully et al., 2004) and buds (Ashworth et al., 1989; Ishikawa et al., 1997). Ice shows a lower water potential than liquid water: below 0 °C, the water potential of ice will decrease about −1.2 MPa with each degree Kelvin decrease in temperature (Rajashekar and Burke, 1982). An ice body will therefore attract water from the surroundings, thereby dehydrating the living cells, depressing their freezing temperature further and making their content strongly viscous (Franks, 1985). Extracellular ice bodies forming in cold hardy plants can be quite massive, and the water stored in them is usually completely absorbed by the living cells after thawing (McCully et al., 2004).

The essential aspect of freezing avoidance is the ability of the cold hardy plant to store ice at specific sites. For example, whereas ice forms randomly in the leaves of freezing sensitive *Eucalyp-*

* Corresponding author.
E-mail addresses: rena.schott@gmx.de, rena.schott@smns-bw.de (R.T. Schott).

http://dx.doi.org/10.1016/j.flora.2017.07.018
0367-2530/

tus species, occurrence of ice is limited to specific positions in the leaves of frost hardy species (Ball et al., 2004). Basic components for limiting the spreading of ice are tissue structure, cell walls, and membranes. Cell walls are suitable to stop a moving ice front because water inside a finely porous material (pores in the nm range) freezes at a much lower temperature compared to unconfined water (Ashworth and Abeles, 1984). Thus, finely porous material can prevent entrance of a moving ice front. Also hydrophobic layers, including artificial ones, can limit spreading of ice (Fuller et al., 2003; Kuprian et al., 2016).

Freezing avoidance and freezing tolerance are coupled mechanisms and both are essential for the ability of cold hardiness. Improving our knowledge of freezing processes in plants is thus essential for understanding cold hardiness, which is a highly relevant aspect of plant evolution (Zanne et al., 2014), ecology (Larcher et al., 2010; Taschler and Neuner, 2004) and agriculture (Lindow et al., 1978; Wisniewski et al., 2014). In the last years, however, the numbers of studies considering freezing avoidance in plants have declined (Wisniewski et al., 2014). Furthermore, gymnosperms and angiosperms are preferentially studied with respect to internal ice formation, whereas spore bearing plants were seldom considered. An outstanding example for a cold hardy spore-bearing plant is the horsetail species *Equisetum hyemale* L., subgenus *Hippochaete* (Husby, 2013). Horsetails are assigned to the monilophytes, a spore-bearing vascular plant group which includes – besides horsetails – the whisk ferns, and eusporangiate and leptosporangiate ferns (Smith et al., 2006).

Equisetum hyemale L., common name "winter scouring rush", shows a wide circumpolar distribution, being native throughout temperate Asia, North America, South America and Europe (Hauke, 1963). Its shoots reach heights from about 0.5 m to 1 m. Usually, *E. hyemale* grows in moist habitats, such as wetlands, riparian environments, swamps or moist forests (Husby, 2013). Horsetails show a unique and characteristic morphology and anatomy (Hauke, 1963, 1979). The hollow stem is organized into nodes and internodes and shows ridges and furrows. As characteristic for plants of moist habitats which are tolerant of flooding, horsetails show an extensive internal system of intercellular air spaces (Bierhorst, 1971). Although the various species of *Equisetum* differ with respect to site soil moisture demand, the structure of their internal canals is similar, consisting of carinal and vallecular canals and a more or less spacious central pith. The carinal canals represent the space originally occupied by protoxylem, and were suggested to support water transport by supplying a low-conductivity pathway (Leroux et al., 2011; Xia et al., 1993).

Horsetails thus represent a special plant construction by showing an extensive and strictly organized intercellular system, consisting of a spacious pith cavity and various longitudinal canals. All canals are more or less circular in cross-section and run continuously along each internodal segment. The shoots of *E. hyemale* persist for about two years (Hauke, 1963), and ice accumulation within their canal system under subzero conditions was reported (Niklas, 1989; Schaffner, 1908). There is evidence that the pith cavity represents the essential site for extracellular ice formation (Niklas, 1989). Because in cold hardy plants extracellular ice formation often takes place at preferred intercellular spaces which are subsequently expanded by the growing ice body and finally occupy the space left by the shrinking dehydrating tissue (McCully et al., 2004), the already extensive canal system of *E. hyemale* appears to be a predestined location for ice storage. Analyzing extracellular ice formation in the canal system of frost hardy *E. hyemale* may contribute to understand the importance and role of intercellular space architecture for freezing avoidance. In this contribution we studied extracellular freezing in *E. hyemale* and the extracellular distribution of ice within its shoots in detail.

2. Material and methods

2.1. Plant material and sample collection

Plants of *Equisetum hyemale* var. *robustum* from the inner courtyard of the State Museum of Natural History Stuttgart (SMNS; 48.793308° latitude, 9.190340° longitude), cultivated as potted plants, and field-grown plants from the Botanical Garden of the Technical University Dresden, Germany (51.040074° latitude, 13.771024° longitude), were used throughout the work. The plants received natural precipitation and potted individuals were additionally watered ad libitum to keep the substrate moist. The plants cultivated in Stuttgart were used for digital microscopy (DM) studies and Scanning Electron Microscopy (SEM), while the plants obtained from the Botanical Garden in Dresden were analyzed with Cryo-Scanning Electron Microscopy (Cryo-SEM).

2.2. Acclimation and freezing

Observations of ice formation were conducted during the winter season, after all plants were acclimated at their growing site under natural conditions. For freezing, acclimated plants were either 1) put into a freezer, or 2) plants were harvested after natural freezing in the field, under subzero conditions. For artificially freezing, whole plants including pot were put into a custom-built freezer (Fryka, Esslingen, Germany), which was set to 0 °C. To protect the root zone, the pot was kept within a polystyrene box. Then, the temperature was decreased to −10 °C, with a cooling rate of 2 °C h^{-1}. With this cooling rate, which is in the range of that experienced by plants in nature (Steffen et al., 1989), plants should have enough time to perform extracellular ice formation. Samples were harvested from the frozen material after keeping it under −10 °C for 16 h.

2.3. Microscopic analysis

2.3.1. Digital microscopy

During the summer, samples were collected from the six potted plants at the SMNS, which were supplied from the same breeder (Pflanzmich GmbH, Hamburg, Germany), and visualized and analyzed with the digital microscope (Keyence VHX-500F, with VH-Z250R and VH-Z20R, Keyence Corp.). During winter, acclimated and unfrozen as well as frozen plants were studied. Artificially frozen samples were harvested with a pre-cooled razor blade. During the transport as well as during the analysis samples were kept frozen on pre-cooled copper plates (−10 °C) in a small cooling box (True North® mini-cooler, Heathrow Scientific, LLC, Vernon Hills, Illinois, U.S.). For both summer and winter, for frozen as well as unfrozen plants, 10–15 shoot samples taken from different shoot heights were studied.

2.3.2. Scanning electron microscopy

For SEM analysis during summer, samples from current year and older shoots were dehydrated for 10 min in absolute methanol before putting them into absolute ethanol for 30 min. This procedure was repeated, according to Talbot and White (2013), before critical point drying (CPD) was applied using a Leica EM CPD300 (Leica Microsystems GmbH, Wetzlar, Germany). Dried samples were subsequently mounted by an adhesive conducting tape on a stub, and sputtered with gold, and examined in the SEM Zeiss EVO LS 15 (Carl Zeiss Microscopy GmbH, Jena, Germany).

2.3.3. Cryo-scanning electron microscopy

Cryo-fixation with subsequent Cryo-SEM allows for preserving and observing the distribution of ice, liquid water and gas spaces

within a tissue structure or cell (Ball et al., 2004). In summer, whole stems were cut and transported in a closed plastic bag with a wetted paper towel. For summer samples from different plant heights 15 shoots were studied, while for winter samples from different heights around 10 shoots were analyzed. All sampled shoot segments were sealed at their cut ends with modelling clay during transport. During analyses in summer, samples were stored in a water-filled glass to keep them hydrated. In winter, samples taken from naturally acclimated and frozen plants were cut, sealed and transported in a cooling box on dry ice. Samples were kept in the box during the analysis, for maximum a day, to preserve the state of harvesting. Spanning the time between analyses, naturally frozen samples were stored for maximum 72 h at −20 °C in a custom laboratory freezer.

Naturally frozen (winter) and unfrozen (summer) samples were mounted on the sample holder of the Cryo-SEM by using polyvinyl alcohol Tissue-Tek, O.C.T. (Sakura Finetek Europe B.V., Alphen aan den Rijn, Netherlands). Subsequently, the samples were treated in the EMITECH K250X cryo-preparation unit (Quorum Technologies Ltd., Ashford, Kent, United Kingdom), first shock-frozen in liquid nitrogen in the slushing-chamber, secondly transferred to the cryo preparation chamber at −140 °C, transversely and longitudinally freeze-fractured with a cool metal blade, and sputter-coated with platinum (layer thickness ca. 6 nm). All cross sections in Fig. 1 were sublimed for 30 min at −70 °C before sputtering. All other samples were not etched, i.e., not sublimed. Then, samples were moved to the cryo-SEM SUPRA 40VP-31-79 (Carl Zeiss SMT Ltd., Oberkochen, Germany) and examined in the frozen state at 5 kV accelerating voltage and −100 °C temperature. Cryo-SEM micrographs were taken using the software Smart SEM 05.03.05 (Carl Zeiss SMT Ltd., Oberkochen, Germany).

The images obtained by DM, SEM and cryo-SEM were qualitatively evaluated for tissue structure and the distribution of ice.

2.4. Determination of ice within the pith cavity

During winter, 11 acclimated shoots from the plants at the SMNS were cut after each third internode from the top. These parts were cooled in plastic bags in a common laboratory freezer, with a cooling rate of 2 °C h^{-1}, until −20 °C. To determine the distribution and amount of ice crystals within the pith cavity, each frozen internode was cut at its base, middle and top (close to the upper node). The samples were analyzed with the digital microscope.

3. Results

In cross-section, the stem shows the genus-specific structure of the cortex surrounding a spacious pith cavity (Fig. 1A). The cortex consists of epidermal and hypodermal tissues, chlorenchyma and two canal systems, the carinal canals and the vallecular canals. The carinal canals show the sites of former protoxylem, with protoxylem remnants still to be found at this position (Fig. 1B). The hypodermal tissue is a fiber-reinforced collenchyma with the function of a hypodermal sterome (Gierlinger et al., 2008; Hauke, 1963; Speck et al., 1998). Together with the two endodermis layers separating pith tissue and cortex, the hypodermal sterome represents a major stabilizing structure of *E. hyemale* shoots (Speck et al., 1998). The amount of the various tissues varies throughout the stem. For example, there are more vallecular canals in the upper part of the stem than in the basal part, and the thickness of the pith parenchyma increases towards the apex (Speck et al., 1998).

The vallecular canals show a sheet-like lining with a high variance (Fig. 1C). It is not uncommon to find these structures segregating the vallecular canals into separate volumes, by forming longitudinal partitionings or horizontal sheets (Fig. 1C), often in an inclined arrangement (Fig. 2A). The lining can be partially absent (Fig. 2B) or continuous over the surrounding cells (Fig. 2C). In the

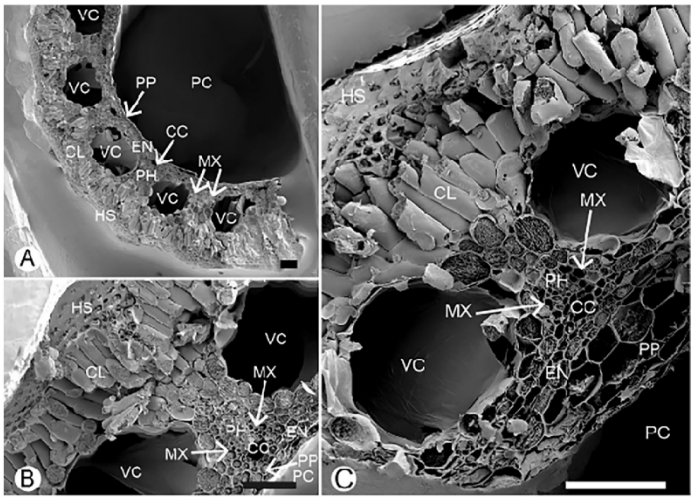

Fig. 1. Cryo-SEM images of cross sections of an *Equisetum hyemale* shoot taken during summer. A. A part of the internodal region, showing the various tissues and canals. B. Details of an older internode illustrating the internal construction with a collapsed parenchymatous pith (PP). C. Details of a younger internode illustrating the internal construction with a still intact parenchymatous pith (PP). CC = carinal canal; CL = chlorenchyma; EN = endodermis; HS = hypodermal sterome; MX = metaxylem tracheid; PC = pith cavity; PH = phloem; VC = vallecular canal. Scale bars = 100 µm.

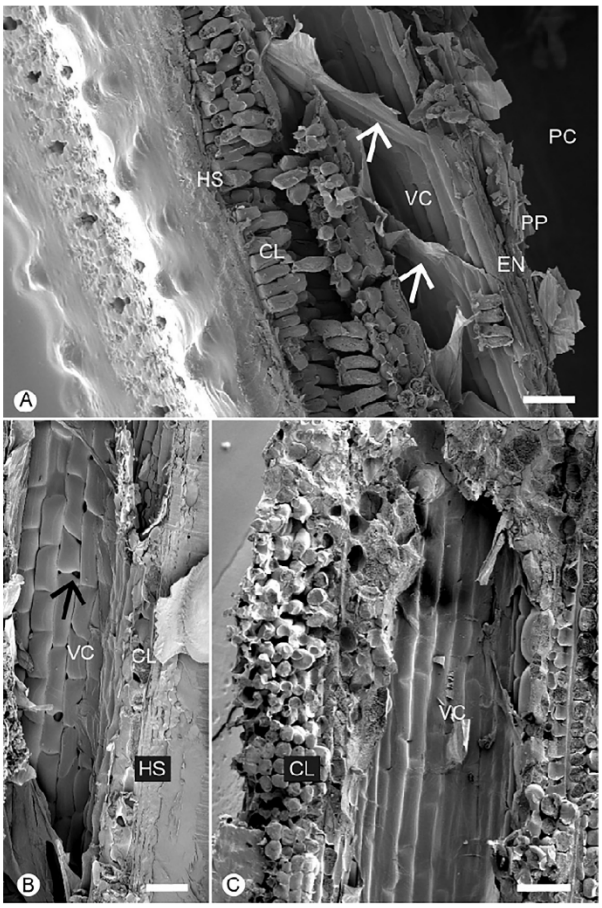

Fig. 2. Cryo-SEM images of longitudinal sections of *Equisetum hyemale* shoots within the internode taken during summer. A. Vallecular canal, showing linings which form sheets, highlighted by white arrows, across the canal. B. Cellular details of the vallecular canal wall at higher magnification. The black arrow indicates a gap between cells. C. Vallecular canal, showing almost no pores in the canal lining. CL = chlorenchyma; EN = endodermis; HS = hypodermal sterome; PC = pith cavity; PP = parenchymatous pith; VC = vallecular canal. Scale bars = 100 µm.

former case, the internal space of the vallecular canal is directly connected with the intercellular space of the cortex by pores which are gaps between adjacent cells (Fig. 2B, arrow).

During summer, all canals, including the pith cavity, were found to be empty in fresh stems. Neither in cryo-SEM preparations (Figs. 1 and 2) nor by optical methods (Fig. 3A) could any water be detected in the internal canals and the pith cavity. When living cells are freeze-fractured in cryo-SEM, their frozen cell content shows characteristic patterns, caused by separation of solute and water upon freezing (Figs. 1 and 2) (McCully et al., 2000). With respect to the carinal canals, optical imaging did not allow to determine presence or absence of water, but in all cryo-SEM images, the carinal canals appeared to be empty as well (Figs. 1 and 2).

Frozen stems showed massive ice bodies within their canal system. The vallecular canals were often found to fill with ice rapidly and completely. Also the pith cavity showed ice, as expected (Figs. 3B and 4). Accumulation of ice in the pith occurred, however, in a more complex pattern, as revealed by inspection of various positions along an internode. In 68% of the 11 samples, the three uppermost internodes of a shoot showed an ice layer covering at least the walls of the pith cavities. The subjacent three internodes showed ice layers in the pith cavity in about 62% of the studied cases, while for the 7th–9th internodes below the apex, pith ice was present in 58% of the samples. There was also variation of ice accumulation within the internodes: the amount of ice within the pith cavity increased with height along the shoot (Fig. 5). Generally, a pith cavity thus becomes filled with ice from bottom to top. Interestingly, the ice bodies in the vallecular canals often showed a pattern that was described by Wisniewski et al. (2014) for an experimentally frozen water film containing fructan (Fig. 4).

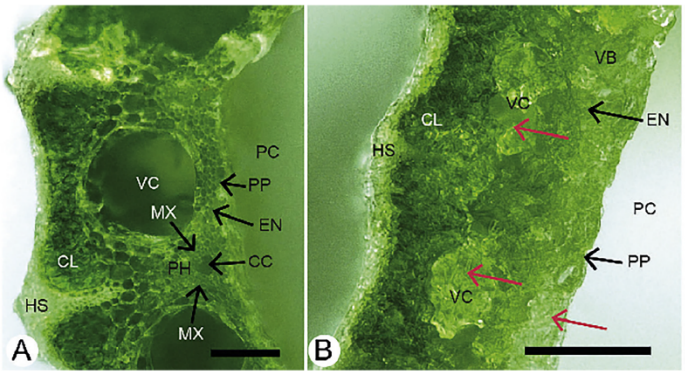

Fig. 3. Cross sections through the internodal region of fresh samples of *Equisetum hyemale* (digital microscopy). A. Shoot during summer. The vallecular canals (VC) are all empty. The carinal canal (CC) appears to be empty as well. B. Shoot during winter, after natural acclimatization and freezing (16 h at −10 °C). The red arrows indicate ice bodies. CC = carinal canal; CL = chlorenchyma; EN = endodermis; HS = hypodermal sterome; MX = Metaxylem tracheid; PC = pith cavity; PH = phloem; PP = parenchymatous pith; VB = vascular bundle. Scale bars = 250 μm.

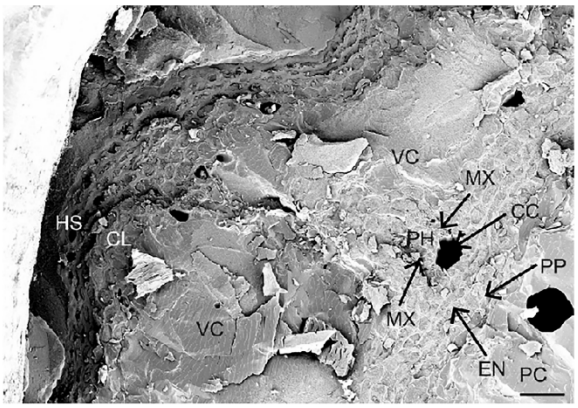

Fig. 4. Cryo-SEM image of a cross section of a naturally acclimated *Equisetum hyemale* shoot, frozen for 72 h at −20 °C. The vallecular canals (VC), the pith cavity (PC) and the intercellular spaces of the chlorenchyma (CL) are filled with ice. The carinal canal (CC) is almost empty. EN = endodermis; HS = hypodermal sterome; MX = metaxylem tracheid; PH = phloem; PP = parenchymatous pith. Scale bar = 50 μm.

Also the carinal canals could contain varying amounts of water in frozen stems (Fig. 4). No differences could be detected between naturally and artificially frozen samples.

In frozen shoots, the living cells lost volume during dehydration. Thick-walled cells of the hypodermal sterome and the epidermis showed a lower degree of shrinkage than the other living cortex cell types (Fig. 4). Hypodermal sterome cells and epidermis cells were readily recognizable in cryo-SEM images whereas pith parenchyma cells and chlorenchyma cells deformed stronger and were difficult to detect in cross-sectional view. Whereas the stomatal antechamber was always ice-free (Fig. 6B and C), the substomatal chamber can be filled with ice (Fig. 6B and C).

4. Discussion

Already Schaffner (1908) noted the presence of ice in the internal canal system of *Equisetum hyemale*, under natural conditions during winter. The results of the present study confirm extracellular ice formation within the shoot canal system. Niklas (1989) focused on extracellular ice accumulating in the pith, by extracting water from the pith of shoots of *E. hyemale* after thawing. As found in the present study, ice formation was also massive within the vallecular canals which were often filled quite rapidly and almost completely with ice whereas ice formation in the pith cavity showed a complex pattern and was dependent on position along the shoot.

Rapid and extensive extracellular ice formation in the vallecular canals appears to be consistent with the structure of the *E. hyemale* stem. The vallecular canals are described as representing schizo/lysigenous intercellular spaces, originating from separation of cortical cells which do not keep up with the growth of hypodermal and procambial cells (Golub and Wetmore, 1948). Due to the shallowness of the cortex cylinder, and the regular circular arrangement of the vallecular canals, practically all cortex cells are quite close to at least one vallecular canal border. Furthermore, pores in the lining of the vallecular canals provide direct connection between intercellular spaces and vallecular canals. Therefore,

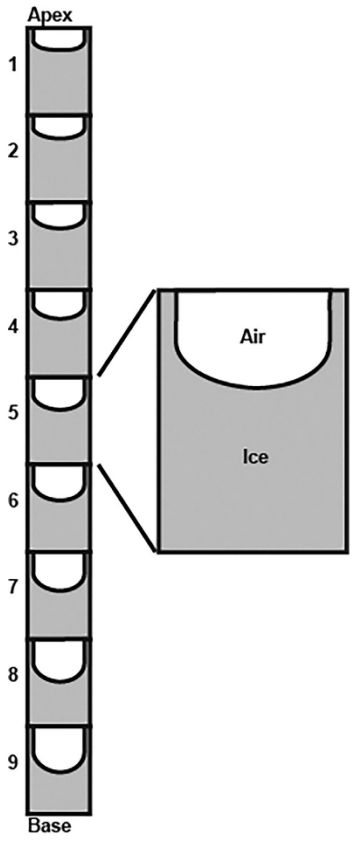

Fig. 5. Schematic sketch of the distribution of air and ice within the pith cavities based on inspection of 9 frozen internodes of an *Equisetum hyemale* stem. The increasing amount of ice from the base to the apex was determined by a cut along the upper part, the middle and the lower part of each internode.

transport distance from the living tissue and from the metaxylem to the vallecular canals is quite short with direct connections whereas the pith is separated from the cortex by a two-layered endodermis showing Casparian thickenings (Speck et al., 1998) which represents possibly a barrier for rapid ice growth.

Ice formation in the pith may be – at least in the early stages of frost events – mainly connected to the pith parenchyma which consists of large and quite thin-walled cells. The amount of pith parenchyma varies along the stem, with larger amounts of pith parenchyma in basal stem parts and increasingly shallow pith parenchyma layers in middle and upper stem sections (Speck et al., 1998). Cryo-SEM images reveal that the pith parenchyma is strongly affected by frost events. In stems which were exposed to freezing, the pith parenchyma has completely collapsed, leaving only some flaky remains. It is probable that the thin walled pith parenchyma cells do not survive freezing events. Further accumulation of ice in the pith may then occur also via water vapor transport. In his experiments, Niklas (1989) reported continuously decreasing water potential of the cortex over several days while the amount of pith cavity ice increased, which would lend support to the idea of slower and continuous ice buildup in the pith.

Ice formation in plants is triggered by heterogeneous nucleation, that is, by substances showing ice nucleation activity (Gusta and Wisniewski, 2013; Marcellos and Single, 1979; Sakai and Larcher, 1987; Wilson et al., 2003). Heterogeneous ice nucleation starts at temperatures several degrees below zero and can be extrinsic or intrinsic. Extrinsic nucleators are not produced by the organism itself. Various bacteria and fungi were reported to have nucleation activity (Lindow et al., 1978; Wisniewski et al., 2002a), and the responsible macromolecules have been partially identified and studied (Pummer et al., 2015). Intrinsic nucleators are produced by the plants themselves (Brush et al., 1994), and their expression can be periodical (Kishimoto et al., 2014). Ice formation in the canal system of *E. hyemale* is therefore very probably also initiated by heterogeneous nucleation, extrinsically or intrinsically.

Extrinsic ice nucleation can occur at the plant surface, with subsequent spreading of ice into the plant interior (Gusta and Wisniewski, 2013; Pearce, 2001; Wisniewski et al., 2014). There is evidence that stomata are entrance sites for spreading ice (Wisniewski and Fuller, 1999) with closed stomata hampering penetration of ice. In the present study, the Cryo-SEM images of naturally frozen samples showed that extracellular ice may be present in the substomatal chamber, but never in the antechamber which was always completely ice-free. The surfaces of the antechamber, the outer sides of the guard cells as well as the shoot surface of the stomatal region are covered with wax crystals which have probably a water-repellent effect (Fig. 6A–C) (Brune and Haas, 2011; Neinhuis and Barthlott, 1997). It was shown that ice nucleation is prevented by water-repellency (Fuller et al., 2003; Wisniewski et al., 2002b). Extrinsic and external nucleation via stomata appears therefore improbable. The genus *Equisetum* shows, however, also hydathodes (Johnson, 1937), which can provide a possible entrance route for ice into the plant after extrinsic nucleation (Pearce and Fuller, 2001). However, also intrinsic nucleation is possible, even in the presence of extrinsic nuclei (Wisniewski et al., 1997). To our knowledge, no information yet exists with respect to intrinsic ice nucleation in *Equisetum*. If different ice nucleators coexist, the "warmest" will cause ice nucleation (Zaragotas et al., 2016).

Internal freezing usually starts in extracellular spaces, including the interior of water-conducting cells. The readiness with which xylem water freezes is due to its low solute content and the continuity of the water columns within the conduits. When ice nucleation starts in the xylem, the ice front progresses rapidly throughout the plant or plant organ (Hacker and Neuner, 2007). Xylem conduits are therefore one preferred site of apoplastic ice formation in plants, and the closeness of vallecular canals and metaxylem in *E. hyemale* may promote ice spreading from conduits to the vallecular canals. However, xylem conduits in the genus *Equisetum* are quite narrow tracheids, and there is evidence that water in this kind of conduit type shows a lower freezing temperature compared to wider elements (Lintunen et al., 2013). The carinal canals in *Equisetum* species were repeatedly reported to be filled with water and therefore suggested to support water transport, at least within an internode because they are not continuous through the nodes (Bierhorst, 1958; Buchholz, 1921). In all our stems, however, we found carinal canals mostly empty, during both summer and winter. The presence of a lacuna close to xylem is thus not sufficient to reliably form an extracellular ice body.

The living cortex cells, such as chlorenchyma and phloem, show shrinkage due to losing water to extracellular ice accumulation but recover during thawing. Interestingly, frozen stems of *E. hyemale* do not suffer from great loss in mechanical stability, because hypodermal sterome and double-layered pith endodermis are the main components of shoot stiffness and not cell turgor (Speck et al., 1998). In contrast, various herbaceous seed plant axes show

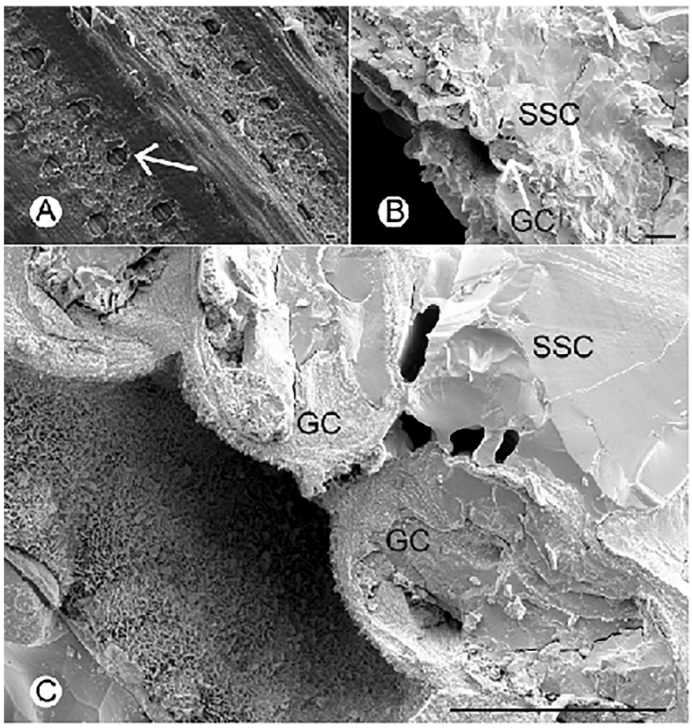

Fig. 6. A. SEM image of the surface of *Equisetum hyemale*, showing the rough surface containing silica bodies and the arrangement of stomata. The white arrow indicates a stoma. B. Cryo SEM image of a cross section through a stoma and the substomatal chamber of a naturally acclimated *E. hyemale* shoot, frozen for 72 h at −20 °C. C: Detail of stoma with ice-filled substomatal chamber, at higher magnification. SSC = substomatal chamber; GC = guard cell. Scale bars = 20 μm.

wilting during freezing when extracellular ice dehydrates living cells (McCully et al., 2004). In cold hardy woody plants, however, thick cell walls and/or special sclerenchymatic structures are common. For example, evergreen leaves of cold hardy *Ilex aquifolium* L. (Aquifoliaceae) or *Buxus sempervirens* L. (Buxaceae) are sclerophyllous, leading also to mechanical stabilization during freezing and dehydration of the living tissues (Hacker and Neuner, 2007). In the same way as for water stress caused by drought, sclerenchymatic structures are a suitable functional trait to prevent wilting under dehydration caused by internal freezing.

In fact, cold acclimation of frost hardy plants includes, among various other complex processes, changes which are related to dehydration. An essential process of acclimation is the change of cell membrane composition during cold acclimation which not only enhances cryostability of the membranes, but also prevents damages during thawing and rehydration of the cells (Xin and Browse, 2000). Furthermore, overwintering organs of woody plants show dehydration and osmotic adjustment, with dehydration often caused by accumulation of dry matter, which improves cold hardiness (Li et al., 2002; Welling, 2003). Cold acclimation of *E. hyemale* probably also includes such processes as osmotic adjustment and a decrease of water content but – to our knowledge – no study exists so far.

The complex pattern of freezing in its canal system, as well as the regular arrangement and spaciousness, of the canals, make *E. hyemale* an ideal object for studying external ice formation. The various canals do not only allow for readily observing ice buildup and anatomical details, such as size or partitioning, by microscopic analysis. Also harvesting of canal fluid is possible, as was demonstrated by Niklas (1989). That *E. hyemale* retains its stiff and upright posture during freezing, without large deformation of its inner structure, also facilitates studies of frozen shoots.

5. Conclusions

It was possible to identify the sites of extracellular ice formation and to document the importance of pre-existing extensive lacunae for the formation of extracellular ice bodies in *E. hyemale*. Previous studies emphasized the spacious pith cavity as the main place for the ice crystal growth. It was shown that the vallecular canals which seem to occupy favorable positions within the cortex also contain a large share of ice bodies under freezing conditions, and that ice accumulation in the pith follows a complex pattern depending on position along the shoot. Furthermore, spreading of extrinsic ice into the shoot is probably prevented by water-repellent waxes covering antechamber and outer sides of stomata.

Acknowledgements

This work has been funded by the German Research Foundation (DFG) as part of the Transregional Collaborative Research

Centre (SFB/Transregio) 141 'Biological Design and Integrative Structures'/A01. The authors would like to thank Dr. Barbara Ditsch (Botanical Garden, Dresden) for providing fresh samples. Furthermore, we are grateful to Markus Günther and Prof. Dr. Christoph Neinhuis (Institute for Botany at the Technical University of Dresden) for allowing us to use the Cryo-SEM, fruitful discussions, and excellent and friendly technical support.

References

Ashworth, E.N., Abeles, F.B., 1984. Freezing behavior of water in small pores and the possible role in the freezing of plant tissues. Plant Physiol. 76, 201–204.

Ashworth, E.N., Davis, G.A., Wisniewski, M.E., 1989. The formation and distribution of ice within dormant and deacclimated peach flower buds. Plant Cell Environ. 12, 521–528.

Ball, M.C., Canny, M.J., Huang, C.X., Heady, R.D., 2004. Structural changes in acclimated and unacclimated leaves during freezing and thawing. Funct. Plant Biol. 31, 29–40.

Bierhorst, D.W., 1958. Vessels in *Equisetum*. Am. J. Bot. 45, 534–537.

Bierhorst, D.W., 1971. Morphology of Vascular Plants. Macmillan, New York.

Brune, T., Haas, K., 2011. Equisetum species show uniform epicuticular wax structures but diverse composition patterns. AoB Plants 2011, http://dx.doi.org/10.1093/aobpla/plr1009.

Brush, R.A., Griffith, M., Mlynarz, A., 1994. Characterization and quantification of intrinsic ice nucleators in winter rye (*Secale cereale*) leaves. Plant Physiol. 104, 725–735.

Buchholz, M., 1921. Über die Wasserleitbahnen in den interkalaren Wachstumszonen monocotyler Sprosse. Flora 114, 119–186.

Franks, F., 1985. Biophysics and Biochemistry at Low Temperatures. Cambridge University Press, Cambridge.

Fuller, M.P., Hamed, F., Wisniewski, M., Glenn, D.M., 2003. Protection of plants from frost using hydrophobic particle film and acrylic polymer. Ann. Appl. Biol. 143, 93–98.

Gierlinger, N., Sapei, L., Paris, O., 2008. Insights into the chemical composition of *Equisetum hyemale* by high resolution Raman imaging. Planta 227, 969–980.

Golub, S.J., Wetmore, R.H., 1948. Studies of development in the vegetative shoot of *Equisetum arvense* L. II. The mature shoot. Am. J. Bot. 35, 767–781.

Gusta, L.V., Wisniewski, M., 2013. Understanding plant cold hardiness: an opinion. Physiol. Plant. 147, 4–14.

Hacker, J., Neuner, G., 2007. Ice propagation in plants visualized at the tissue level by infrared differential thermal analysis (IDTA). Tree Physiol. 27, 1661–1670.

Hauke, R., 1963. A taxonomic monograph of the genus *Equisetum* subgenus *Hippochaete*. Beih. Nova Hedwigia 8, 123pp.

Hauke, R., 1979. A taxonomic monograph of *Equisetum* subgenus *Equisetum*. Nova Hedwigia, 385–456.

Husby, C., 2013. Biology and functional ecology of *Equisetum* with emphasis on the giant horsetails. Bot. Rev. 79, 147–177.

Ishikawa, M., Price, W.S., Ide, H., Arata, Y., 1997. Visualization of freezing behaviors in leaf and flower buds of full-moon maple by nuclear magnetic resonance microscopy. Plant Physiol. 115, 1515–1524.

Johnson, M.A., 1937. Hydathodes in the genus *Equisetum*. Bot. Gaz. 98, 598–608.

Kishimoto, T., Sekozawa, Y., Yamazaki, H., Murakawa, H., Kuchitsu, K., Ishikawa, M., 2014. Seasonal changes in ice nucleation activity in blueberry stems and effects of cold treatments in vitro. Environ. Exp. Bot. 106, 13–23.

Kuprian, E., Tuong, T.D., Pfaller, K., Wagner, J., Livingston III, D.P., Neuner, G., 2016. Persistent supercooling of reproductive shoots is enabled by structural ice barriers being active despite an intact xylem connection. PLoS One 11, e0163160.

Larcher, W., Kainmüller, C., Wagner, J., 2010. Survival types of high mountain plants under extreme temperatures. Flora – Morphol. Distrib. Funct. Ecol. Plants 205, 3–18.

Leroux, O., Knox, J.P., Masschaele, B., Bagniewska-Zadworna, A., Marcus, S.E., Claeys, M., van Hoorebeke, L., Viane, R.L.L., 2011. An extensin-rich matrix lines the carinal canals in *Equisetum ramosissimum*, which may function as water-conducting channels. Ann. Bot. 108, 307–319.

Levitt, J., 1980. Responses of Plants to Environmental Stress, Volume 1: Chilling, Freezing, and High Temperature Stresses. Academic Press, London, New York.

Li, C., Puhakainen, T., Welling, A., Viherä-Aarnio, A., Ernstsen, A., Junttila, O., Heino, P., Palva, E.T., 2002. Cold acclimation in silver birch (*Betula pendula*): development of freezing tolerance in different tissues and climatic ecotypes. Physiol. Plant. 116, 478–488.

Lindow, S.E., Arny, D.C., Upper, C.D., 1978. Distribution of ice nucleation-active bacteria on plants in nature. Appl. Environ. Microbiol. 36, 831–838.

Lintunen, A., Hölttä, T., Kulmala, M., 2013. Anatomical regulation of ice nucleation and cavitation helps trees to survive freezing and drought stress. Sci. Rep. 3, 2031.

Marcellos, H., Single, W.V., 1979. Supercooling and heterogeneous nucleation of freezing in tissues of tender plants. Cryobiology 16, 74–77.

McCully, M.E., Shane, M.W., Baker, A.N., Huang, C.X., Ling, L.E.C., Canny, M.J., 2000. The reliability of cryoSEM for the observation and quantification of xylem embolisms and quantitative analysis of xylem sap in situ. J. Microsc. 198, 24–33.

McCully, M.E., Canny, M.J., Huang, C.X., 2004. The management of extracellular ice by petioles of frost-resistant herbaceous plants. Ann. Bot. 94, 665–674.

Molisch, H., 1897. Untersuchungen über das Erfrieren der Pflanzen. Cryo-Lett. 3, 332–390, Reprinted in English.

Neinhuis, C., Barthlott, W., 1997. Characterization and distribution of water-repellent self-cleaning plant surfaces. Ann. Bot. 79, 667–677.

Neuner, G., Xu, B., Hacker, J., 2010. Velocity and pattern of ice propagation and deep supercooling in woody stems of *Castanea sativa*, *Morus nigra* and *Quercus robur* measured by IDTA. Tree Physiol. 30, 1037–1045.

Niklas, K.J., 1989. Extracellular freezing in *Equisetum hyemale*. Am. J. Bot. 76, 627–631.

Pearce, R.S., Fuller, M.P., 2001. Freezing of barley studied by infrared video thermography. Plant Physiol. 125, 227–240.

Pearce, R.S., 2001. Plant freezing and damage. Ann. Bot. 87, 417–424.

Prillieux, E., 1869. Sur la formation de glaçons a l'intérieur des plantes. Annales des Sciences Naturelles 12, 125–134.

Pummer, B.G., Budke, C., Augustin-Bauditz, S., Niedermeier, D., Felgitsch, L., Kampf, C.J., Huber, R.G., Liedl, K.R., Loerting, T., Moschen, T., Schauperl, M., Tollinger, M., Morris, C.E., Wex, H., Grothe, H., Pöschl, U., Koop, T., Fröhlich-Nowoisky, J., 2015. Ice nucleation by water-soluble macromolecules. Atmos. Chem. Phys. 15, 4077–4091.

Rajashekar, C.B., Burke, M.J., 1982. Liquid water during slow freezing based on cell water relation and limited experimental testing. In: Li, P.H., Sakai, A. (Eds.), Plant Cold Hardiness and Freezing Stress. Mechanisms and Crop Implications. Academic Press, New York.

Roden, J., Canny, M., Huang, C., Ball, M., 2009. Frost tolerance and ice formation in *Pinus radiata* needles: ice management by the endodermis and transfusion tissues. Funct. Plant Biol. 36, 180–189.

Sakai, A., Larcher, W., 1987. Frost Survival of Plants Responses and Adaptation to Freezing Stress. Springer, Berlin.

Schaffner, J.H., 1908. The air cavities of *Equisetum* as water reservoirs. Ohio Nat. 9, 393–394.

Smith, A.R., Pryer, K.M., Schuettpelz, E., Korall, P., Schneider, H., Wolf, P.G., 2006. A classification for extant ferns. Taxon 55, 705–731.

Speck, T., Speck, O., Emanns, A., Spatz, H.C., 1998. Biomechanics and functional anatomy of hollow stemmed Sphenopsids: III. *Equisetum hyemale*. Bot. Acta 111, 366–376.

Steffen, K.L., Arora, R., Palta, J.P., 1989. Relative sensitivity of photosynthesis and respiration to freeze-thaw stress in herbaceous species: importance of realistic freeze-thaw protocols. Plant Physiol. 89, 1372–1379.

Talbot, M.J., White, R.G., 2013. Methanol fixation of plant tissue for scanning electron microscopy improves preservation of tissue morphology and dimensions. Plant Methods 9, 36.

Taschler, D., Neuner, G., 2004. Summer frost resistance and freezing patterns measured in situ in leaves of major alpine plant growth forms in relation to their upper distribution boundary. Plant Cell Environ. 27, 737–746.

Utsumi, Y., Sano, Y., Fujikawa, S., Funada, R., Ohtani, J., 1998. Visualization of cavitated vessels in winter and refilled vessels in spring in diffuse-porous trees by cryo-scanning electron microscopy. Plant Physiol. 117, 1463–1471.

Welling, A., 2003. Overwintering in Wood Plants: Involvement of ABA and Dehydrins. Institute of Biotechnology and Department of Biosciences, Division of Genetics, Faculty of Science, University of Helsinki, Finland, Helsinki, Academic Dissertation.

Wilson, P., Heneghan, A., Haymet, A., 2003. Ice nucleation in nature: supercooling point (SCP) measurements and the role of heterogeneous nucleation. Cryobiology 46, 88–98.

Wisniewski, M., Fuller, M., 1999. Ice nucleation and deep supercooling in plants: new insights using infrared thermography. In: Margesin, R., Schinner, F. (Eds.), Cold-Adapted Organisms: Ecology, Physiology, Enzymology and Molecular Biology. Springer, Berlin, Heidelberg, pp. 105–118.

Wisniewski, M., Lindow, S.E., Ashworth, E.N., 1997. Observations of ice nucleation and propagation in plants using infrared video thermography. Plant Physiol. 113, 327–334.

Wisniewski, M., Fuller, M., Glenn, D.M., Gusta, L., Duman, J., Griffith, M., 2002a. Extrinsic ice nucleation in plants. In: Li, P.H., Palva, E.T. (Eds.), Plant Cold Hardiness. Springer, Berlin, Heidelberg, pp. 211–221.

Wisniewski, M., Glenn, D.M., Fuller, M.P., 2002b. Use of a hydrophobic particle film as a barrier to extrinsic ice nucleation in tomato plants. J. Am. Soc. Hortic. Sci. 127, 358–364.

Wisniewski, M., Gusta, L., Neuner, G., 2014. Adaptive mechanisms of freeze avoidance in plants: a brief update. Environ. Exp. Bot. 99, 133–140.

Xia, Y., Sarafis, V., Campbell, E.O., Callaghan, P.T., 1993. Non invasive imaging of water flow in plants by NMR microscopy. Protoplasma 173, 170–176.

Xin, Z., Browse, J., 2000. Cold comfort farm: the acclimation of plants to freezing temperatures. Plant Cell Environ. 23, 893–902.

Zanne, A.E., Tank, D.C., Cornwell, W.K., Eastman, J.M., Smith, S.A., FitzJohn, R.G., McGlinn, D.J., O'Meara, B.C., Moles, A.T., Reich, P.B., Royer, D.L., Soltis, D.E., Stevens, P.F., Westoby, M., Wright, I.J., Aarssen, L., Bertin, R.I., Calaminus, A., Govaerts, R., Hemmings, F., Leishman, M.R., Oleksyn, J., Soltis, P.S., Swenson, N.G., Warman, L., Beaulieu, J.M., 2014. Three keys to the radiation of angiosperms into freezing environments. Nature 506, 89–92.

Zaragotas, D., Liolios, N.T., Anastassopoulos, E., 2016. Supercooling, ice nucleation and crystal growth: a systematic study in plant samples. Cryobiology 72, 239–243.

Published manuscript 2: Ice nucleation in stems of trees and shrubs with different frost resistance

Schott, Rena T. & Roth-Nebelsick, Anita (**2018**) Ice nucleation in stems of trees and shrubs with different frost resistance. *IAWA Journal* **39,** 177–190.

The Editor-in-Chief gave the permission to republication!

BRILL

IAWA Journal 39 (2), 2018: 177–190

Ice nucleation in stems of trees and shrubs with different frost resistance

Rena T. Schott and **Anita Roth-Nebelsick***

State Museum of Natural History Stuttgart, Rosenstein 1, 70191 Stuttgart, Germany
*Corresponding author; e-mail: rena.schott@smns-bw.de

Accepted for publication: 19 January 2018

ABSTRACT

In this study, the ice nucleation activity (INA) and ice nucleation temperature (INT) as well as extracellular ice formation within the bark were determined for three woody species with different degrees of frost resistance, *Betula nana*, *Betula albosinensis* and *Castanea sativa*. Current-year stems and at least 2-year old stems of *B. nana* and *C. sativa* as well as current-year stems of *B. albosinensis* were compared, during summer (non-acclimated state) and winter (acclimated state), to evaluate possible ontogenetic and seasonal differences. Acclimated plant parts of the selected species revealed nearly similar results, with an INT from -7.52 to -8.43 °C. The current-year stems of *B. nana* had a somewhat higher INT than the older stems. Microscopic analysis showed that extracellular ice formation occurred in the intercellular spaces within the bark of stems of *B. nana*, *B. albosinensis* and *C. sativa*. Size of the intercellular spaces of the bark were species-specific, and *B. nana* showed the largest intercellular space volume. While freezing behavior and extracellular ice formation thus followed principally the same pattern in all considered species, *B. nana* is obviously capable of dealing with large masses of extracellular ice which accumulate over extended periods of frost, making *B. nana* capable of protecting living tissue in colder regions from freezing damage.

Keywords: Wood, bark, ice nucleation activity, temperature, intercellular spaces, *Betula nana*, *Betula albosinensis*, *Castanea sativa*.

INTRODUCTION

Frost resistance plays a crucial role for the survival of plants growing in regions with cold winters and many aspects are not yet completely understood. Full acclimation is necessary for plants to survive freeze-thaw cycles (Améglio *et al.* 2001), comprising various physiological processes. Acclimation is triggered by environmental factors, particularly decreasing temperature. A common process during frost is extracellular ice formation in plant tissue: extracellular water showing lower solute concentration than the content of living cells freezes first and subsequently draws water from the living tissue, thereby dehydrating it (Mazur 1969; Améglio *et al.* 2001). This study focuses on the process of freezing initiation in woody stems which is usually triggered

DOI 10.1163/22941932-20180201

by ice nucleating substances which are extrinsic or intrinsic to the plant (Pearce 2001; Kishimoto *et al.* 2014b).

Different methods for determining the ice nucleation temperatures (INT) exist. Infrared differential thermal analysis (IDTA) is based on image processing and visualizes intra-plant freezing events, as shown by Neuner *et al.* (2010) for different species such as *Castanea sativa*. Another method to determine INT is described by Kishimoto *et al.* (2014a; 2014b). This method also provides the content of ice nucleating particles within a sample, INA (Ice nucleating activity). By calculating the median T_{INT} for different species, a standard value can be determined which allows for interspecific comparison. Additionally, the determination of the cumulative ice nucleation per gram fresh weight or per water volume provides information of ice nucleation activity at defined temperatures. Both values can also show seasonal adaptations. These values are important for analysis of frost hardiness and the comparison of different species, tissues, ontogenetic changes and seasonal differences with respect to frost resistance and susceptibility to freezing.

In this study, INT and INA of three different woody species with different degrees of frost resistance are investigated: the dwarf birch *Betula nana*, the Chinese red birch *Betula albosinensis*, and the sweet chestnut *Castanea sativa*. *Betula nana*, which can endure the lowest temperatures of these three species, is a small shrub, up to 1 m high, and native especially to northern Europe and the western Asia tundra. *Betula nana* shows characteristic adaptations to its natural habitat, the cold tundra, such as a reduced height. The stiff and dull dark brown twigs are pubescent and not warty, with resin dots covering the young twigs (de Groot *et al.* 1997). The older and heavier twigs grow downwards, to the ground. *Betula nana* does therefore not gain much height during growth but grows mostly in width. This growth habit is interpreted as an adaptation of *B. nana* to long frost periods and strong winds (de Groot *et al.* 1997).

Betula albosinensis is a tree with a maximum height of 30 m and is native to China. This species is also frost-resistant but does not occur in the extremely cold habitats of *B. nana*. It has a thin papery bark, ranging from whitish pink to orange red or pink violet. *Castanea sativa* also reaches a maximal height of 30 m and the bark changes during aging from grey and smooth to grey brown with typical cracks. *Castanea sativa* is also frost-resistant, but occurs in warm-temperate climates. Its distribution is from southern Europe to northern Africa and the region of the Black Sea (Coombes 2012). All three examined deciduous species need to protect their stems from freezing damage during dormancy in winter, but under different degrees of low temperature and differently long frost periods.

In this study, INA is determined for the stem tissue of the three considered species for the first time, by using the adapted method of Kishimoto *et al.* (2014a; 2014b). Additionally, also for the first time, stems are inspected with respect to intercellular spaces for extracellular ice formation. Extracellular ice formation in frost hardy plants is usually concentrated at defined intercellular locations (Prillieux 1869; McCully *et al.* 2004; Roden *et al.* 2009), and the volume of these spaces comply with the mass of accumulated ice. The results are compared to evaluate possible interspecific differences between INA and capacity for extracellular ice formation.

Table 1. List of taxa and samples.

Abbreviations: CSOW: *Castanea sativa*, stems ≥ 2 years "old", "winter material" = acclimated. – CSYW: *Castanea sativa*, "young" current-year stems, "winter material" = acclimated. – BAOW: *Betula albosinensis*, stems ≥ 2 years "old", "winter material" = acclimated. – BAYW: *Betula albosinensis*, "young" current-year stems, "winter material" = acclimated. – BNOW: *Betula nana*, stems ≥ 2 years "old", "winter material" = acclimated. – BNYW: *Betula nana*, "young" current-year stems, "winter material" = acclimated. – BNOS: *Betula nana*, stems ≥ 2 years "old", "summer material" = not acclimated. – BNYS: *Betula nana*, "young" current-year stems, "summer material" = not acclimated.

Species	*C. sativa*	*C. sativa*	*B. albosinensis*	*B. albosinensis*	*B. nana*	*B. nana*	*B. nana*	*B. nana*
Age of material	"old" ≥ 2 years	"young" current-year	"old" ≥ 2 years	"young" current-year	"old" ≥ 2 years	"young" current-year	"old" ≥ 2 years	"young" current-year
Acclimation / season	Naturally in winter	Naturally in winter	Naturally in winter	Naturally in winter	Artificially in winter	Artificially in winter	Naturally in late summer	Naturally in late summer
Growing site	SMNS; Wilhelma; Hohenheimer Gardens	SMNS; Wilhelma; Hohenheimer Gardens	Hohenheimer Gardens	Hohenheimer Gardens	SMNS; Wilhelma; Hohenheimer Gardens	SMNS; Wilhelma; Hohenheimer Gardens	SMNS; Wilhelma; Hohenheimer Gardens	SMNS; Wilhelma; Hohenheimer Gardens
Used for	INT / INA microscopic analysis	INT / INA microscopic analysis	microscopic analysis	INT / INA microscopic analysis	INT / INA microscopic analysis	INT / INA microscopic analysis	INT / INA microscopic analysis	INT / INA microscopic analysis
Abbreviation	CSOW	CSYW	BAOW	BAYW	BNOW	BNYW	BNOS	BNYS

MATERIALS AND METHODS

Plant material, sample collection and acclimation

Samples of *Betula nana* and *Castanea sativa* were collected in the Wilhelma (Stuttgart, Germany) and the Hohenheimer Gardens (Stuttgart, Germany). Furthermore, young potted plants, ~5 years old and kept in the inner yard of the State Museum of Natural History Stuttgart (SMNS), were used. The samples of *Betula albosinensis* were solely provided by the Hohenheimer Gardens. The twigs for the different experiments were collected from the end of summer 2015 till the middle of December 2016, and thus during different stages of natural acclimation. All plant material is listed and described in Tables 1 and 2.

Material from the Wilhelma was used for *B. nana* in the summer (non-acclimated plants) and in winter for *C. sativa* (acclimated plants).

All samples were collected fresh at the day of the experiment, and used for imaging or INT as fast as possible. "Summer" twigs which had to be transported over a certain distance (Wilhelma and Hohenheim) were put into water with their cut ends.

In winter, after some nights with frost, material of fully acclimated but yet unfrozen plants was collected. The samples were wetted and transported in closed plastic bags and were used for the experiments as fast as possible.

Potted plants of *B. nana* were artificially acclimated in November 2016 during one week at 5 °C and another week at 0 °C in the custom-built freezer from Fryka, equipped with a triple glazed door and showing a temperature accuracy of ± 1.2 °C at -20 °C (Esslingen, Germany; www.fryka.de). The artificially acclimated plant was used for the INA and the microscopic analysis. The various samples are summarized in Table 1, in which also the acronyms used in the following text are explained.

Determination of ice nucleation temperature (INT)

In this study, the method of Kishimoto *et al.* (2014a; 2014b) was used, but some alterations were required. The basic procedure is as follows. Glass tubes containing 250 ml ultrapure (Type 1) water were autoclaved at 121 °C for 20 minutes. One glass tube each received one of 40 pieces per twig sample. Length and weight of the twig samples for the different species are summarized in Table 2. The limited amount of

Table 2. Length [mm] and maximum weight [mg] of samples of *Betula nana* (current-year and 2-years-old stems), *Betula albosinensis* (current-year stems) and *Castanea sativa* (current-year and 2-years-old stems).

Species	*B. nana*	*B. albosinensis*	*C. sativa*
Length of the used part of the current-year stems [mm]	30	20	7
Maximum weight of the current-year stems [mg]	74.7	115.3	238.9
Length of the used part of the 2-years-old stems [mm]	10	–	3
Maximum weight of the 2-years-old stems [mg]	123.1	–	329

B. nana material required a reduction of the water volume from originally 500 ml to 250 ml. To get comparable results this adaptation was made for all species. The experiment was repeated 4 times.

To be sure that the ultrapure (Type 1) H_2O would not influence the results, the ice nucleation temperature of the water control was determined in a pre-experiment: -16.45 °C ± SE 0.05.

For each measurement cycle, eight glass tubes solely filled with autoclaved ultrapure (Type 1) H_2O served as control. All glass tubes, with and without tissue samples, were put into the precooled (0 °C) freezer. The samples were cooled down by 1° every 20 minutes while the already frozen tubes were counted during each step. The beginning of the experiment started when the plant parts reached the bottom of the glass tubes.

To support reliable identification of frozen samples, the glass tubes were placed onto a small wooden shelf with a black background. This arrangement provided sufficient contrast between sample and background to observe ice crystal growth. In pre-experiments, the temperature development of the shelf in the freezer was measured to exclude any bias by the equipment.

The results provide the median T_{INT} of ice nucleating temperature and the ice nuclei concentration per g fresh weight (Kishimoto *et al.* 2014b).

$$\text{Median } T_{INT} = T_1 + (T_2 - T_1) * (2^{-1} * n - F_1) * (F_2 - F_1)^{-1} \qquad \text{(eqn 1)}$$

T_1 is the threshold temperature before the content of half of the glass tubes freezes and T_2 is the temperature after half of the tubes are frozen. F_1 and F_2 are the corresponding numbers of frozen tubes at these temperatures, and n is the total number of tubes.

The results of the calculation of the cumulative concentration (per unit mass of the sample) of ice nuclei that acted at all temperatures warmer than T ($K'(T)$) (Vali 1995) can best be shown and compared with literature results by a log10 ($K'(T)$) graph.

$$K'(T) = -\ln(f) * M^{-1} \qquad \text{(eqn 2)}$$

With f = (n– FT) * n-1, M = fresh weight [g], FT is the cumulative number of frozen tubes at temperature T. Further details can be found in Kishimoto *et al.* (2014b) and Vali (1995).

Image analysis – Light microscopy

Fresh samples collected from the potted *Betula nana* plants at the SMNS during late summer were analyzed directly with incident light microscopy (Keyence VHX-500F, with VH-Z250R and VH-Z20R). Thicker cross sections were used to obtain suitable pictures for comparison with winter images.

Fresh, acclimated winter samples of all species were collected from an artificially acclimated potted plant of *B. nana* at the SMNS and later from naturally acclimated potted plants (*Castanea sativa*) and from plants growing in the Hohenheimer Gardens (*C. sativa, B. albosinensis*). During transport the stems were handled as explained in

the above section "Plant material, sample collection and acclimation". The cutting ends of the twigs from *C. sativa* and *B. albosinensis* were sealed with clay to prevent water loss by evaporation. In this state they were put into the freezer. After this, the stems were cooled down from 0 °C to -10 °C by 2 °/h. After 72 hours images were taken. For this, samples were cut with a precooled razor blade. During the experiments, the frozen samples were stored on five precooled copper plates within a small cooling box.

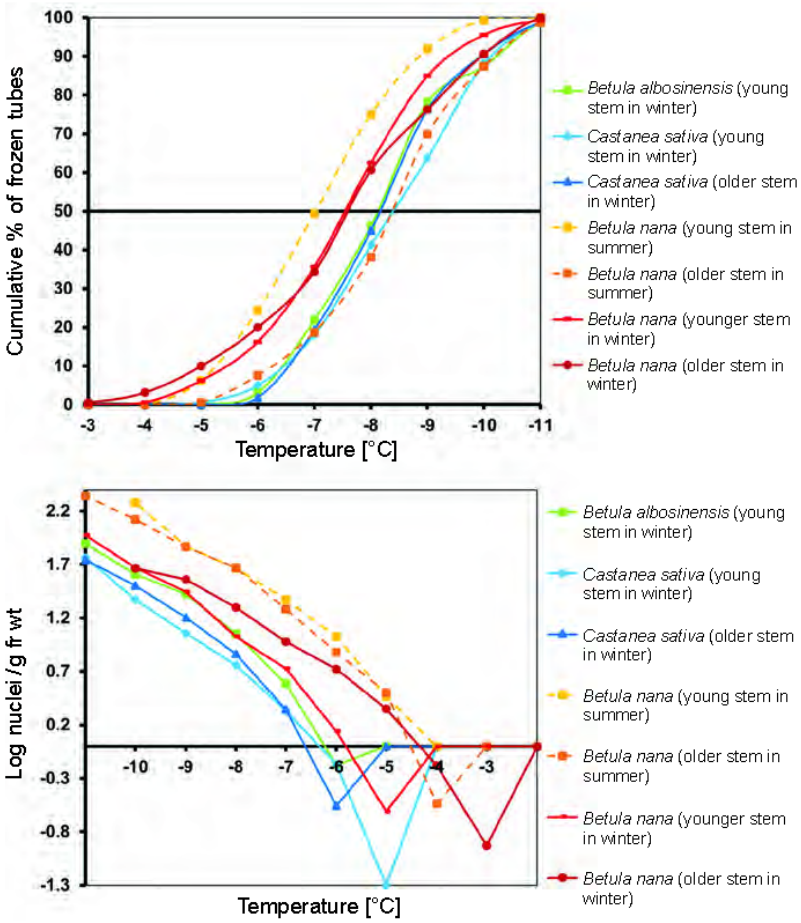

Figure 1. A: Distribution of ice nucleation activity (INA) shown as cumulative percentage of frozen tubes. – B: Cumulative ice nucleation showing K'(T) (ice nuclei per g fresh weight) for BNYS, BNOS, BNYW, BNOW, BAYW, CSYW and CSOW.

RESULTS

Betula nana

Ice nucleation activity

Various differences in INT occurred between summer and winter samples as well as between young and older samples (Fig. 1A). Median INT courses against temperature were different for the summer samples, BNYS and BNOS, but were almost identical for both winter samples, BNOW and BNYW (Fig. 1A and Table 3; see Table 1 for description of the acronyms). INA, however, was lower for the winter samples (Fig. 1B). Figure 2 further illustrates the distribution of freezing for the samples of *B. nana*. Acclimated stems, particularly older material (BNOW), show an early initia-

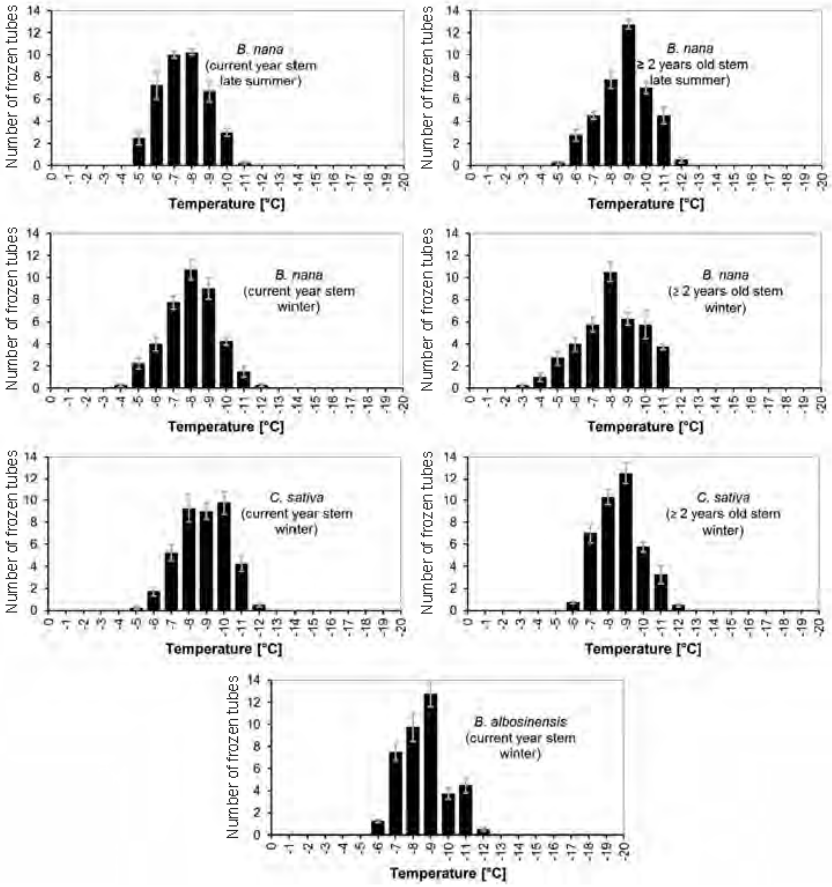

Figure 2. Distribution of ice nucleation activity of BNYS, BNOS, BNYW, BNOW, BAYW, CSYW and CSOW.

Table 3. Results of ice nucleation temperature and median of ice nuclei active at -8 °C for *Castanea sativa*, *Betula albosinensis* and *Betula nana*.

Species	*C. sativa*	*C. sativa*	*B. albosinensis*	*B. albosinensis*	*B. nana*	*B. nana*	*B. nana*	*B. nana*
Age of material	"old" ≥ 2 years	"young" current-year stems	"old" ≥ 2 years	"young" current-year stems	"old" ≥ 2 years	"young" current-year stems	"old" ≥ 2 years	"young" current-year stems
Season	winter	winter	winter	winter	winter	winter	summer	summer
Median INT [°C] ± SE (n = 4)	-8.14 ± 0.14	-8.43 ± 0.25	n.a.	-8.06 ± 0.20	-7.52 ± 0.26	-7.56 ± 0.19	-8.38 ± 0.20	-7.01 ± 0.23
Median of ice nuclei active at -8 °C	9	7	n.a.	12	21	12	54	49

tion of freezing events, compared to non-acclimated stems. The latter group shows first freezing at -5 °C, whereas acclimated samples started to show freezing at -4 °C or even -3 °C.

Betula nana INT of current-year stems in October was lower than in November (Table 3).

Intercellular spaces

Since we used younger twig material, the largest part of the bark is represented by cortex in our samples. The following descriptions and discussions refer therefore – for all considered species –to cortex tissues.

During summer, older as well as younger stems of *B. nana* showed visible intercellular spaces within the bark (Fig 3A, D; 4A, D). During winter, after acclimation, the intercellular spaces within the bark became substantially larger (Fig. 3B, E; 4B, E). After freezing, at -10 °C, ice bodies formed within these intercellular spaces

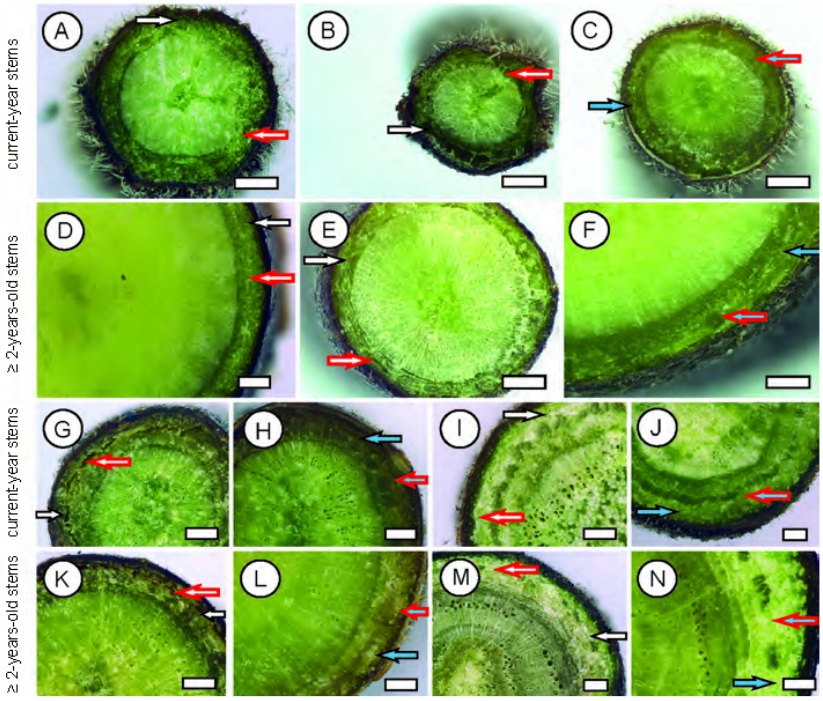

Figure 3. Microscopy images of fresh and frozen cross sections of stems. The arrows point at intercellular spaces filled with air (white) or ice (blue). Red arrows indicate sites that are enlarged in Figure 4. – A: fresh BNYS. – B: fresh BNYW. – C: frozen BNYW. – D: fresh BNOS. – E: fresh BNOW. – F: frozen BNOW. – G: fresh BAYW. – H: frozen BAYW. – I: fresh CSYW. – J: frozen CSYW. – K: fresh BAOW. – L: frozen BAOW. – M: fresh CSOW. – N: frozen CSOW. – Scale bars = 250 µm.

(Fig. 3C, F; 4C, F). For comparison a naturally acclimated potted plant showing the same wide intercellular spaces within the current-year stems was analyzed to exclude freezer depending damage.

Betula albosinensis

Ice nucleation activity

For acclimated younger stems, freezing of the samples started at -6 °C (Fig. 1, Fig. 2). Further freezing then proceeded more rapidly, with a peak at -9 °C, with decreasing rate of freezing events with further decreasing temperature.

Intercellular spaces

Acclimated young stems of *B. albosinensis* already showed visible intercellular spaces within the bark (Fig. 3G, K; 4G, K). These became filled with ice during freezing (Fig. 3H, L; 4H, L).

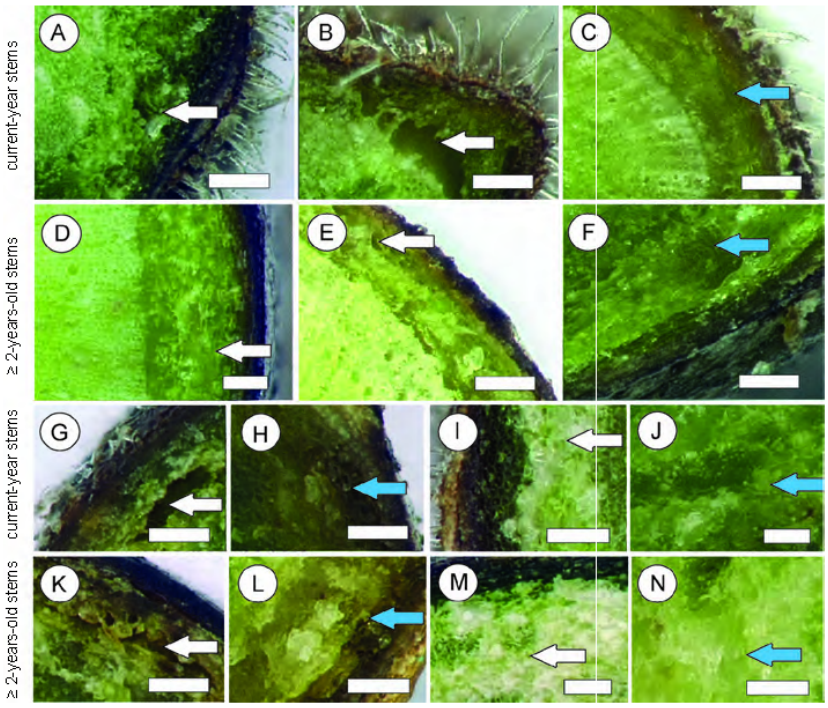

Figure 4. Detailed view of intercellular spaces of the bark (as indicated in Figure 3 by red arrows). Arrows point at intercellular spaces filled with air (white) or ice (blue). – A: fresh BNYS. – B: fresh BNYW. – C: frozen BNYW. – D: fresh BNOS. – E: fresh BNOW. – F: frozen BNOW. – G: fresh BAYW. – H: frozen BAYW. – I: fresh CSYW. – J: frozen CSYW. – K: fresh BAOW. – L: frozen BAOW. – M: fresh CSOW. – N: frozen CSOW. — Scale bars = 100 µm.

Castanea sativa

Ice nucleation activity

With respect to initiation of freezing, CSYW and CSOW were quite similar (Fig. 1). Also, the Median T_{INT} were almost identical for both groups (Table 3). However, there was no pronounced peak for younger stems (Fig. 2). INA results for *C. sativa* were quite low (≥ 2-years-old stems: 9; current-year stems: 7) (Table 3).

Intercellular spaces

Castanea sativa showed quite small and nearly not detectable intercellular spaces within its bark (Fig. 3 I, M; 4 I, M). After freezing, ice crystals formed within these spaces (Fig. 3 J, N; 4 J, N).

Interspecific comparison

INT of *Betula albosinensis* (current-year stems: -8.06 °C ± 0.20) and *C. sativa* (≥ 2-years-old stems: -8.14 °C ± 0.14; current-year stems: -8.43 °C ± 0.25) tend to lower values when compared to acclimated material of *B. nana* (≥ 2-years-old stems: -7.52 °C ± 0.26; current-year stems: -7.56 °C ± 0.19), meaning that freezing was triggered at lower temperatures (Table 3). This was particularly the case for *Castanea sativa* whose current-year stems showed a very wide peak of INT against temperature. Furthermore, *C. sativa* (≥ 2-years-old stems: 9; current-year stems: 7) tended to a lower number of INA, compared to all other taxa (*B. albosinensis*: current-year stems: 12; *B. nana*: ≥ 2-years-old stems: 21; current-year stems: 12).

All species and sample groups had visible intercellular spaces (Fig. 3 and 4), albeit with different dimensions, within the living tissue which filled with ice during freezing (Fig. 3C, F, H, J, L, N; 4C, F, H, J, L, N). The stems of *B. nana* (Fig. 3B, E; 4B, E) showed larger intercellular air spaces than the other two species (*B. albosinensis*, Fig. 3H, L; 4H, L; *C. sativa*, Fig. 3J, N; 4J, N).

To obtain a quantitative comparison, intercellular air spaces in the cortex were measured in fresh sections, for all species. Non-acclimated plants ("summer state") were used, to determine pre-existing differences (with respect to acclimation and freezing). Three sections of three individual twigs current-year, and ≥ 2-years-old, for each species were used. Measurements were performed for cortex sectors which appeared to be not deformed or damaged by sectioning. It should be emphasized that this may lead to an underestimation of the total intercellular air spaces, because regions with wider air spaces may be more prone to damage during cutting, and therefore not be included in the measurements. Thus, all values have to be considered to be approximate.

For *Castanea sativa*, 1.24% ± 0.49 (SD) was obtained, followed by *Betula albosinensis* with 8.22% ± 3.08. *Betula nana* showed the largest air space volume, with 16.15% ± 6.24. The area of the intercellular spaces of the current-year stems amounted for *C. sativa* to 2.04% ± 1.11, while *B. albosinensis* (9.26% ± 2.43) and *B. nana* were quite similar (7.19% ± 2.44).

DISCUSSION

In *Betula nana*, the decreasing number of active ice nuclei from summer to winter as well as the convergence of INT and INA in both BNYW and the BNOW, as a result of acclimation, may represent components of controlled freezing. Some of the INA results reported in Kishimoto *et al.* (2014a) for blueberry (*Vaccinium corymbosum* L. cv. Weymouth and *Vaccinium ashei* Reade cv. Woodard) showed a possible correlation between decrease in INA with freezing damage of the bark in not yet acclimated stems. However, despite the different levels of cold hardiness of the species considered in the present study, ice nucleation activity was in fact very similar for all species in winter. Kishimoto *et al.* (2014a) published similar results for two blueberry species with different cold hardiness levels, also showing adaptation of their INA during the year with the highest INA in November, albeit with narrower distribution of test tube nucleation. The distribution of test tube nucleation (Fig. 2) for *B. nana* obtained in the present study slightly shifted to a higher temperature while the temperature span did not change. Compared with *Betula albosinensis* and *Castanea sativa* the temperature span was quite similar.

The results for INT and INA of the various considered species are similar to those of Kishimoto *et al.* (2014a, b). Also, the INT obtained for *C. sativa* is close to the results obtained by Neuner *et al.* (2010) based on IDTA. The smaller water volume used in the present study may have influenced the results slightly, because, according to the volume effect, the smaller the amount of water, the higher the probability and level of supercooling. The distribution of freezing temperature may then be shifted towards lower temperature values (Kishimoto *et al.* 2014a). This volume effect would explain the moderate difference between the results obtained by Neuner *et al.* (2010) for *C. sativa* based on IDTA and our results. Neuner *et al.* (2010) cooled down twigs (about 3 cm long and 1.41 cm wide) in a freezing chamber (-24 °C h^{-1}) which resulted in INTs of -2.8 to -7.4 °C from August to April. The somewhat higher values for INT obtained by Neuner *et al.* (2010) for *C. sativa* might therefore be closer to the natural value. Additionally, in the case of *B. nana*, the potted individual was younger than the plants from Wilhelma and Hohenheim, which could have influenced the results of the INA slightly (Kishimoto *et al.* 2014a). Despite these various influences, the results found in the present study indicate the magnitude of freezing temperature for the species considered.

Early initiation of ice by INA may avoid excessive supercooling which can lead to damage by internal ice formation (Kishimoto *et al.* 2014b). In blueberry stems, intrinsic INA is located in bark tissue, and therefore probably promoting the formation of extracellular ice within this tissue (Kishimoto *et al.* 2014b). In the present study, ice bodies were observed in the intercellular spaces of the bark of the considered species (Pearce 2001; Kishimoto *et al.* 2014b; Eurich *et al.* 2016). All acclimated twigs, yet unfrozen, showed larger intercellular spaces than during the summer. This may represent an adaptation to the cold period, caused by a certain degree of dehydration and therefore volume loss of the bark cells. In fact, dehydration is a widely observed component of acclimation (Welling 2003). The *Betula* species showed larger intercellular spaces in

the bark than *C. sativa*, which may represent an adaptation to longer freezing periods and/or lower temperatures. As described above, freezing will occur firstly in extracellular water, due to its low solute content. After its formation, extracellular ice acts as a dehydrating agent, because its water potential decreases about -1.2 MPa for each degree decrease in temperature below zero (Rajashekar & Burke 1982). During an extended period of severe frost, extracellular ice bodies will therefore grow by attracting water from surrounding tissues, making availability of sufficient deposition space mandatory.

In fact, particularly large intercellular spaces could be found in the bark of *B. nana* which seem to grow during the first winter. Acclimated *B. nana* plants survived all freeze thaw cycles showing a healthy appearance, indicating that the large intercellular air spaces did not represent freezing damage. Thus, the intercellular space volume in the bark of *B. nana* may represent an adaptation to the winter conditions of the natural habitat. The results of this study indicate that the observed intercellular spaces for extracellular ice formation are mainly located in the cortex parenchyma. However, the considered material consisted mostly of twigs of about 2 years, or somewhat younger or older. Extracellular ice deposits may possibly also develop at other sites of the bark. Accumulation of ice is therefore another function requiring extended intercellular air spaces, besides aeration paths in species from waterlogged habitats (Angyalossy *et al.* 2016).

CONCLUSIONS

Despite differences in frost hardiness, INT of *Betula nana*, *Betula albosinensis* and *Castanea sativa* were within the typical range reported for woody plants. However, *B. nana* tended towards higher values, particularly in the acclimated state which can be interpreted as ensuring controlled freezing during colder temperatures. The two *Betula* species, especially *B. nana*, showed larger intercellular spaces than *C. sativa*, probably to provide sufficient space for external ice buildup within the bark.

ACKNOWLEDGEMENTS

This work has been funded by the German Research Foundation (DFG) as part of the Transregional Collaborative Research Centre (SFB/Transregio) 141 'Biological Design and Integrative Structures'/ A01. The authors would like to thank Dr. Björn Schäfer (Wilhelma, Stuttgart, Germany), Günter Koch and Dr. Robert Gliniars (Hohenheimer Gardens, Stuttgart, Germany) for providing fresh samples. We thank the editor and two anonomyous reviewers for their constructive comments which improved the manuscript.

REFERENCES

Améglio T, Cochard H, Ewers FW. 2001. Stem diameter variations and cold hardiness in walnut trees. J. Experim. Bot. 52 (No. 364): 2135–2142.

Angyalossy V, Pace MR, Evert RF, Marcati CR, Oskolski AA, Terrazas T, Kotina E, Lens F, Mazzoni-Viveiros SC, Angeles G, Machado SR, Crivellaro A, Rao KS, Junikka L, Nikolaeva N, Baas P. 2016. IAWA List of Microscopic Bark Features. IAWA Journal 37 (4): 517–615.

Coombes AJ. 2012. Blätter und ihre Bäume: Haupt, Berne.

de Groot WJ, Thomas PA, Wein RW. 1997. *Betula nana* L. and *Betula glandulosa* Michx. J. Ecol. 85: 241–264.

Eurich L, Schott R, Wagner A, Roth-Nebelsick A, Ehlers W. 2016. Fundamentals of heat and mass transport in frost-resistant plant tissues. In: Knippers J, Nickel KG, Speck T (eds.), Biomimetic research for architecture and building construction. Biological design and integrative structures. Bd. 8. Springer Biologically-Inspired Systems 9: 97–108. Springer, Berlin.

Kishimoto T, Sekozawa Y, Yamazaki H, Murakawa H, Kuchitsu K, Ishikawa M. 2014a. Seasonal changes in ice nucleation activity in blueberry stems and effects of cold treatments in vitro. Environm. Experim. Bot. 106: 13–23.

Kishimoto T, Yamazaki H, Saruwatari A, Murakawa H, Sekozawa Y, Kuchitsu K *et al.* 2014b. High ice nucleation activity located in blueberry stem bark is linked to primary freeze initiation and adaptive freezing behaviour of the bark. AoB Plants 6. DOI: 10.1093/aobpla/plu044.

Mazur P. 1969. Freezing injury in plants. Annl. Rev. Plant Physiol. 20: 419–448.

McCully ME, Canny MJ, Huang CX. 2004. The management of extracellular ice by petioles of frost-resistant herbaceous plants. Ann. Bot. 94 (5): 665–674.

Neuner G, Xu B, Hacker J. 2010. Velocity and pattern of ice propagation and deep supercooling in woody stems of *Castanea sativa*, *Morus nigra* and *Quercus robur* measured by IDTA. Tree Physiol. 30 (8): 1037–1045.

Pearce R. 2001. Plant freezing and damage. Ann. Bot. 87 (4): 417–424.

Prillieux M (ed.). 1869. Effet de la gelée sur les plantes. Formation de glaçons dans les tissus des plantes. Bull. Soc. Bot. France 16 (4): 140–152.

Rajashekar CB, Burke MJ. 1982. Plant cold hardiness and freezing stress. In: Li PH, Sakai A (eds.), Mechanisms and crop implications. Vol. 1. Academic Press, New York. pp. 395–416.

Roden JS, Canny MJ, Huang CX, Ball MC. 2009. Frist tolerance and ice formation in *Pinus radiata* needles: ice management by the endodermis and transfusion tissue. Funct. Plant Biol. 36: 180–189.

Vali G.1995. Principles of ice nucleation. In: Lee R, Warren GJ, Gusta LV (eds.): Biological ice nucleation and its applications. APS Press: 1–28.

Welling A. 2003. Overwintering in wood plants: involvement of ABA and dehydrins. Academic Dissertation. Institute of Biotechnology and Department of Biosciences, Division of Genetics, Faculty of Science, University of Helsinki, Finland, Helsinki.

Submitted manuscript 1: A model for extracellular freezing based on observations on *Equisetum hyemale*

Konrad, Wilfried; **Schott, Rena;** Roth-Nebelsick, Anita (**submitted**) A model for extracellular freezing based on observations on *Equisetum hyemale*

A model for extracellular freezing based on observations on *Equisetum hyemale*

Wilfried Konrad[a,b], Rena Schott[c], Anita Roth-Nebelsick[c]

[a]*Department of Geosciences, University of Tübingen, Hölderlinstrasse 12, D-72074 Tübingen, Germany*
[b]*Institute of Botany, Technical University of Dresden, Zellescher Weg 20b, D-01062 Dresden, Germany*
[c]*State Museum of Natural History Stuttgart, Rosenstein 1, D-70191 Stuttgart, Germany*

Abstract In frost hardy plants, the lethal intracellular formation of ice crystals has to be prevented during frost periods. Besides the ability for supercooling and pre-frost dehydration of tissues, extracellular ice formation is another strategy to control ice development in tissues. During extracellular ice formation, partially large ice bodies accumulate in intercellular spaces, often at preferred sites which can also be expandable. In this contribution, the physico-chemical processes underlying the water movements towards the sites of extracellular ice formation are studied theoretically, based on observations on the frost hardy horsetail species *Equisetum hyemale*, with the overall aim to obtain a better understanding of the physical processes involved in extracellular ice formation. In *E. hyemale*, ice accumulates in the extensive internal canal system. The study focuses on the processes which are triggered in the cellular osmotic-mechanic system by falling, and especially subzero temperatures. It can be shown that when the temperature falls, 1) water flow out of cells is actuated and 2) "stiff-walled" cells lose less water than "soft-walled" cells. Furthermore, 3) cell water loss increases with increasing (= less negative) turgor loss point. These processes are not related to any specific activities of the cell but are solely a consequence of the structure of the cellular osmotic system. On this basis, a directed water flow can be initiated triggered by subzero temperatures. The suggested mechanism may be quite common in frost hardy species with extracellular ice formation.

Keywords Ice, freezing avoidance, cell dehydration, frost hardiness, cell water potential, elastic modulus

1. Introduction

Frost hardiness is crucial for plants living in regions with frost occurrence. For plants which maintain their aboveground parts during the winter season, various mechanisms are relevant. One is (deep) supercooling, partially based on the production of anti-freezing proteins. For supercooling, freezing is prevented by avoiding nucleation which keeps the water liquid despite negative Celsius temperatures (Wilson, 2012). Another strategy is to strongly dehydrate the tissue before freezing sets in (Lenné et al., 2010). Also common is the mechanism of extracellular freezing. Here, freezing within a tissue happens, but the living cells are protected from lethal intracellular ice crystal growth and ice forms instead in extracellular spaces. (Neuner, 2014). Buildup of extracellular ice bodies is placed into the category of freezing avoidance which sums up all physical mechanisms which control the formation of ice in the plant (Gusta and Wisniewski, 2012). Ice crystal growth starts at specific sites within the plant in intercellular spaces and the low water potential of ice draws out water from adjacent cells, leading to further intracellular freezing point depression by increasing solute concentration in the cells (Guy, 1990; Mazur, 1969; Lenné et al., 2010; Beck et al., 2007). Extracellular accumulation of ice results in a shrinkage of the protoplast and a freeze cytorrhysis (Lenné et al., 2010) which expands the intercellular spaces as places for ice formation and is only possible in soft and not rigid tissues (Beck et al., 2007).

Analysis of freezing processes within plants began in the middle of the 19th century and since then extracellular ice formation and coupled tissue dehydration mechanism as adaptation to frost could be found in many different plant taxa and tissues (e.g. petioles (McCully et al., 2004; Prillieux, 1869), leaves (Ball et al., 2004; Hacker and Neuner, 2007), stems (Niklas, 1989; Schott et al., 2017), buds (Ishikawa et al., 1997) and woody tissue (Ashworth et al., 1988; Schott and Roth-Nebelsick, 2018; Hacker and Neuner, 2007). A conspicuous feature of extracellular ice formation is that most of the ice accumulates in specific intercellular storage spaces which can also be specifically constructed to allow for expansion during ice buildup (Ball et al., 2004; McCully et al., 2004). Whereas various observations and descriptions of extracellular ice formation and the structure of related tissues exist so far, there is scarce information on the involved processes. In the present study, an analysis is performed of the osmotic and flow processes on cell and tissue level which are triggered by subzero temperatures. The analysis is based on observations on the frost hardy *Equisetum hyemale* var. *robustum* which shows massive accumulation of extracellular ice in its characteristic and spacious shoot internal canal system (Niklas, 1989; Schott et al., 2017).

As typical for all Equisetopsida, *E. hyemale* shows a large central canal which is surrounded by a tissue ring (see cross section, Figure 1). The tissue ring itself contains a row of narrower canals, the vallecular canals, and a second row of small canals, the carinal canals which occupy the spaces of the former protoxylem. Upon freezing, ice forms predominantly in the vallecular canals and the pith cavity (Figure 1) (Niklas, 1989; Schott et al., 2017). The formerly air filled vallecular canals (Figure 1B) expand through the shrinkage of the chlorenchyma cells and fill up with ice (Figure 1C). Freezing and extracellular ice buildup are accompanied by substantial dehydration of living cells. This becomes particularly visible for the pith parenchyma cells which surround the pith cavity (Schott et al., 2017). Two tissues, the two layered endodermis (Spatz and Emanns, 2004) and the hypodermal sterome (Speck et al., 1998) represent effective supporting tissue which prevents the stem from wilting during the freezing process (Schott et al., 2017).

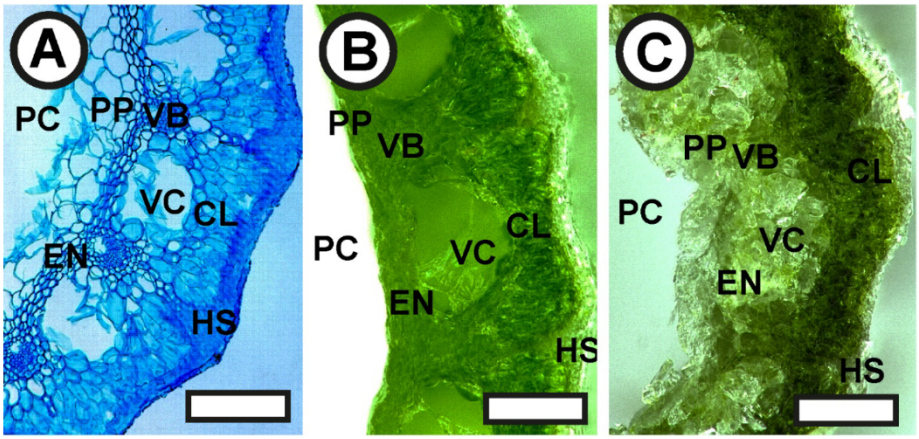

Figure 1: Microscopic images of cross-sections of *E. hyemale* stems. (a) Sample embedded in glycerol gelatin and stained with Astrablue and Safranin. (b) Fresh stem. (c) Frozen stem (18 hours at −15 °C). CL = chlorenchyma; HS = hypodermal sterome; EN = endodermis; PC = pith cavity; PP = parenchymatous pith; VB = vascular bundle; VC = vallecular canal. The carinal canal is a small canal within the VB. Scale bars: 250 µm

This contribution deals with the water movements which allow for ice accumulation and how the physical processes driving this mechanism can be quantified coherently in a mathematical model. From the viewpoint of physico-chemical relationships between the cellular osmotic system and its immediate surroundings, the most important factor is the water potential and its dependence on the aggregate state of water (solid, liquid, vapourous), on cell wall construction (such as elastic properties and thickness), on solute concentration within

the cells, and on temperature. It will be demonstrated that the concentration of extracellular ice at specific sites can be explained via gradients of cell mechanics. The overall motivation for this study is to obtain a better understanding of the physical processes controlling extracellular ice formation as essential factor of freezing avoidance.

2. Basics of cell water relations

2.1. Cell water potential

Within a plant cell, water potential is the sum of the turgor (or hydrostatic) pressure p_{tu} exerted by the cell wall on the cell sap and of the osmotic pressure caused by the presence of solutes within the cell (Nobel (2005), we will focus on situations in which external pressure = atmospheric pressure):

$$\psi_{cell} = p_{tu} + \frac{\mathcal{R}T}{V_m} \log a_w \tag{1}$$

$\mathcal{R} \approx 8.314\,\mathrm{J/mol}$ denotes the gas constant, T (absolute) temperature, a_w is the activity of the cell sap and $V_m \approx 18 \times 10^{-6}\,\mathrm{m^3/mol}$ is the molar volume of (liquid) water.

(i) It is reasonable to assume that change of cell volume is proportional to change in turgor pressure (Philip, 1958; Steudle et al., 1977; Nobel, 2005). Then, turgor pressure p_{tu} can be expressed as $p_{tu} = \epsilon (V - V_0)/V_0$, where ϵ is the volumetric elastic modulus of the cell (not to be confused with bulk modulus (Cosgrove, 1988)), V is the cell volume, and V_0 denotes the cell volume corresponding to $p_{tu} = 0$. Denoting the number of water molecules and of solute molecules in V by N_w and N_s, respectively, and assuming that a water molecule and a molecule of solute occupy roughly the same volume, we may conclude

$$p_{tu} = \epsilon \left[\frac{N_s + N_w - (N_0 + N_s)}{N_0 + N_s} \right] = \epsilon \left[\frac{c_0 - c}{c} \right] \tag{2}$$

N_0 denotes the number of water molecules in the volume V_0. The last expression follows by introducing the mole fractions $c := N_s/(N_w + N_s)$ and $c_0 := N_s/(N_0 + N_s)$. The turgor pressure p_{tu} may be positive (if the turgid case, equivalent to $c < c_0$, is realised), zero ($c = c_0$) or even negative (cytorrysis case, $c > c_0$). Notice that c_0 is closely related to the turgor loss point where p_{tu} vanishes.

The definition of c implies

$$\frac{dc}{c} = -\frac{dV}{V} \tag{3}$$

that is, changes in solute concentration c and cell volume are related, such that the relative increase in c equals the relative decrease in V and vice versa.

In principle, the elastic modulus ϵ can increase with turgor (Cosgrove, 2015) but for our case we assume it to be approximately constant (Philip, 1958; Steudle et al., 1977; Nobel, 2005).

(ii) The activity a_w can be expressed in terms of the mole fraction c, yielding

$$a_w = N_w/(N_s + N_w) = 1 - N_s/(N_s + N_w) = 1 - c \tag{4}$$

Using the results (2) and (4), expression (1) becomes

$$\psi_{cell} = \epsilon \left[\frac{c_0 - c}{c} \right] + \frac{\mathcal{R}T}{V_m} \log(1 - c) \tag{5}$$

Notice that for the turgid case, that is, in the absence of wilting, the first term on the right hand side is positive whereas the logarithm term is generally negative because $N_s < N_w$ implies $0 \leq c < 1$ which implies in turn $\log(1-c) < 0$.

For later usage we note

$$\frac{\partial \psi_{cell}}{\partial T} = \frac{\mathcal{R}}{V_m} \log(1-c) < 0 \tag{6}$$

$$\frac{\partial \psi_{cell}}{\partial c} = -\epsilon \frac{c_0}{c^2} - \frac{\mathcal{R}T}{V_m} \frac{1}{(1-c)} < 0 \tag{7}$$

$$\frac{\partial \psi_{wv}}{\partial T} = \frac{\mathcal{R}}{V_m} \log \varphi < 0 \tag{8}$$

where the inequality signs are due to the fact that all parameters in ψ_{cell} have to be positive in order to make sense and that c is furthermore restricted to the range $0 \ldots 1$.

2.2. Water potential in the intercellular air space

Depending on the physical state of the water in the intercellular air space, ψ_{ias} equals ψ_{liq} (liquid), ψ_{ice} (frozen) or ψ_{wv} (vaporous).

Liquid, solute-free water Water in the intercellular air spaces contains usually only negligible amounts of solutes. Thus, the water potential reads (Nobel, 2005)

$$\psi_{liq} = 0 \tag{9}$$

Ice Below freezing temperature $T_f \approx 273\,\mathrm{K}$, the water layer covering the walls of the intercellular air spaces freezes and the water potential becomes (Guy (1990))

$$\psi_{ice} = \frac{H_{fus}\left(T - T_f\right)}{T_f V_m} \tag{10}$$

where $H_{fus} \approx 6.01\,\mathrm{kJ/mol}$ denotes the fusion enthalpy of ice.

Water vapour The water potential of water vapour is given by (Nobel (2005))

$$\psi_{wv} = \frac{\mathcal{R}T}{V_m} \log\left(\frac{p_{wv}}{p_{sat}}\right) = \frac{\mathcal{R}T}{V_m} \log \varphi \tag{11}$$

p_{wv} and p_{sat} denote the partial pressure and the saturation pressure, respectively, of water vapour. $\varphi := p_{wv}/p_{sat}$ is the relative humidity.

2.3. Freezing point depression

Pure water at atmospheric pressure freezes at the temperature $T = T_f := 273.15\,\mathrm{K}$, that is, at the null point of the Celsius scale. If the water contains solutes of (total) molar fraction $c := N_s/(N_w + N_s)$ the freezing point of this solution is decreased to the value (Atkins, 1997)

$$T = T_f - \frac{\mathcal{R}T_f^2}{H_{fus}} c \tag{12}$$

3. The effect of decreasing temperature on cell water relations

3.1. Basic mechanism of freezing-induced cell dehydration

If the tissue is allowed to equilibrate with respect to the exchange of water molecules between cells and intercellular air spaces the water potentials in these compartments adopt finally the same value. Depending on whether the temperature is above or below freezing point two cases have to be distinguished.

(i) As long as the *Equisetum* sample is above the freezing point T_f, equilibrium of the water potentials means $\psi_{cell}(c,T) = \psi_{wv}(\varphi,T)$ or, employing expressions (5) and (11),

$$\epsilon\left[\frac{c_0 - c}{c}\right] + \frac{\mathcal{R}T}{V_m}\log(1-c) = \frac{\mathcal{R}T}{V_m}\log\varphi \tag{13}$$

Because the cell sap concentrations of living plants are within the range $0 \leq c \leq c_0 < 1$ (and because of $\epsilon > 0$) the first term on the left hand side of this equation is positive. Minor manipulations lead first to $\log\varphi \geq \log(1-c)$ and imply finally the condition

$$\varphi \gtrapprox 1 - c \tag{14}$$

for equilibrium of the water potentials of cells and intercellular air spaces. Since in most plants $c_0 \lessapprox 0.03$ we may conclude $\varphi \gtrapprox 0.97$, that is, almost saturation for the relative humidity in intercellular air spaces.

If equilibrium of the water potentials prevails (meaning that equation (13) is valid) and temperature T is *reduced* both ψ_{cell} and ψ_{wv} increase, according to expressions (6) and (8). Because of (14), the increase in ψ_{cell} is stronger, implying temporarily $\psi_{cell}(c,T) > \psi_{wv}(\varphi,T)$.

Cell water follows this water potential gradient into the intercellular air spaces. Since the semi-permeable membrane which encloses the cell vacuole retains the solute only (pure) water can leave the cell. This loss of water increases the solute concentration c in the cell, leading to a decrease of ψ_{cell} (see (7)) which terminates once a new equilibrium $\psi_{cell}(\tilde{c},\tilde{T}) = \psi_{wv}(\varphi,\tilde{T})$ at lower temperature $\tilde{T} < T$ and higher solute level $\tilde{c} > c$ has been established.

(ii) Below the freezing point T_f, the water potentials of water vapour and ice compete for the water drained from the cell. This can be understood by means of Figure 2 which depicts the water potentials of liquid water, water vapour and ice. For Celsius temperatures $t \gtrapprox -20\,°\mathrm{C}$ and $\varphi \lessapprox 0.8$ the water potential of water vapour is more negative (and therefore attracts liquid water stronger) than ice. Hence water molecules "prefer" the gaseous state instead of forming a solid (i.e. ice). Ice forms only if combinations of temperature and relative humidity lying above the blue line prevail. More precisely, equating $\psi_{wv}(\varphi,T)$ and $\psi_{ice}(T)$ (see (11) and (10)) and solving for T one obtains

$$T_\varphi := \frac{H_{fus}T_f}{H_{fus} - \mathcal{R}T_f\log\varphi} \tag{15}$$

This means, water molecules entering an intercellular air space with relative humidity φ will vapourise if the temperature satisfies $T > T_\varphi$, for $T < T_\varphi$, however, they will form ice. Therefore, equation (13), describing equilibrium of the water potentials, is valid not only above freezing point but down to the temperature $T_\varphi < T_f$.

Below T_φ, equilibrium may develop between cell water potential and ice water potential in the intercellular air space, i.e. $\psi_{cell}(c,T) = \psi_{ice}(T)$. Insertion of expressions (5) and (10) yields

$$\epsilon\left[\frac{c_0 - c}{c}\right] + \frac{\mathcal{R}T}{V_m}\log(1-c) = \frac{H_{fus}\left(T - T_f\right)}{T_f V_m} \tag{16}$$

If this equation is valid (indicating equilibrium between the two water potentials) and temperature T is reduced ψ_{cell} increases (with the same argument as above) and ψ_{ice} decreases. Thus, similarly as above, this disturbance of equilibrium forms a temporary water potential gradient which drives cell water from the cell interior into the intercellular air spaces until a new equilibrium $\psi_{cell}(\tilde{c},\tilde{T}) = \psi_{ice}(\tilde{T})$ is achieved.

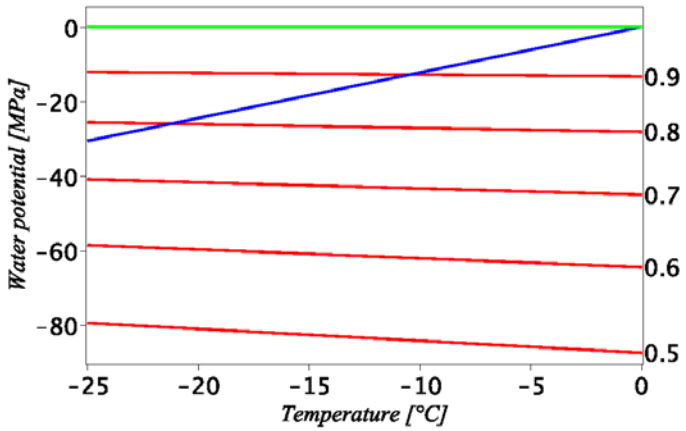

Figure 2: Water potential of liquid water (green line), ice (blue line) and water vapour (family of red lines), according to expressions (9), (10) and (11), as a function of Celsius temperature t. The different red lines represent different relative humidities, from $\varphi = 0.5$ (lowermost line) up to $\varphi = 0.9$ (uppermost line).

Introducing the Celsius temperature $t := T - T_f$ into equations (13), (16) and (15), the equilibrium relations between the solute concentration c within the cell and t simplify slightly to

$$0 = \epsilon\left[\frac{c_0 - c}{c}\right] + \frac{\mathcal{R}\left(t + T_f\right)}{V_m}\log\left(\frac{1-c}{\varphi}\right) \qquad \text{if } t > t_\varphi \qquad (17)$$

$$0 = \epsilon\left[\frac{c_0 - c}{c}\right] + \frac{\mathcal{R}\left(t + T_f\right)}{V_m}\log\left(1-c\right) - \frac{H_{fus}\,t}{T_f V_m} \qquad \text{if } t < t_\varphi \qquad (18)$$

where

$$t_\varphi := \frac{\mathcal{R}T_f^2 \log\varphi}{H_{fus} - \mathcal{R}T_f \log\varphi} \qquad (19)$$

Figure 3 depicts relations (17) and (18) for several values of the volumetric elastic modulus of the cell ϵ, of the relative humidity φ and of the mole fraction c_0 for which the turgor pressure p_{tu} vanishes. The black, dotted line indicates the relation between t and c implied by the freezing point depression, equation (12). Thus, according to Figure 3, cell water of a given solute mole fraction c remains liquid for all temperatures t related to (c, t)-combinations above the black, dotted line. Each of the coloured curves represents a slow, quasistatic cooling process (respective freezing process, once the black, dotted line is crossed), that is, the water potentials are assumed to restore equilibrium between successive infinitesimal temperature reductions during which they are allowed to abandon equilibrium temporarily.

The two families of curves in Figure 3 are distinguished by the value of c_0; red, blue and green curves within each family are related to different values of ϵ. The vanishing of the term proportional to ϵ in expression (18) implies that the members of each family intersect at $c = c_0$, the solute concentration where plasmolysis occurs and turgor pressure vanishes. The intersection points lie very close to the freezing point depression curve (12). Noting that $c_0 \ll 1$, which is usually the case (Bartlett et al., 2012; Larcher, 2003), justifies to approximate the logarithm in (18) as $\log(1 - c_0) \approx -c_0$. Equation (12) yields $t = -(\mathcal{R}T_f^2/H_{fus})\,c_0$, that is, antifreeze protection over larger temperature intervals requires higher values of c_0 (cf. Figure 3).

The slopes of the curves in Figure 3 are very steep for $t > t_\varphi$. This means that solute concentration c is practically unaffected by temperature changes. For $t < t_\varphi$, by contrast, already a moderate temperature decrease

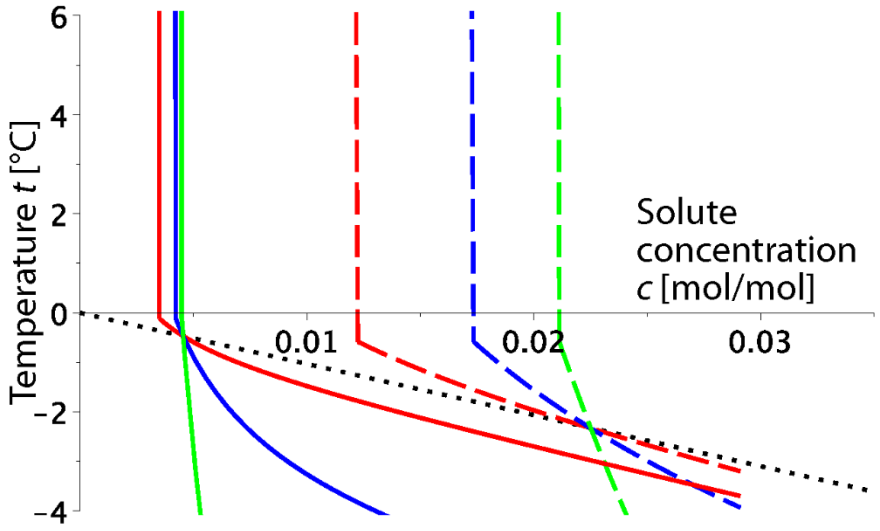

Figure 3: Visualisation of the relation between Celsius temperatures t (ordinate axis) and cell solute concentration c (abscissa) according to equations (17) and (18). Black, dotted line: Freezing point depression (according to equation (12)). If a plant cell contains a solute of mole fraction c cell water remains liquid for all Celsius temperatures t (ordinate axis) between the c-axis (abscissa) and the black, dotted line. Coloured lines (solid or dashed) represent equilibrium of the water potentials in a cell and in intercellular air spaces containing water vapour (for $t > t_\varphi$) or ice (for $t < t_\varphi$). Elastic modulus ϵ of the cell wall is indicated by the colours (red, blue, green) = (1 MPa, 5 MPa, 30 MPa) while the line styles represent the mole fraction c_0 for which the turgor pressure p_{tu} vanishes: (solid, dashed) = (0.0045 mol/mol, 0.0225 mol/mol). The t_φ have been calculated via (19) with $\varphi = 0.998$ (for the curves related to $c_0 = 0.0045$ mol/mol) and $\varphi = 0.994$ (for the curves related to $c_0 = 0.0225$ mol/mol).

causes a considerable increase in c. This is a consequence of equation (17) and (18): solving them for $t(c)$ and differentiating them with respect to c yields

$$\frac{dt}{dc} = \begin{cases} -\frac{\epsilon V_m}{\mathcal{R}} \left[\frac{c\,(c_0 - c) + c_0\,(1-c) \log\left(\frac{\varphi}{1-c}\right)}{c^2\,(1-c)\left[\log\left(\frac{\varphi}{1-c}\right)\right]^2} \right] & \text{if } t > t_\varphi \\ -\frac{\epsilon V_m T_f \left\{c_0\,(1-c)\left[H_{fus} - \mathcal{R}T_f \log(1-c)\right] + \mathcal{R}T_f\,c\,(c_0 - c)\right\} + H_{fus}\mathcal{R}T_f c^2}{c^2\,(1-c)\left[H_{fus} - \mathcal{R}T_f \log(1-c)\right]^2} & \text{if } t < t_\varphi \end{cases} \tag{20}$$

The steep slope of $t(c)$ in the case $t > t_\varphi$ is caused by the logarithm in the denominator of the upper line of this expression which becomes very small (i.e. close to zero) due to condition (14), which implies in turn $\partial T / \partial c \approx \infty$. The expression in the lower line of (20) (the case $t > t_\varphi$) behaves, by contrast, inconspicuously.

3.2. Water flux towards ice

Figure 4 illustrates that many cells in *Equisetum hyemale* have no direct access to large intercellular spaces because they are surrounded by other cells. This raises the question how the water released by these "interior" cells is guided towards an intercellular space where ice formation is non-hazardous for the plant. The following reasoning provides an answer.

(i) If equilibrium prevails at a given temperature above freezing point, cell water potential ψ_{cell} (expression (5)) has the same value in all cells and equals the water potential ψ_{wv} of the water vapour in the intercellular spaces. Because a water potential gradient does not exist, no water flows.

(ii) It is evident from microscopic images of *Equisetum hyemale* tissue (see, for instance, Figures 1 and 4) that cell volume and cell wall thickness vary with cell type. This suggests a related variation of the elasto-mechanical properties of cell walls as represented, for instance, by the volumetric elastic modulus ϵ of the cell wall (Steudle et al., 1977).

Quantitative measurements of Young's modulus (Speck et al., 1998) of the hypodermal sterome layer of the cell wall corroborate this supposition. Young's modulus and the volumetric elastic modulus ϵ are quite differently defined and it makes no sense to compare their absolute values; nonetheless, they are not unrelated but proportional to each other, as Saito et al. (2006) have shown. Therefore, we may conclude from the measurements of Speck et al. (1998) that ϵ varies with cell type. With regard to the cell water potential ψ_{cell} this means that the first term in expression (5) (the turgor term) varies from cell type to cell type (or even from cell to cell). Hence, constant water potential across all cells can only be preserved if the second term in ψ_{cell} compensates the variations of the turgor term. Since temperature is kept constant in an equilibrium situation the solute concentration c of the cell sap has to vary between cell types in order to fulfill this requirement.

In order to examine this situation quantitatively we take the total derivative of ψ_{cell} = const. under the conditions T = const. and c_0 = const. and obtain

$$0 = d\psi_{cell} = -\left[\frac{\epsilon c_0}{c^2} + \frac{\mathcal{R}T}{V_m\,(1-c)}\right] dc + \left[\frac{c_0 - c}{c}\right] d\epsilon \tag{21}$$

This implies

$$\frac{dc}{d\epsilon} = \frac{V_m\,c\,(1-c)\,(c_0 - c)}{\mathcal{R}T\,c^2 + \epsilon V_m\,c_0\,(1-c)} \tag{22}$$

Because for living plants usually $0 < c < c_0 < 1$, the expression on the right hand side which stands for the slope of the function $c(\epsilon)$ is positive.

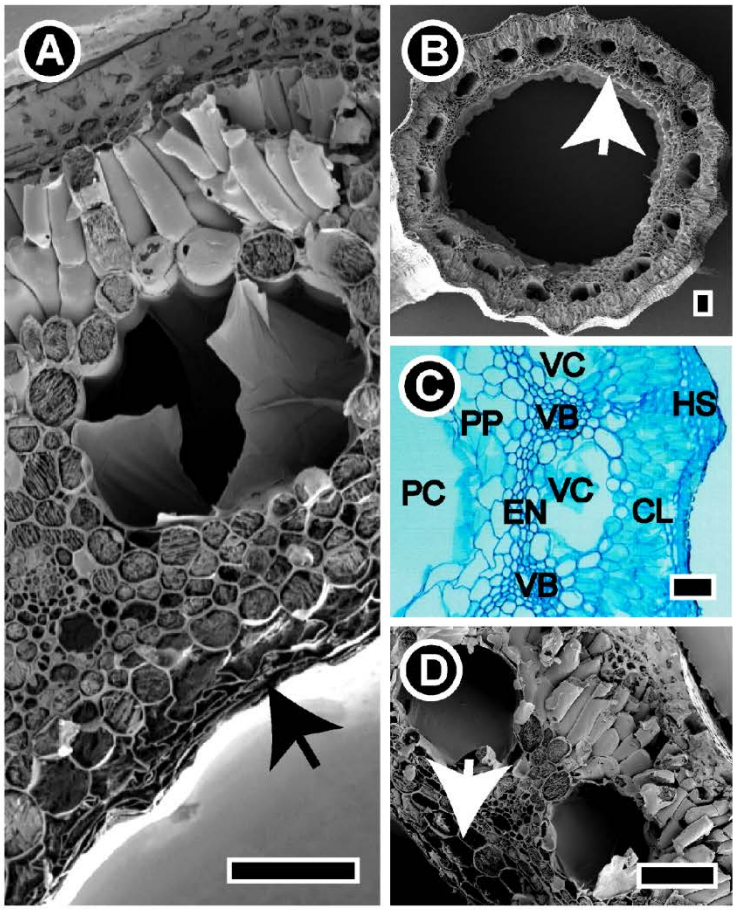

Figure 4: Cross sections of *E. hyemale* stems. (a) CryoSEM image of a detailed cross section of a stem. (b) CryoSEM image of a cross section of a stem, overview. (c) cross-section of an embedded and stained stem (see Figure 1). (d) CryoSEM image of a cross section of a stem, higher magnification. CL = chlorenchym; HS = hypodermal sterome; EN = endodermis; PC = pith cavity; PP = parenchymatous pith; VB = vascular bundle; VC = vallecular canal. Scale bars: 100 µm.

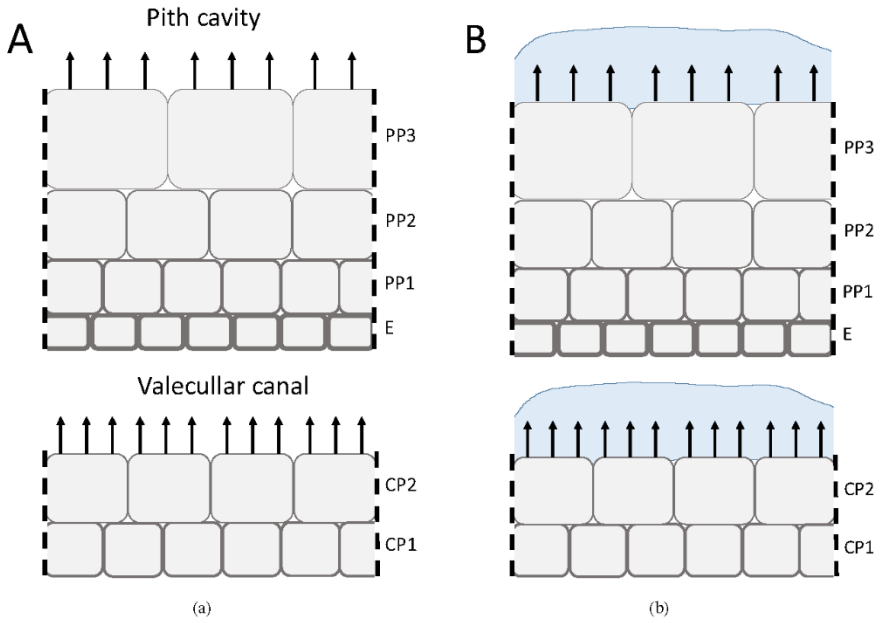

Figure 5: Schematic representation of tissue showing gradients in cell size and cell wall thickness (indicating differences in cell volumetric elastic modulus ϵ). A temperature decrease triggers water flow, shown as arrows.
(a) A temperature drop causes the cell water potential ψ_{cell} to increase. The "softest" and largest cells experience the highest increase; this gradient generates a flow of liquid water with low solute content towards pith cavity and vallecular canal. If the temperature is higher than t_{φ} (defined in (19)) extracellular water vapourizes into pith cavity and vallecular canal.
(b) If temperature falls below the temperature t_{φ} extracellular water freezes whereas intracellular sap remains liquid because of freezing point depression due to increased solute concentration. Water flows out of cells until water potential of cells and extracellular ice is equilibrated.
Cell layers: E: Endodermis (also representing a flow barrier), PP1: pith parenchyma layer 1, PP2: pith parenchyma layer 2, PP3: pith parenchyma layer 3, CP1: cortex parenchyma layer 1, CP2: cortex parenchyma layer 2.

Figure 5 shows a schematic representation of the different cell layers which differ with respect to volume and cell wall thickness. The endodermis cells feature the thickest cell walls, together with a small cell volume. The cell volume of the pith parenchyma cells increases towards the pith cavity (i.e. from layer E towards layer PP3, see Figures 1 and 4). In the same direction, the cell wall appears to become thinner. This is also suggested by the tendency of the innermost (= closest to the pith cavity) cells to collapse (see Figure 4). With respect to the cells on the other side of the endodermis, their volume tends to increase while their cell wall thickness apparently tends to decrease somewhat from CP1 towards CP2 (with the exception of the cells within the vascular bundles, see Figures 1 and 4). These observations suggest that the values of the volumetric elastic moduli in the cell layers are ordered as $\epsilon_E > \epsilon_{PP1} > \epsilon_{PP2} > \epsilon_{PP3}$ and $\epsilon_{CP1} > \epsilon_{CP2}$, that is, in a decreasing order of stiffness from the innermost layer towards the cells adjacent to the pith cavity and the vallecular canal.

Since the right hand side of (22) is positive, this gradient of the volumetric elastic moduli implies a gradient of the solute concentration which points into the same direction, i.e. $c_E > c_{PP1} > c_{PP2} > c_{PP3}$ and $c_{CP1} > c_{CP2}$.

Finally, we may conclude from equation (6) that layers E and CP1 experience the strongest and layers PP3 and CP2 the smallest increase of the water potential if temperature decreases. Since the drained cell water follows the gradient of the water porential it flows from layer E to layer PP3 and from layer CP1 to layer CP2, from stiffer to softer cells.

(iii) As already discussed in section 3.1, a temperature reduction which disturbes equilibrium causes the second term in expression (5) for ψ_{cell} to increase. Expression (6) implies that due to the factor $\log(1-c) < 0$, cells with different solute concentrations $c = 0 \ldots 1$ experience different increases of ψ_{cell} and that higher c-values are related to higher increases of ψ_{cell}.

A temperature decrease generates thus a patchwork of different ψ_{cell}-values, that is, a network of water potential gradients which act as driving forces for water flow between the cells, and eventually into the intercellular spaces that are adequate to accommodate ice in a hazard-free way, such as the pith cavity or the vallecular canals (see Figures 4 and 5).

It is instructive to calculate the cell volume change dV caused by a temperature change dt. Relation (3) yields in a first step

$$\frac{dV}{dt} = -\frac{V}{c}\frac{dc}{dt} \tag{23}$$

and then, upon insertion of (20),

$$\frac{dV}{dt} = \begin{cases} \dfrac{\mathcal{R}V}{\epsilon V_m}\left[\dfrac{c(1-c)\left[\log\left(\frac{\varphi}{1-c}\right)\right]^2}{c(c_0-c)+c_0(1-c)\log\left(\frac{\varphi}{1-c}\right)}\right] & \text{if } t > t_\varphi \\ \dfrac{Vc(1-c)\left[H_{fus}-\mathcal{R}T_f\log(1-c)\right]^2}{\epsilon V_m T_f\left\{c_0(1-c)\left[H_{fus}-\mathcal{R}T_f\log(1-c)\right]+\mathcal{R}T_f c(c_0-c)\right\}+H_{fus}\mathcal{R}T_f c^2} & \text{if } t < t_\varphi \end{cases} \tag{24}$$

Three properties of this result are conspicuous:

— The right hand sides of these expressions are positive, provided $0 < c < c_0 < 1$ (which is reasonable for living plants). That is, if temperature increases cell volume increases likewise, and if temperature decreases, cell volume decreases also.

— The logarithm in the numerator in the case $t > t_\varphi$ is very close to zero if condition (14) applies; thus, falling (i.e. $dt < 0$) temperatures above freezing point generate very little water drain ($dV \lessapprox 0$) from the cells. A similar temperature decrease generates in the case $t < t_\varphi$ a more pronounced drain $dV < 0$.

— The volumetric elastic modulus ϵ appears on the right hand sides only in the denominators. Therefore, if subjected to the same temperature reduction $dt < 0$, stiffer cells (high ϵ values) drain a smaller volume $dV < 0$ of cell water than softer cells (low ϵ values) (cf. Figures 4 and 5).

The relocation mechanism of cell water to intercellular spaces described so far may be enhanced by a gradient in water conductivity, possibly just due to differences in cell wall thickness.

4. Discussion and conclusions

In section 3.2 we suggested a mechanism based on gradients of volumetric elastic cell wall modulus ϵ and related gradients of solute concentration c which generate water potential gradients that cause excess water drained from cells to flow into the desired direction. Moreover, this mechanism is triggered by falling temperatures and initiates at sub-zero temperatures a swift ice buildup at specific sites to which the flow is directed. After first ice bodies have formed, these then draw more water, due to the low water potential of ice, leading to a further accumulation of ice on the expense of cell water. In this way, living cells are dehydrated, their freezing point further depressed, while "innocuous" ice accumulates at specific sites of the intercellular air space.

The suggested mechanism demands that cell layers furthest away from the ice layers (cf. Figure 5) should feature the stiffest (thickest) cell walls (highest ϵ) and the highest solute concentration c. Observations on anatomy and ice distribution in *E. hyemale* stems support these assumptions (Schott et al., 2017). With respect to the central pith cavity, the parenchyma cells surrounding this cavity are large and show thin cell walls. The supposed gradient points from the outermost pith cells towards the pith space. The cells closest to the cavity are larger than those further away. The large cells lining the cavity are also the ones which deform most during freezing and finally collapse entirely, consistent with the model assumption of strongest water loss of the cells featuring the "softest" cell walls.

The vallecular canals are mostly surrounded by quite large and thin-walled parenchyma cells. On the central (towards the pith cavity) side of the valecullar canals, the thin-walled and large parenchyma cells border smaller cells with thicker cell walls, and on the peripheral site, they are surrounded by the chlorenchyma cells. These correspond to palisade parenchyma which usually shows quite stiff cell walls (Larcher, 2003). Also, the most peripheral tissue layers, hypodermal sterome and the epidermis cells feature stiff and thick cell walls (both cell layers were identified by Speck et al. (1998) to contribute substantially to the stiffness of the entire stem). In the (naturally) frozen state, all cell types featuring stiff and thick cell walls show minor deformation and shrinkage, whereas large and thin-walled cells deform strongly or even collapse (Schott et al., 2017). According to the results described in section 3, the low deformation is not only due to the high cell wall stiffness, preventing strong deformation, but also due to the lower water loss featured by these cells (Figure 5). Water loss in consequence of a temperature decrease depends according to equation (24) (illustrated by Figure 3) on the elastic modulus ϵ: soft cells (i.e. low ϵ) lose much more water than stiff cells (high ϵ).

The results are also supported by another observation. Schott et al. (2017) noted (see their Figure 5) that the distribution of air and ice within the pith cavities varies with height: the amount of ice increases from the base to the apex of the stem. This observation can be understood as follows. Speck et al. (1998) found (see their Figure 8) that Young's modulus of the hypodermal sterome is a function of the (relative) height of the stem; it drops from roughly 4 GPa at its base to around 1.5 GPa at its apex. Furthermore, Saito et al. (2006) showed that Young's modulus is proportionally related to the volumetric elastic modulus ϵ. Therefore, we may conclude that ϵ of *E. hyemale* cells show a similar behaviour.

Again, these observations can be explained by the finding that soft cells (i.e. low ϵ) lose more water than stiff cells (high ϵ). Recalling that the drained water contains no solutes (the cell membrane keeps the solute within the cells) and starts therefore to freeze close to the cells that emitted it, it is evident that pith cavities in the apex region where ϵ is small accumulate thicker ice layers than those in the base region where ϵ is high (cf. Figure 4 in Schott et al. (2017)). Additionally, observations on the appearance and disappearance of ice in samples of *E. hyemale* made with the ESEM (Environmental Scanning Electron microscope) support the results of section 3. This is described and discussed in A.

We would like to emphasize that the interrelationships between temperature, water flows, and gradients of cell wall mechanics, solute concentration and water potential which were presented in section 3 are not dependent on specific activities of living cells. All these effects and their interdependencies are, in fact, a consequence of the structures of the plant tissue, or rather, of presumed structural gradients of cell elasticity, conductivity and solute concentration and of thermodynamics. Therefore, the suggested mechanisms may be quite common, i.e. they do not only explain observations on extracellular ice accumulation in *E. hyemale*, but also site-specific ice buildup in tissues of other frost-hardy plant taxa. The crucial quantity for frost resistance, c_0, is — as already noted — closely related to the turgor loss point which has drawn substantial attention due to its probable importance for drought tolerance (BARTLETT ET AL., 2012). The findings presented in this contribution indicate a further substantial role for this quantity in frosthardiness.

A. Experiments with samples of *Equisetum hyemale* in the ESEM

Observation

When samples of *Equisetum hyemale* are placed into an ESEM (Environmental Scanning Electron Microscope) and cooled below freezing point patches of ice crystals begin to form within the intercellular air spaces (e.g. in the pith cavity) whereas the fluid within the cells remains liquid. After a while, the ice crystals vanish. Figure 6 shows the typical development.

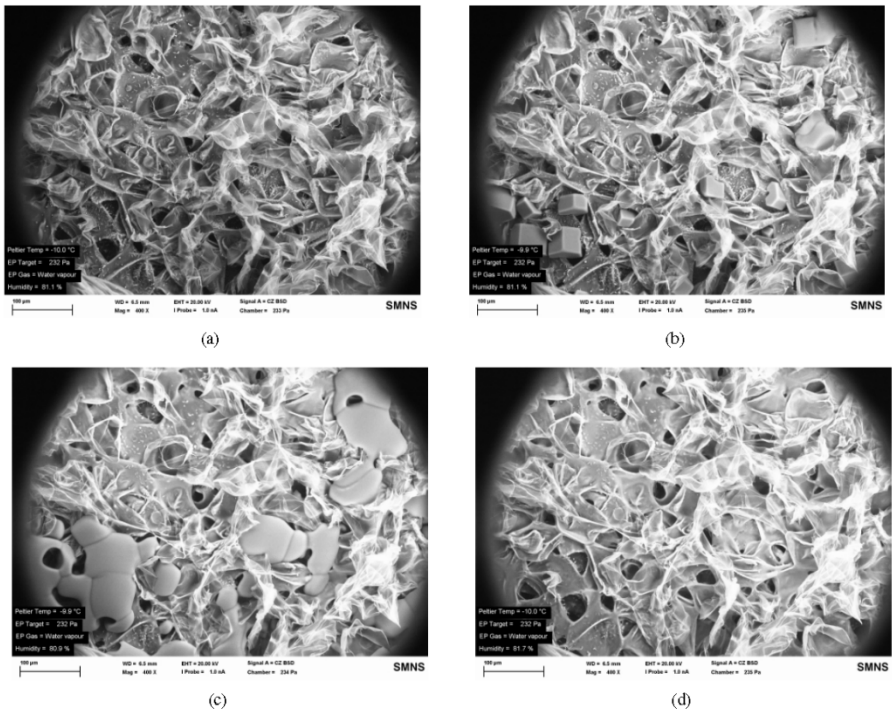

Figure 6: SEM pictures of *Equisetum hyemale*, nodium from below. (a) Begin of cooling, (b) ice crystals emerge, (c) maximum ocurrence of ice crystals, (d) ice crystals have vanished.

Explanation

The emergence and disappearance of the ice crystals depicted in Figure 6 can be explained by the superposition of two mechanisms that operate on different time scales:

(i) When the *Equisetum* sample is placed in the ESEM, Celsius temperature is positive, i.e. no ice crystals are present. As cooling takes place water moves — as explained already in section 3 — from the cell interior into the intercellular spaces. After the temperature has fallen below zero, the solute-free water in the intercellular spaces starts to freeze, producing the ice crystals displayed in Figure 6. The cell sap, however, remains liquid, due to the presence of solute whose concentration depresses the freezing point sufficiently. Once the final temperature $t = -10\,°\mathrm{C}$ is attained, no more water molecules are supplied from the cell interiors to the intercellular spaces.

(ii) Figure 6 has been obtained while a relative humidity $\varphi = 80\,\%$ and a temperature $t = -10\,°\mathrm{C}$ was maintained in the ESEM after the initial cooling period. Under these conditions (cf. expressions (10) and (11) and Figure 2) sublimation exceeds condensation in the intercellular air spaces (such as the pith cavity), that is, the ice layer loses permanently water molecules. Once these losses are no longer replaced from the cell interiors the ice crystals will eventually vanish, which is corroborated by the sequence of images shown in Figure 6.

Hence, we have two antagonistic effects: the one described in (i) generates the ice, the one explained in (ii) removes it. But, (i) is a transient effect — it stops once a constant temperature level is reached — and effect (ii) acts permanently. Clearly, effect (ii) dominates in the long run.

Figure 2 suggests that condensation would dominate sublimation at temperature $t = -10\,°\mathrm{C}$ if the ESEM would maintain a relative humidity of, for instance, $\varphi = 95\,\%$ instead of $\varphi = 80\,\%$. Under such conditions the ice crystals should prevail and even grow.

Patchy emergence of ice crystals ESEM pictures of larger fractions of the pith cavity show that ice crystals do not emerge uniformly on the outside walls of the cells, they rather appear (and disappear) as isolated patches in the intercellular spaces. This can be understood, taking into account (i) the antagonistic effect described above and assuming (ii) that the conductance for liquid water across cell walls varies spatially: above, we tacitly assumed that during the cooling phase cells lose more liquid water per time into the intercellular spaces than is instantly vapourised. If, however, the cell wall conductance for liquid water is low enough, all the liquid water entering the intercellular spaces is vapourised before freezing sets in, that is, in these areas ice crystals do not form.

Acknowledgements

This work has been funded by the German Research Foundation (DFG) as part of the Transregional Collaborative Research Centre (SFB/Transregio) 141 'Biological Design and IntegrativeStructures'/A01.

References

Ashworth, E., Echlin, P., Pearce, R., Hayes, T., 1988. Ice formation and tissue response in apple twigs. Plant, Cell & Environment 11, 703–710.

Atkins, P.W., 1997. Physical Chemistry. W H Freeman & Co.

Ball, M.C., Canny, M.J., Huang, C.X., Heady, R.D., 2004. Structural changes in acclimated and unacclimated leaves during freezing and thawing. Functional Plant Biology 31, 29–40.

Bartlett, M.K., Scoffoni, C., Sack, L., 2012. The determinants of leaf turgor loss point and prediction of drought tolerance of species and biomes: a global meta-analysis. Ecology Letters 15, 393–405.

Beck, E.H., Fettig, S., Knake, C., Hartig, K., Bhattarai, T., 2007. Specific and unspecific responses of plants to cold and drought stress. Journal of Biosciences 32, 501–510.

Cosgrove, D.J., 1988. In defence of the cell volumetric elastic modulus. Plant, Cell and Environment 11, 67–69.

Cosgrove, D.J., 2015. Plant cell wall extensibility: connecting plant cell growth with cell wall structure, mechanics, and the action of wall-modifying enzymes. Journal of Experimental Botany 67, 463–476.

Gusta, L.V., Wisniewski, M., 2012. Understanding plant cold hardiness: an opinion. Physiologia Plantarum 147, 4–14.

Guy, C.L., 1990. Cold acclimation and freezing stress tolerance: role of protein metabolism. Annual review of plant biology 41, 187–223.

Hacker, J., Neuner, G., 2007. Ice propagation in plants visualized at the tissue level by infrared differential thermal analysis (IDTA). Tree physiology 27, 1661–1670.

Ishikawa, M., Price, W.S., Ide, H., Arata, Y., 1997. Visualization of freezing behaviors in leaf and flower buds of full-moon maple by nuclear magnetic resonance microscopy. Plant physiology 115, 1515–1524.

Larcher, W., 2003. Physiological Plant Ecology. Springer Berlin Heidelberg.

Lenné, T., Bryant, G., Hocart, C.H., Huang, C.X., Ball, M.C., 2010. Freeze avoidance: a dehydrating moss gathers no ice. Plant, Cell & Environment 33, 1731–1741.

Mazur, P., 1969. Freezing injury in plants. Annual Review of Plant Physiology 20, 419–448.

McCully, M.E., Canny, M.J., Huang, C.X., 2004. The management of extracellular ice by petioles of frost-resistant herbaceous plants. Annals of Botany 94, 665–674.

Neuner, G., 2014. Frost resistance in alpine woody plants. Frontiers in Plant Science 5, 654.

Niklas, K.J., 1989. Extracellular freezing in *Equisetum hyemale*. American journal of botany 76, 627–631.

Nobel, P.S., 2005. Physicochemical and environmental plant physiology. Academic press.

Philip, J.R., 1958. The Osmotic Cell, Solute Diffusibility, and the Plant Water Economy. Plant Physiology 33, 264.

Prillieux, M., 1869. Effet De La Gelée Sur Les Plantes. Formation De Glaçons Dans Les Tissus Des Plantes. Bulletin de la Société Botanique de France 16, 140–152.

Saito, T., Soga, K., Hoson, T., Terashima, I., 2006. The Bulk Elastic Modulus and the Reversible Properties of Cell Walls in Developing Quercus Leaves. Plant and Cell Physiology 47, 715–725.

Schott, R.T., Roth-Nebelsick, A., 2018. Ice nucleation in stems of trees and shrubs with different frost resistance. IAWA Journal 39, 177–190.

Schott, R.T., Voigt, D., Roth-Nebelsick, A., 2017. Extracellular ice management in the frost hardy horsetail *Equisetum hyemale* L. Flora 234, 207–214.

Spatz, H.C., Emanns, A., 2004. The mechanical role of the endodermis in *Equisetum* plant stems. American Journal of Botany 91, 1936–1938.

Speck, T., Speck, O., Emanns, A., Spatz, H.C., 1998. Biomechanics and functional anatomy of hollow stemmed sphenopsids: III. *Equisetum hyemale*. Botanica acta 111, 366–376.

Steudle, E., Zimmermann, U., Lüttge, U., 1977. Effect of turgor pressure and cell size on the wall elasticity of plant cells. Plant Physiology 59, 285–289.

Wilson, P., 2012. Supercooling of water, in: Supercooling. InTech.

Manuscript in preparation 1: Detailed 2- and 3- dimensional evaluation of the freezing process within important structures of *Equisetum hyemale* L. var. *robustum*

Schott, Rena T. & Roth-Nebelsick, Anita (**in prep**) Detailed 2- and 3- dimensional evaluation of the freezing process within important structures of *Equisetum hyemale* L. var. *robustum*

Detailed 2- and 3- dimensional evaluation of the freezing process within important structures of Equisetum hyemale L. var. robustum

Rena T Schott[a] and Anita Roth-Nebelsick[a]

[a]State Museum of Natural History Stuttgart, Rosenstein 1, 70191 Stuttgart, Germany

Corresponding author: Rena T Schott, State Museum of Natural History Stuttgart, Rosenstein 1, D-70191 Stuttgart, Germany, telephone: +49 (0) 711 8936185, e-mail: rena.schott@smns-bw.de

Abstract:
The focus within this contribution is on the morphological adaptation to freezing events of the spore-bearing plant *Equisetum hyemale* L. var. *robustum*. Naturally acclimated stems were collected and analyzed during summer and winter with different imaging techniques – digital microscopy, scanning electron microscopy, environmental scanning electron microscopy, cryo scanning electron microscopy or via µ-CT -. During a freezing event ice accumulated within the intercellular spaces of the chlorenchyma, within the vallecular canal, at the borders of the pith cavity and on the upper and lower side of the node as well as in the substomatal chamber. Different formed protuberance could be found attached on cells adjacent to some intercellular spaces of the chlorenchyma or to the vallecular canal. The ice growth through the different parts of *E. hyemale* is time depended and more ice accumulates over time. Only well acclimated plants are able to undergo this reversible process completely.

Keywords: intercellular spaces, frost, X-ray micro-CT, cryo-SEM, canals, Pteridophyte

1. Introduction

Frost resistant plants developed many strategies to survive longer freezing events (winter) as well as repeating short term freezing periods (thawing and freezing cycles = mostly day and night). One of these strategies is (deep) supercooling, supported by, for example, antifreeze protein production (AFP), also known as ice restructuring proteins, which prevent the cell content from freezing. AFPs could modify the ice crystal growth (Sharma & Deswal 2014). Another interesting protection mechanism is dehydration by initiating extracellular freezing within the intercellular spaces of living tissues in various plant parts. The extracellular water within the intercellular spaces freezes first because it has a higher freezing point than cell water (reviewed in Jan, Ul-Hussain & Andrabi (2009)). The ice has a low water potential and attracts water from adjacent cells (especially from the vacuoles) which leads to cell shrinkage (cythorrhysis), depending on cell wall stiffness, which may expand the intercellular spaces further (Lenné *et al.* 2010; Jan *et al.* 2009) leads to widened intercellular spaces for the ice crystal growth. Substantial shrinkage is only possible in softer cells. In rigid cells, the stiff cell walls prevent shrinkage and this may result in the formation of (reversible) water vapor bubbles within the vacuoles by cavitation (Beck *et al.* 2007). The entire process is similar to drought stress. Frost resistance has to be build up by acclimation during which various changes take place, such as the lipid composition of the plasma membrane (Yamazakia, Kawamura & Uemura 2014, reviewed in Mazur 1969). In general, frost hardiness is increased or decreased by acclimation and de-acclimation, triggered by changing

environmental conditions (day length and temperature) over time (Beck, Heim & Hansen 2004).

In this study, freezing-induced dehydration processes occurring in the spore-bearing *Equisetum hyemale* L. var. *robustum* are considered. The genus *Equisetum*, also termed horse tail, consists of 15 living species, is distributed nearly worldwide except Australia and New Zealand. The class Equisetopsida can be traced back to the Carboniferous (Sporne 1979, reviewed in Husby 2013). The stem of *E. hyemale*, as in all members of the Equisetopsida, is organized into internodes and microphyll-bearing nodes, with branches being almost absent. *E. hyemale* is a moisture-loving species. (Ludwigs 1911, Speck *et al.* 1998). *Equisetum hyemale* L. var. *robustum* has several interesting properties, for example with respect to biomechanics (Zajączkowska *et al.* 2017) and its mechanical load capacity is quite high, especially due to a hypodermal sterome and a two layered endodermis (Spatz & Emanns 2004; Speck et al. 1998;). The special structure of *E. hyemale* with its large and small intercellular spaces and canals and its dealing with subzero temperatures also makes it an interesting subject for extracellular freezing. For that, the interrelationships between structure and freezing mechanisms within *E. hyemale* must be completely understood.

The freezing process within *Equisetum hyemale* has been previously studied (Niklas 1989; Schott, Voigt & Roth-Nebelsick 2017; Schaffner 1908). Schaffner (1908) was the first to report freezing of water during winter in the canal system of *E. hyemale*. Niklas (1989) found ice within the pith cavity and analyzed it with respect to its accumulation over time. In a previous paper (Schott *et al.* 2017), first details of ice accumulation at the border of the pith cavity, within the vallecular canals and within the intercellular spaces of the chlorenchyma cells were studied. This study attempts to answer open questions of the process of extra cellular ice accumulation within the *E. hyemale* by various investigations using microscopic techniques (digital microscope (DM), scanning electron microscope (SEM), environmental scanning electron microscope (ESEM), cryo scanning electron microscope (cryo-SEM)) and micro CT.

2. Material and Methods

2.1 Plant material

Cultivated, potted plants in the inner courtyard of the State Museum of Natural History Stuttgart, Germany (SMNS; 48.793308° latitude, 9.190340° longitude) supplied from the same breeder (Pflanzmich GmbH, Hamburg, Germany) and from the border of the Rhine near Bad Säckingen, Germany (47.5562231° latitude, 7.9435877° longitude) as well as field-grown plants from the Botanical Garden of the Technical University Dresden, Germany (51.040074° latitude, 13.771024° longitude) were used for this study. The potted plants, consisting of the plants from the breeder and Bad Säckingen, were watered and fertilized when needed. The samples obtained from Dresden were analyzed with the Cryo-Scanning Electron Microscopy (Cryo-SEM), while the potted plants from Stuttgart were used for digital microscopy (DM), Scanning Electron Microscopy (SEM), Environmental Scanning Electron Microscopy (ESEM) and micro-computed tomography (µCT).

Freezing experiments were conducted during cold spells of the winter season, exclusively with acclimated plants. Images for comparison were taken with natural acclimated plants during the hot summer months. For identifying and observing the freezing sites within the plants, either artificially frozen plants or naturally frozen plants were taken. For artificial freezing in Stuttgart, the potted plants were put in a polystyrene box for protection of the roots in a precooled (0 °C) custom-built freezer (Fryka, Esslingen, Germany). The desired temperature of -10 °C or lower was achieved with a

cooling rate of 2 °/h, which matched a natural one (Steffen, Arora & Palta 1989) and gave the plants enough time to initiate ice crystallization. Or the plant tissue was constantly frozen at -15 °C. For artificially freezing in Dresden a laboratory freezer constantly at -20 °C was used.

2.2 Microscopic analysis

2.2.1 Digital microscope (DM)

For thin cross sectioning (50 µm; Leitz 1516 Microtome) samples were embedded in blocks of PEG 2000 after Rüggeberg et al. (2008). For this, fresh cuts of stems were put into a 1:1 mix of PEG 2000 and $H_2O_{dest.}$ for 3 days and stored in a dry cabinet (60°C). Afterwards the samples were transferred into a mixture of PEG 2000 and glycerol (100 g PEG 2000: 2,5 ml glycerol) and stored in the dry cabinet (60°C) for another 24 hours before it was filled into small ceramic blocks and cooled down for hardening in a refrigerator. The stained cross sections (Astrablue and Safranin) were mounted on slides with glycerol gelatin. The images were produced with a Keyence VHX-500F (with VH-Z250R and VH-Z20R, Keyence Corp.)

During summer, samples of thicker cross sections of the internode region were prepared after Schott *et al.* (2017) and analyzed for comparison with the samples of the freezing experiments conducted during winter. For this, naturally acclimated plants, either to summer or winter temperatures, were studied in the unfrozen and frozen state. The artificially frozen samples were collected with a precooled razor and stored during transport and the experiment on precooled copper plates (-10 °C) in a small cooling box (True North®mini-cooler, Heathrow Scientific, LLC, Vernon Hills, Illinois, U.S.). All in all, over 10 shoots were studied, with sections taken at different heights along the plant axis.

2.2.2 SEM/ESEM

For the SEM, sample preparation was performed after (Talbot & White 2013). Freshly cut samples were transferred into pure Methanol for 10 minutes. Afterwards they were put in pure Ethanol for 30 minutes. This step was repeated. This method largely maintains the native structure and avoids artificial deformation to a large degree. The dehydrated samples were critical point dried (Leica EM CPD300; Leica Microsystems GmbH, Wetzlar, Germany) before mounting on adhesive conducting tape on a stub. The prepared stubs were sputtered with gold before the examination in the SEM (ZeissEVO LS 15; Carl Zeiss Microscopy GmbH, Jena, Germany).

The ESEM experiments were conducted with the same equipment. First the pressure was set at ~ 500 Pa, the precooled peltier temp was set at 1 °C and the Humidity varied between ~75 - 85 % or ~95 %. For other, longer freezing experiments with the ESEM the chamber was precooled at 0 °C. After the sample was mounted, it was cooled down to -10 °C with a humidity around 80 % and a pressure of around 234 Pa. Pictures were taken for a pressure of ~500 Pa and with different temperatures.

Various ice crystals and their development were detected and observed, and used to support identification of ice (Supp.1).

2.2.3 CryoSEM

During summer whole stems were cut, sealed with modelling clay and transported in a closed plastic bag with a wetted paper towel. The stems were analyzed as fast as possible. Part of the stems were mounted on the stubs with Tissue-Tek, O.C.T. (Sakura Finetek Europe B.V., Alphen aanden Rijn, Netherlands). The sample holder was shock-

frozen with liquid nitrogen before the samples was transferred in the precooled (-140 °C) slushing-chamber EMITECH K250X cryo-preparation unit (Quorum TechnologiesLtd., Ashford, Kent, United Kingdom). The transversely or longitudinally freeze-fractured samples were sputter-coated with a ca. 6 mm thick platinum layer. Nearly all samples were not etched for 30 min at -70 °C before sputtering. Carefully and fast the samples were moved to the cryo-SEM SUPRA 40VP-31-79 (Carl Zeiss SMT Ltd.,Oberkochen, Germany) and analyzed at 5 kV accelerating voltage and a temperature around -100 °C.

2.2.4 X-ray micro-CT

A fresh sample was taken from a potted plant, sealed with nail polish and put into plastic tubes containing a drop of water, which was tightly sealed, directly before scanning with a Skyscan 1272; Bruker. The scans with a resolution of 1344x896 and an image pixel size of 8 µm were reconstructed with NRecon. The obtained scan was analyzed with Avizo 9.4.

3. Results

3.1 In general

Fig. 1 shows an embedded and stained cross section of an *E. hyemale* stem, revealing the essential morphological structure. The various peripheral tissues comprise epidermis, stomata and substomatal chambers (both encircled in black), hypodermal sterome and chlorenchyma. To the center of the axis, vallecular canals, parenchyma, endodermis, pith parenchyma and pith cavity are visible. The hypodermal sterome as well as the endodermis consist of stiffer and smaller cells (Fig. 1A, B). Over time the freezing process, starting on the outside and triggering the ice crystal growth within the different intercellular spaces and canals, the ice accumulates more within these compartments over time. The frozen cross section in supplement 2 shows the development of the freezing process from the left to the right side after ice grew within the intercellular spaces of the chlorenchyma cells, within the vallecular canals, at the border of the pith cavity and on top of the node. The freezing within the *E. hyemale* stems occurred mainly at these three different sites.

During the sample preparation the cut cryoSEM images revealed the typical structure in the extracellular ice of separation of water and solute content (Fig. 2G) (Schott *et al.* 2017) or the cut during fractioning leads to the special freezing patterns of vacuole and the other cell content visible in the cryo-SEM while the ice in the intercellular spaces show a structure similar to flaky pastry.

3.1.1 Chlorenchyma and stomata

The chlorenchyma of *E. hyemale* stems consists of two or more layers of bigger, overlapping and mostly oval cells with a thinner cell wall (Fig. 1A), higher water content and surrounded by intercellular spaces (Fig. 3, 4B, C, 5, Supp. 3A). The stomatal apparatus consists of guard cells, sub-stomatal chamber and antechamber (Supp. 4A). The rough surface of the antechamber (Fig. 6A, Supp. 4B) which is probably covered by water repellent waxes was also recognized between the contact zones of the guard cells following a little further inside the sub-stomatal chamber the waxes decrease in numbers and density (Fig. 2C, 6B - D).

The intercellular spaces of the elongated and thin walled chlorenchyma cells are partly or completely filled with ice during freezing events. The water loss from the adjacent cells expands the intercellular spaces due to cell shrinkage (Fig. 7, Supp. 4 A-C, E). The sub-

stomatal chamber (Fig. 6E) is filled with ice during a freezing event, while the antechamber and the space between the guard cell remains ice free (Fig. 1C, 2G, H, 6F, G). Ice can be found as small lines between the chlorenchyma cells and the cells of the sub-stomatal chamber (Fig. 2E, F).

Protuberances in general in *E. hyemale* showing different shapes from long and filaments to scala, to strands and to warts (Fig. 8) exist for example between many chlorenchyma cells (Fig. 2D, 8F) or on the cells within small intercellular spaces (Fig. 8E). Before breaking into the vallecular canals (Fig. 3B, D, 4A, B, 5D) most protuberances with different forms and sizes (Fig. 3B, 4A, B, 8A – C) seems to start growing under the membranes. Next to protuberances water droplets could even be detected within many sub-stomatal chambers (Fig. 2A – F, 6D) and also on some protuberances (Fig. 8C, D, 9E, F).

3.1.2 Vallecular canal

During the fresh and unfrozen state the vallecular canals have a nearly circular form, but are sometimes also slightly oval (Fig. 1B, 3). Some parts of vallecular canals can have a nearly smooth surface without or with few perforations (Fig. 4D, 5A, Supp. 4C, D). Within the vallecular canals, different structures can be found. The most frequent ones are the nearly diagonal sheets or membranes which are sometimes covered with small water droplets (Fig. 9 C, D) and which partly divide the canal in different compartments (Fig. 3A, C, D, 4B – D, 5). These membranes can also cover a part of the border of the vallecular canals (Fig. 5, Supp. 4E) and sometimes water could be found between the sheets and the chlorenchyma cells (Fig. 9A, G).

While the vallecular canals do have a more circular cross section during the fresh state, they are deformed in frozen state (Fig. 1, Supp. 2, Supp. 3D, Supp. 4F). During the freezing process water and solute content separate, which leaves the typical structure on the surface of the cryoSEM images (Supp. 3A, D).

Bigger protuberance grew only within the vallecular canals (Fig. 1A, 3B, 4, 5D, 8B) sometimes under or close to the diagonal sheets partly dividing or being covered by membranes covering the borders of the vallecular canals (Fig. 3B, 4, 5). While smaller protuberances could also be recognized within the vallecular canals next to the within the sub-stomatal chamber and within bigger and smaller intercellular spaces of the chlorenchyma.

3.1.3 Pith cavity and the parenchymatous pith

The pith cavity is surrounded by the parenchymatous pith and separated by the nodes which are curved upwards and show a rough surface (Fig. 10). The parenchymatous pith is surrounded by the smaller and stiffer endodermis cells and consists of a few rows of big cells (Fig. 1A, B). Before their first winter those cells are fluffy and afterwards more or completely compressed (Fig. 1A, B, 3). This results in a pith cavity cover similar to a stack of paper sheets (Fig. 10 A – C, Supp. 4F) which is shown in the fresh state by ESEM images in supplement 4.

The pith cavity fills with ice over some time. The ice crystals start growing at the borders and at the nodes (Fig. 1C, Supp. 2, Supp. 4F) till the canal is complete filled (Supp. 3A). During frost, the forming ice results in the above mentioned compression of the parenchymatous pith cells (Fig. 1C, Supp. 2, 4). Some of little rest of water found during summer within a few stretched or compressed cells of the parenchymatous piths (Fig. 9 A, H) stayed within the cells of the parenchymatous pith in frozen state (Supp. 3B,C, E) and it remains after thawing (Fig. 9B).

3.2 3D structure

The segmentation of a µCT scan (Fig. 11) of *E. hyemale* stem part revealed the distribution of the intercellular spaces of the chlorenchyma existing along the entire length of the scan even around the node. The vallecular canals and pith cavity are bordered by the nodes. The porosity of this structure becomes visible. The hypodermal sterome a structure for stability can be seen between the clusters of segmented intercellular spaces as part of the surface reconstruction. Due to the sealing with nail polish, stomata became filled and are thus not visible.

3.3 Dynamics of the freezing of parts of an *E. hyemale* stem

The ESEM experiments focused mostly on the analyzation of the pith cavity, the top and lower part of the nodes and their connection. With respect to the vallecular canals, mostly longitudinal sections were considered. The ice crystal growth within the chlorenchyma proved to be too small and fast to be observed.

Before ice crystallization, the pith cavity started to deform (Fig. 12, Supp. 6). Afterwards, on the longitudinal sections, shadows within the parenchymatous pith could be detected (Fig. 12B, C) before ice crystals grew (Fig. 12C, D). The vallecular canals behaved in a similar way but deformed stronger, probably because they were not stabilized by an endodermis. On top and lower side of the nodes the ice crystals grew between the structures of the node surface till they merged and covered the surface (Fig. 13). A small movement towards the borders of the pith cavity could be detected (Supp. 6). Through raising the temperature the ice vanished and no damage from ice growth were left on the tissue.

During the ESEM experiments different humidities (~80 % and ~95 %) were tested with nearly no differences. The main difference recognized were between the still acclimated and the slowly de-acclimating plants. Especially ice growth on the surface underneath the node changed. The ice crystals occurred between the structures of the rough surface and vanished again after a short time. It seems that the ice growth started earlier on the better acclimated plants. The ice crystals on the nodes moved slowly to the borders of the pith cavity. This movement was stronger in the more de-acclimated plants while the ice crystals covered faster the surface within the more acclimated plants which might hide a stronger movement.

4. Discussion

Ludwigs (1911) started to analyze the *Equisetum hyemale* followed by Niklas (1989) and Schott *et al.* (2017). This study aimed at obtaining further insight into the process of extracellular ice formation and its relationship to structure and cell dehydration. The vallecular canals directly seated next to the cortex and connected with by holes in the membrane between cells (Fig. 3, 5) serve as big storage spaces for the first big ice crystal growth as the tissue cools down from the outside to the inside over time and gets rapidly filled by ice. The thickness of the ice layer within the pith cavity depends on the position along the shoot and internode (Schott *et al.* 2017) which might get influenced by the slight changes in structure (Speck *et al.* 1998). Ice grew within the sub-stomatal chamber but not on the rough surface of the ante chamber which indicates the existence of the probably water repellent waxes (Fig. 2G, 6F, G) (Schott *et al.* 2017). Showing no signs of wilting as many herbaceous plants with higher water content (McCully *et al.* 2004) the hypodermal sterome and the two-layered endodermis keep the upright position during the freezing process (Speck *et al.* 1998; Spatz & Emanns 2004; Schott *et al.* 2017).

The analyzation of DM, SEM and cryo-SEM images (Fig. 1 – 10) revealed additional structural details. The water repellent waxes on the antechamber of a stoma are even between the two contact sides of the guard cells (Fig. 2, 6) which highlights their importance from separating the outer space from the sub-stomatal chamber completely filled with ice. Protuberances of different shape and size are present which were already described by Kisser (1928), but are rarely mentioned today. Protuberances are usually mentioned with tissue expansion and formation of intercellular spaces (Potgieter & van Wyk 1992). Few suggestions of possible functions of protuberances were made but remained - to the authors knowledge - unconclusive. Within *E. hyemale* Potgieter & van Wyk (1992) review protuberances in form of warts exist, but as figure 8 shows more forms can be found and water has been spotted around some protuberances (Fig. 9E, F). They might influence the water/ice layer within the air filled spaces.

Distinguishing ice from tissue (*e.g.* protuberances) was supported by the ESEM which allows for direct observation of ice growth (Supp. 1). By comparing these results with the descriptions made by Voigt *et al.* (2012), who tested small, sprayed water droplets on different surfaces and Jeffree *et al.* (1987) who analyzed “water droplets and ice deposits in leaf intercellular spaces”, ice and tissue could be identified. Within the ESEM experiments (Fig. 12, 13, Supp. 1, 6), effects of the acclimation state became visible, particularly when observing the lower side of the node. The ice occurred later for the less acclimated plants on the lower side of the node and it melted again. This might indicate that the dehydration effect was lower within the less acclimated plants which might not be sufficient during longer freezing periods. On the upper side of the node growing ice crystals were drawn to the borders of the pith cavity until it was covered with ice. Afterwards the ice kept growing on the upper side of the node. The ice development started at all sites - the borders and on the lower and upper side of the node - of the pith cavity. Before ice crystals grew at the borders on the parenchymatous pith moving shadows under the layers of the parenchymatous pith were seen. The shadows allowed a prediction of occurring ice crystals. This is indicates the importance of the paper like layers of parenchymatous pith cells around the pith cavity for the water transport during the dehydration mechanism. The ice might grew faster at the borders since more water from adjacent cells had to be removed at the beginning of the freezing event and over time.

The collapse of pith parenchyma cells at older portions of the stem was already observed by (Schott *et al.* 2017) and was confirmed in the ESEM experiments. A few ice crystals could be spotted within formerly frozen and thawed samples within the CryoSEM (Fig. 9A, B, H, Supp. 3 B, C, E). This leads to the assumption that the cells of the parenchymatous pith are deformable and that their main role during the freezing process is the directing of the cell water to the pith cavity. This means that they might play a bigger role within the regulation of the humidity within the pith cavity.

The water efflux from the protoplast through a semipermeable membrane is described by a chemical potential. With higher solute concentration due to water loss the osmotic potential of the cells increases (Niklas 1992). During dropping temperatures with the corresponding pressure changes specialized surface structures could help during the freezing process. Protuberances and the membranes within and at the borders of the vallecular canals might have a rougher surface and maybe could such structures for improving the water adhesion (Fig. 9C, D, G). Within the node capillary tubes, long tubes with narrow bores which can draw water upwards against the gravity (Niklas 1992) might

also be essential for water transport between internodes and affect extracellular ice formation.

The leaf cells of stressed *G. hirsutum* L. plants (Cutler *et al.* 1977) were smaller in size and thicker cell walled and as Cutler *et al.* (1977) reviewed lesser cell size seem to be an adaptation to moisture stress. The lesser cell size and thicker cell walls of the hypodermal sterome and the endodermis (Fig. 1A) might be responsible for their stable stiffness.

The current study confirmed the former interpretations and provides substantially more information and insight of the extracellular freezing process and its interrelationship with structure. Studies analyzing the structure of plants with a µCT scanner with respect to freezing resistance or the direct impact of frost are for the authors' knowledge scarce. For example Zhao & Takhar (2017) analyzed the impact of freeze-thaw cycles on potatoes.

The focus of this study was on the interesting structural adaptations of *Equisetum hyemale* var. *robustum* to recurring frost events within bigger (vallecular canals and pith cavity) as well as within smaller air filled spaces (intercellular spaces within the chlorenchyma) as part of this porous medium as well as the distribution of the probably water repellent waxes and the protuberances. In the future for being able to use *E. hyemale* as a role model for porous building materials a theoretical model has to be developed. So far – to the authors´ knowledge - mainly pore network models based on artificial materials have been calculated. To presume that we have a high humidity within the intercellular spaces and the canals water drops will occur with dropping temperatures. The border of the pith cavity, the vallecular canals and especially of the nodes and the intercellular spaces of the chlorenchyma have rougher surfaces. Next to the surface the deformation and the ice crystallization needs to be included in this future study.

Acknowledgements:

This work has been funded by the German Research Foundation (DFG) as part of the Transregional Collaborative Research Centre (SFB/Transregio) 141 'Biological Design and Integrative Structures'/A01. The authors would like to thank Dr. Barbara Ditsch (Botanical Garden, Dresden, Germany) for providing fresh samples. Furthermore, we are grateful to Markus Günther, Dr. Dagmar Voigt and Prof. Dr. Christoph Neinhuis (Institute for Botany at the Technical University of Dresden, Germany) for allowing us to use the cryo-SEM, fruitful discussions, and excellent and friendly technical support.

References

Beck E.H., Fettig S., Knake C., Hartig K. & Bhattarai T. (2007) Specific and unspecific responses of plants to cold and drought stress. *Journal of Biosciences* **32,** 501–510.

Beck E.H., Heim R. & Hansen J. (2004) Plant resistance to cold stress: Mechanisms and environmental signals triggerung frost hardening and dehardening. *J. Biosci.,* 449–459.

Cutler J.M., Rains D.W. & Loomis R.S. (1977) The Importance of Cell Size in the Water Relations of Plants. *Physiologia Plantarum* **40,** 255–260.

Husby C. (2013) Biology and Functional Ecology of Equisetum with Emphasis on the Giant Horsetails. *The Botanical Review* **79,** 147–177.

Jan N., Ul-Hussain M. & Andrabi K.I. (2009) Cold resistance in plants. A mystery unresolved. *Electronic Journal of Biotechnology* **12**.

Jeffree C.E., Read N.D., Smith J.A. & Dale J.E. (1987) Water droplets and ice deposits in leaf intercellular spaces: redistribution of water during cryofixation for scanning electron microscopy. *Planta* **172,** 20–37.

Kisser (1928) J. Untersuchungen über das Vorkommen und die Verbreitung von Pektinwarzen. In *Jahrbücher für wissenschaftliche Botanik. - Berlin: Borntraeger*, pp. 206–232.

Lenné T., Bryant G., Hocart C.H., Huang C.X. & Ball M.C. (2010) Freeze avoidance: a dehydrating moss gathers no ice. *Plant, cell & environment* **33,** 1731–1741.

Ludwigs K. (1911) Untersuchungen zur Biologie der Equiseten. *Flora,* 385–440.

Mazur P. (1969) Freezing Injury in Plants. *Annu. Rev. Plant. Physiol.,* 419–448.

McCully M.E., Canny M.J. & Huang C.X. (2004) The management of extracellular ice by petioles of frost-resistant herbaceous plants. *Annals of botany* **94,** 665–674.

Niklas K.J. (1989) Extracellular freezing in Equisetum hyemale. *American Journal of Botany,* 627–631.

Niklas K.J. (1992) Plant biomechanics. An engineering approach to plant form and function. Univ. of Chicago Press, Chicago, Ill.

Potgieter M.J. & van Wyk A.E. (1992) Intercellular pectic protuberance in plants: their strcuture and taxonomic significance. *Bot. Bull. Acad. Sin.,* 295–316.

Rüggeberg M., Speck T., Paris O., Lapierre C., Pollet B., Koch G. & Burgert I. (2008) Stiffness gradients in vascular bundles of the palm Washingtonia robusta. *Proceedings. Biological sciences* **275,** 2221–2229.

Schaffner J.H. (1908) The Air Cavities of Equisetum as Water Reservoirs. *Ohio Nat.,* 393–394.

Schott R.T., Voigt D. & Roth-Nebelsick A. (2017) Extracellular ice management in the frost hardy horsetail Equisetum hyemale L. *Flora* **234,** 207–214.

Sharma B. & Deswal R. (2014) Antifreeze proteins in Plants: an overview with an insight into the detection techniques including nanobiotechnology. *Journal of proteins and proteomics* **5,** 89–107.

Spatz H.-C. & Emanns A. (2004) The mechanical role of the endodermis in Equisetum plant stems. *American Journal of Botany,* 1936–1938.

Speck T., Speck O., Emanns A. & Spatz H.-C. (1998) Biomechanics and Functional Anatomy of Hollow Stemmed Sphenopsids: III. Equisetum hyemale. *Bot. Acta* **111,** 366–376.

Sporne K.R. (1979) The Morphology of pteridophytes. The Structure of Ferns and Allied Plants. Hutchinson & Co (Publishers) Ltd, London.

Steffen K.L., Arora R. & Palta J.P. (1989) Relative Sensitivity of Photosynthesis and Respiration to Freeze-Thaw Stress in Herbaceous Species. Importance of Realistic Freeze-Thaw Protocols. *Plant Physiology,* 1372–1379.

Talbot M.J. & White R.G. (2013) Methanol fixation of plant tissue for Scanning Electron Microscopy improves preservation of tissue morphology and dimensions. *Plant methods* **9,** 36.

Voigt D., Roth-Nebelsick A., Miranda T., Ebner M. & Gorb S. (2012) Visualization of Small Water Droplets on Surfaces with Different Degree of Wettability by Using Cryo-Scanning Electron Microscopy. *Journal of Advanced Microscopy Research* **7,** 64–67.

Yamazakia T., Kawamura Y. & Uemura M. (2014) Extracellular freezing-induced mechanical stress and surface area regulation on the plasma membrane in cold-acclimated plant cells. *Plant Signaling & Behavior* **4,** 231–233.

Zajączkowska U., Kucharski S., Nowak Z. & Grabowska K. (2017) Morphometric and mechanical characteristics of Equisetum hyemale stem enhance its vibration. *Planta* **245,** 835–848.

Zhao Y. & Takhar P.S. (2017) Micro X-ray computed tomography and image analysis of frozen potatoes subjected to freeze-thaw cycles. *LWT - Food Science and Technology* **79,** 278–286.

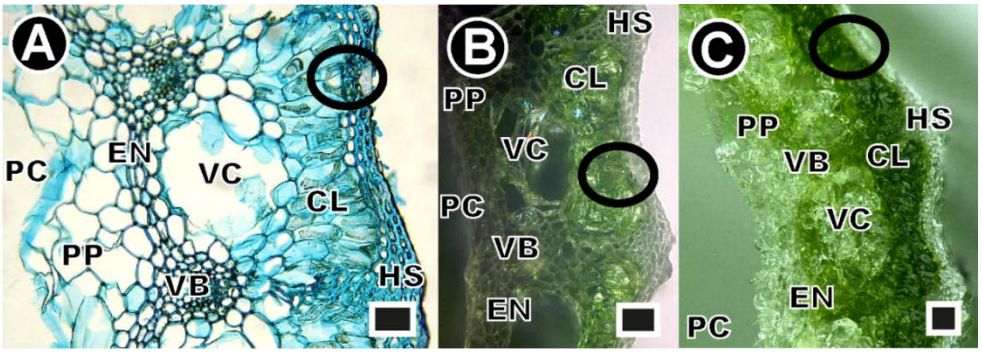

Fig. 1: Detailed parts of cross sections of *Equisetum hyemale* var. *robustum* stems. A: embedded and stained stem. B: fresh stem. C: frozen stem (15 hours at -15 °C). The circles are around a stomata. HS = hypodermal sterome; CL = chlorenchym; VC = vallecular canal; VB = vascular bundle; EN = endodermis; PP = parenchymatous pith; PC = pith cavity. Scale bars: 100 µm

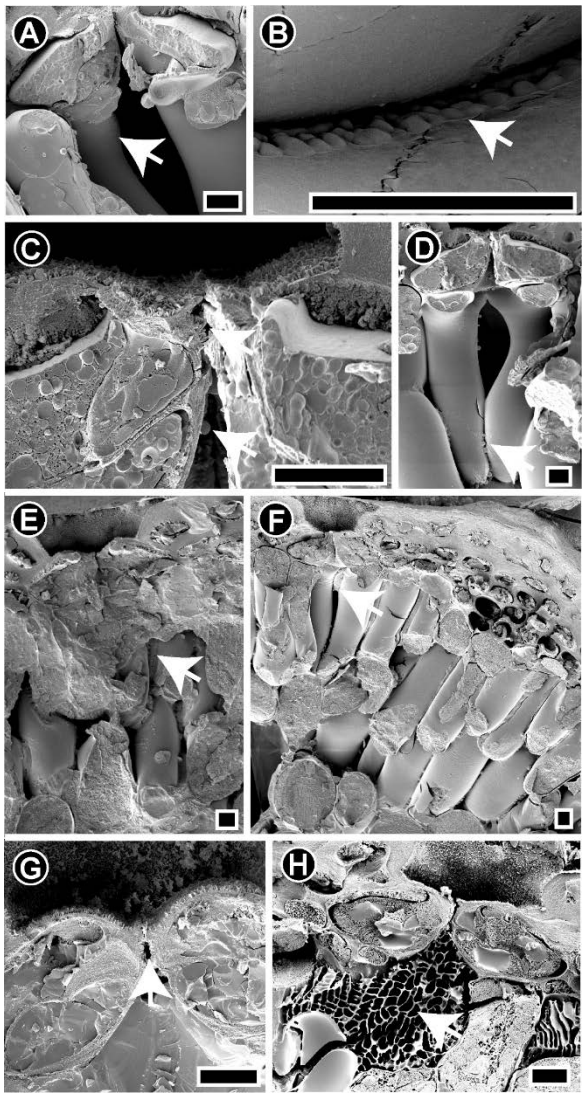

Fig. 2: Cryo SEM images of cross sections of stomata of *Equisetum hyemale* var. *robustum* during summer of older stems (A – D) and during winter of current year stems (E - H). White arrows point at highlights. A – B: water droplet can be found on the cells of the substomatal chamber. C: wax crystals between the two guard cells are revealed. C – D: protuberances can be seen on the cells of the substomatal chamber. E – H: naturally frozen samples (E – G; ice as solid mass) and artificially frozen (H; 24 h at -20 °C; ice as gratings) show an ice filled substomatal chamber and an ice free ante chamber. E – F: ice can be located between the chlorenchyma cells. G - H: no ice can be detected on the wax cystrals between the two guard cells. Scale bars: 10 µm

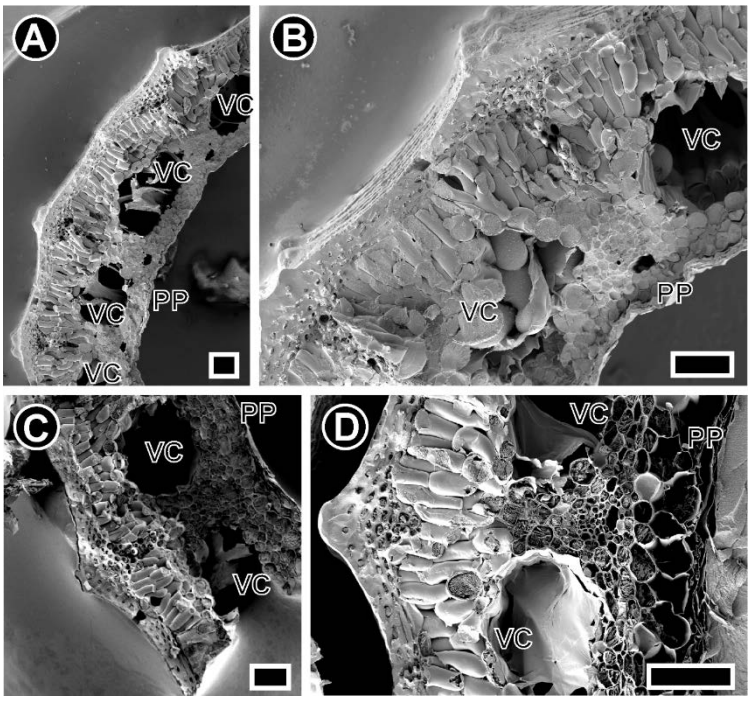

Fig. 3: CryoSEM images of cross sections of older (A, B) and current year (C, D) stems of *Equisetum hyemale* var. *robustum* in summer showing the distribution of the tissue and the intercellular spaces as well as the membranes and the growth within the vallecular canals (VC). The older stems (A, B) show a visible shrinkage in the parenchymatous pith (PP) compared with the current year stems (C, D). . D: is etched. Scale bars: 100 µm

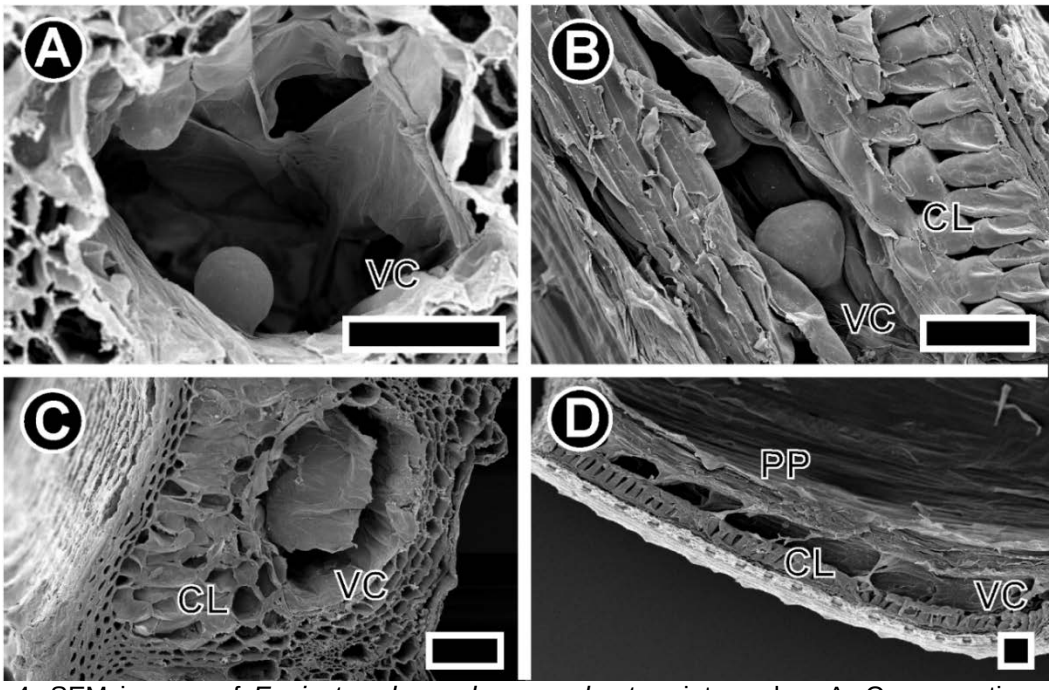

Fig. 4: SEM images of *Equisetum hyemale* var. *robustum* internodes. A: Cross section of a vallecular canal (VC) including bigger growth and membranes. B: Longitudinal section of a vallecular canal (VC) with growth and membranes and showing the intercellular space within the chlorenchyma (CL) with small growth on them. C: cross section of a vallecular canal (VC) showing the dimensions of a membrane and of the intercellular spaces within the chlorenchyma (CL). D: Longitudinal section showing the orientation of membranes within a vallecular canal (VC) and the possible number as well as the structure of the parenchymatous pith (PP) and the chlorenchyma (CL). Scale bars: 100 µm

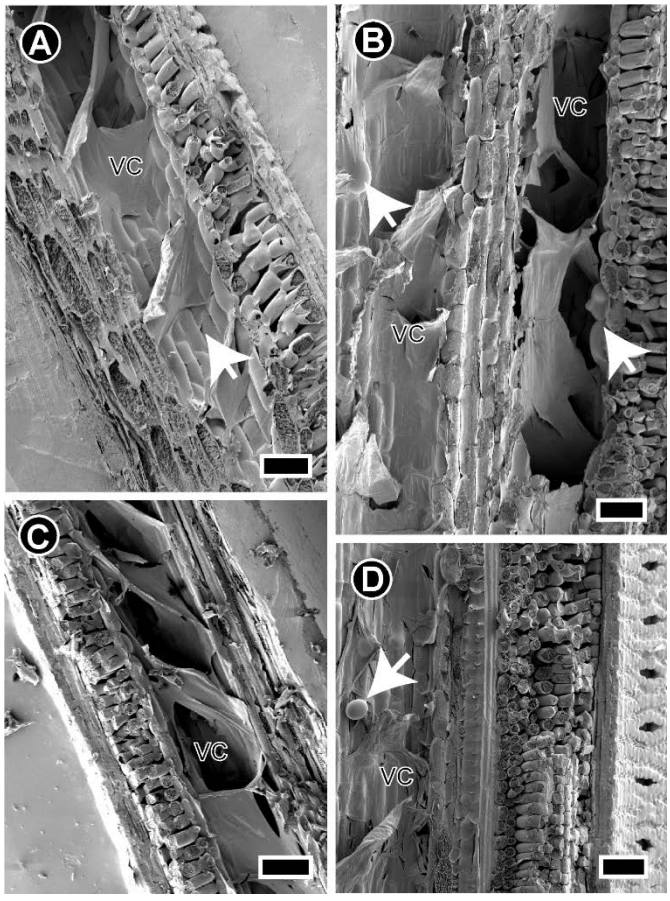

Fig. 5: CryoSEM images of longitudinal sections of older (B, D) and current year (A, C) stems of *Equisetum hyemale* var. *robustum* in summer showing mainly the vallecular canals (VC). A: Holes between cells within the vallecular canals can be spotted and it is showing membrane layers on the cells of the border of the vallecular canal as well as bases of these membranes. B: protrusions can be spotted. B and C: showing nearly complete membranes within the vallecular canals as well as their possible number and orientation. D: protuberances breaking through the membranes of the vallecular canal can be seen. White arrows highlight some important features. Scale bars: 100 µm

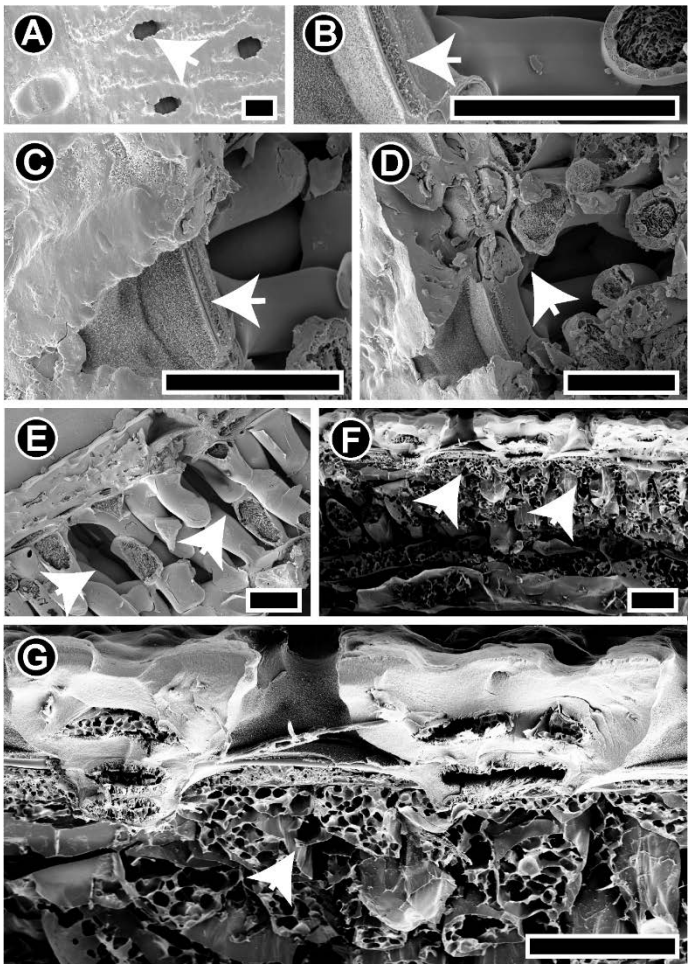

Fig. 6: CryoSEM images of longitudinal sections of stomata of older (A – D) and current year (E-G) *Equisetum hyemale* var. *robustum* stems during summer (A – E) and winter (F, G). A: An overview of the surface and the distribution of stomata is given. B – D: probably water repellent wax crystals on the antechamber on the outside and growing inside the substomatal chamber can be seen. B, D: protuberances are displayed in the substomal chamber. E: the size of a substomal chamber is displayed. F, G: frozen for 29 h at -20 °C are showing the ice crystals as gratings in the substomal chamber and clean and ice free wax crystals on the antechamber. G is an enlargement of F. White arrows point at highlights. Scale bars: 50 µm

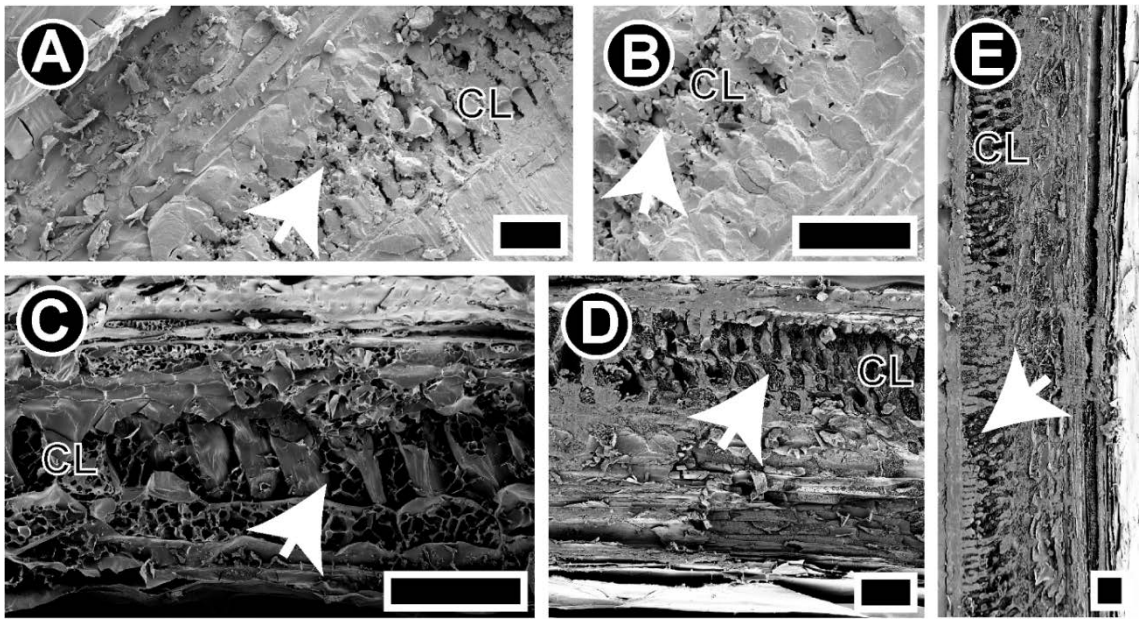

Fig. 7: CryoSEM images of longitudinal sections of older and naturally frozen (A, B) and artificially frozen (29 h at -20 °C), current year (C – E) *Equisetum hyemale* var. *robustum* stems. A and B display the ice especially between the chlorenchyma cells (CL) as solid ice bobbels while the ice has a grating like structure (white arrow). Scale bars: 100 µm

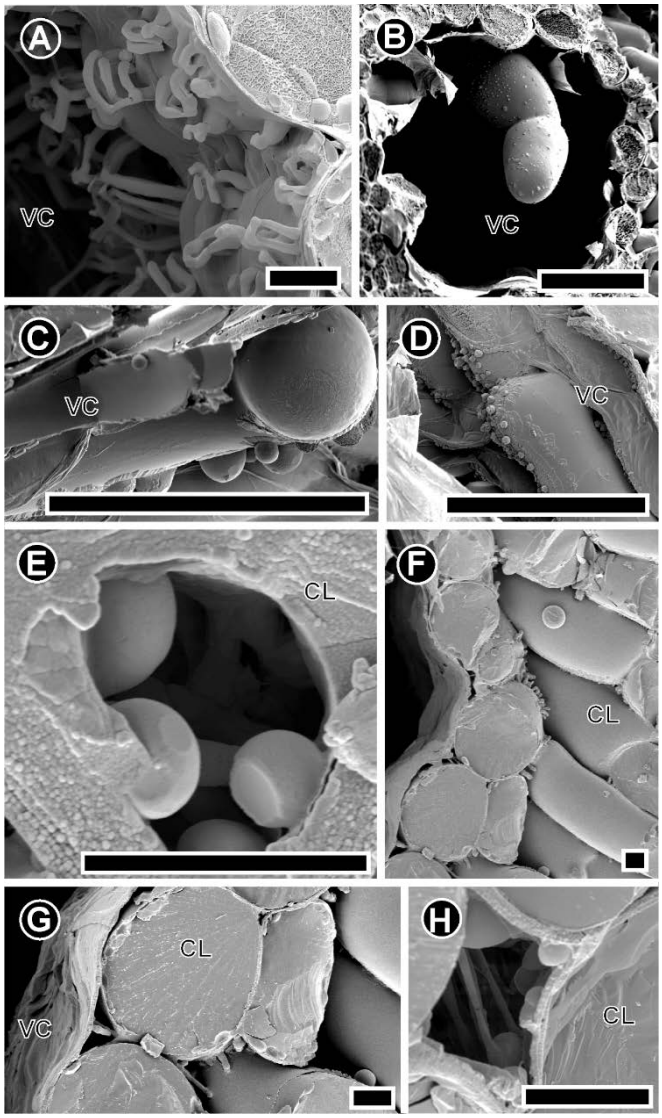

Fig. 8: CryoSEM images of cross (A, B, E, F) and longitudinal sections (C, D) of older (A - D) and current year (E - H) *Equisetum hyemale* var. *robustum* stems during summer showing different protuberances and water droplets. A: showing small protuberances within the vallecular canal (VC). B: displaying big protuberances growing within the vallecular canals (VC). C: Showing bigger protuberances within the vallecular canal (VC) with water around them. D: showing ice crystals within the vallecular canal (VC) with the same ice carpet as around the protuberances in C. E: displaying small protuberances within small intercellular spaces in the chlorenchyma. F: finger like protuberances within the big intercellular spaces of the chlorenchyma. Scale bars: 10 µm (A, F-H), 5 µm (E), 100 µm (B – D)

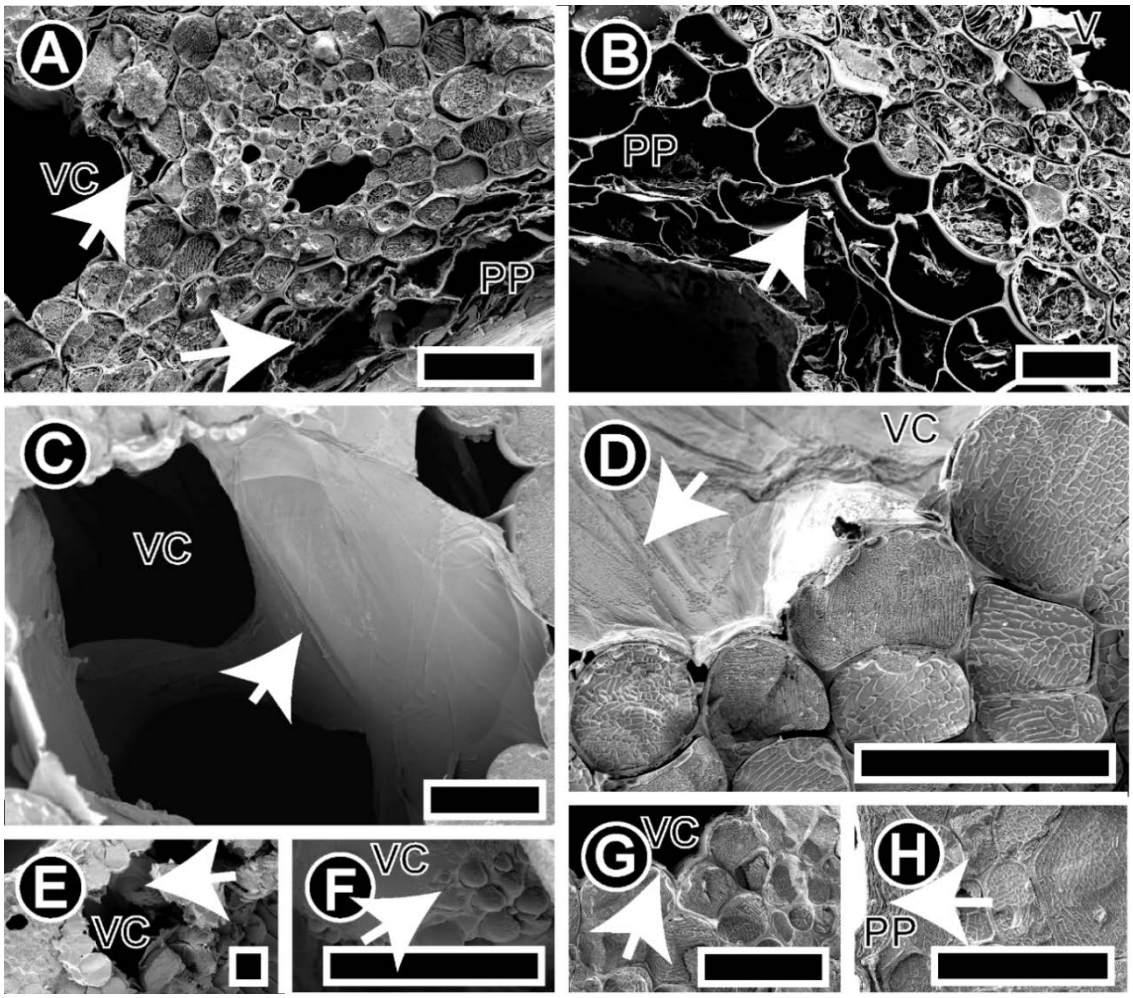

Fig. 9: CryoSEM images of cross sections of older (A, C – H) stems taken during summer and of current year (B) *Equisetum hyemale* var. *robustum* stems frozen and thawed during winter. Water as grating or ice crystals (white arrows) can be seen at the borders of the vallecular canals (VC) (A, D, G), on membranes within the vallecular canals (C, D, G), on growth within the vallecular canals (VC) (E and its enlargement F) and within the partly or completely deformed parenchymatous pith (PP) (A, H). The frozen and thawed sample (B) is still containing water within the parenchymatous pith (PP) during summer. Scale bars: 50 µm

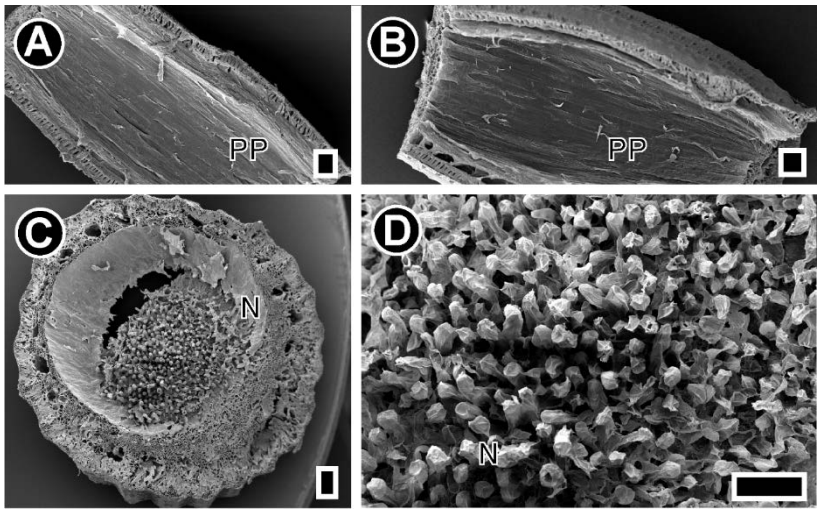

Fig. 10: SEM images of *Equisetum hyemale* var. *robustum* internodes and nodes. A & B: longitudinal sections showing the paper like structure of parenchymatous pith (PP) with a few holes. C: cross section showing the top view of a node (N) with its typical bobble like structure. D: enlargement of the bobbles of the node (N) in C. Scale bars: 200 µm

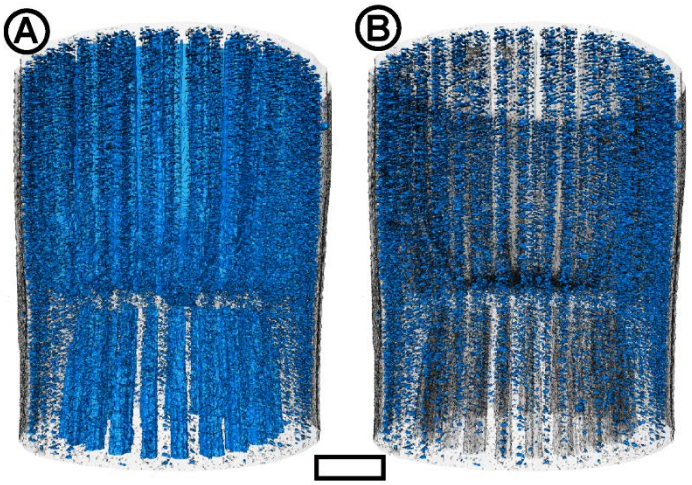

Fig. 11: Segmented (blue) µCT scan of a fresh and with nail polish sealed *E. hyemale* stem inside a small plastic tube with a drop of water displayed with the isosurface (grey). A: upper pith cavity as well as the vallecular canals and the intercellular spaces between the chlorenchyma cells are segmented. B: only the segmented intercellular spaces between the chlorenchyma cells are displayed. Scale bar: 1 mm.

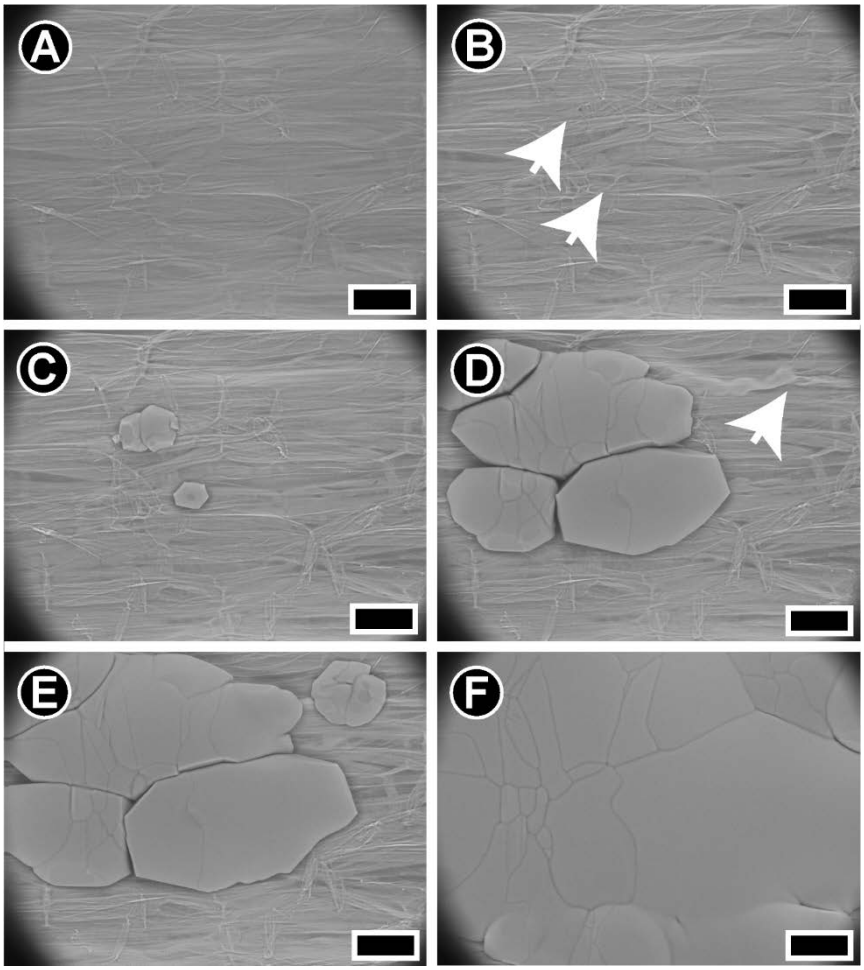

Fig. 12: Selected ESEM images of the border of an *Equisetum hyemale* var. *robustum* pith cavity (humidity: ~85 %; pressure: 275 Pa; temperature: -10 °C) of continuous recordings. A: different layers of the parenchymatous pith can be recognized. B: Movement of the whole parenchymatous pith were noted as well as movement underneath the layers. Few were marked with the white arrows. C: first different formed ice crystals occurred at the in B marked places. D: The ice layer is growing and new movement underneath the parenchymatous pith can be detected (white arrow). E: The ice crystals continue to grow and start to merge. A new different formed crystal grew at the in D marked side. F: The merged ice crystals cover nearly the whole parenchymatous pith as the border of the pith cavity. Scale bars: 100 µm.

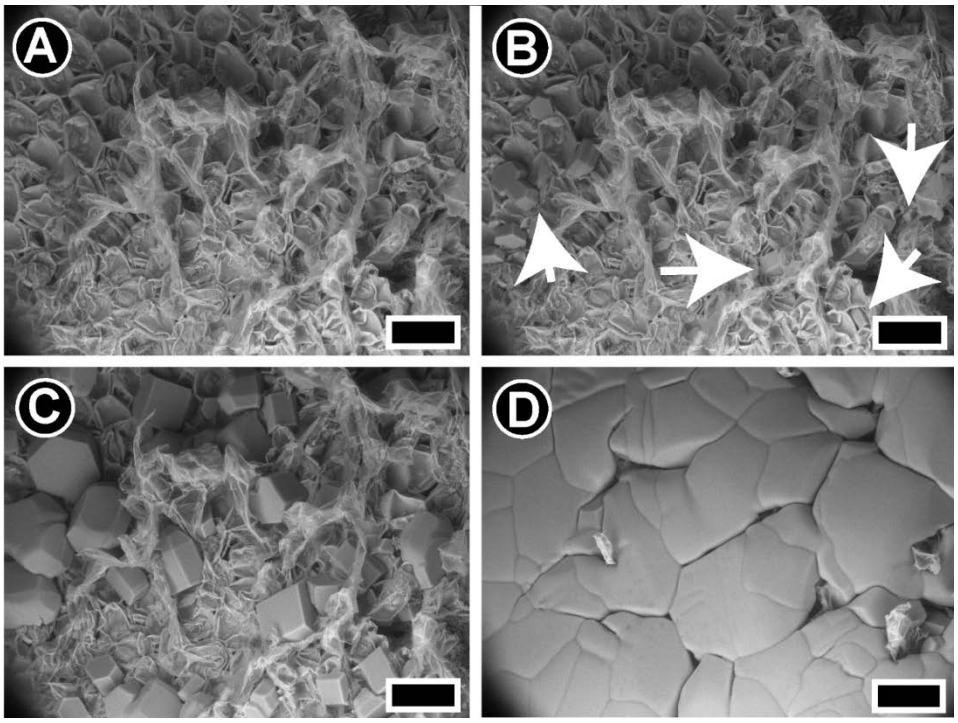

Fig. 13: Selected ESEM images of a node top of an *Equisetum hyemale* var. *robustum* pith cavity stem (humidity: ~95 %; pressure: 273 Pa; temperature: -10 °C) of continuous recordings. White arrow point at small ice crystals. Scale bars: 100 µm

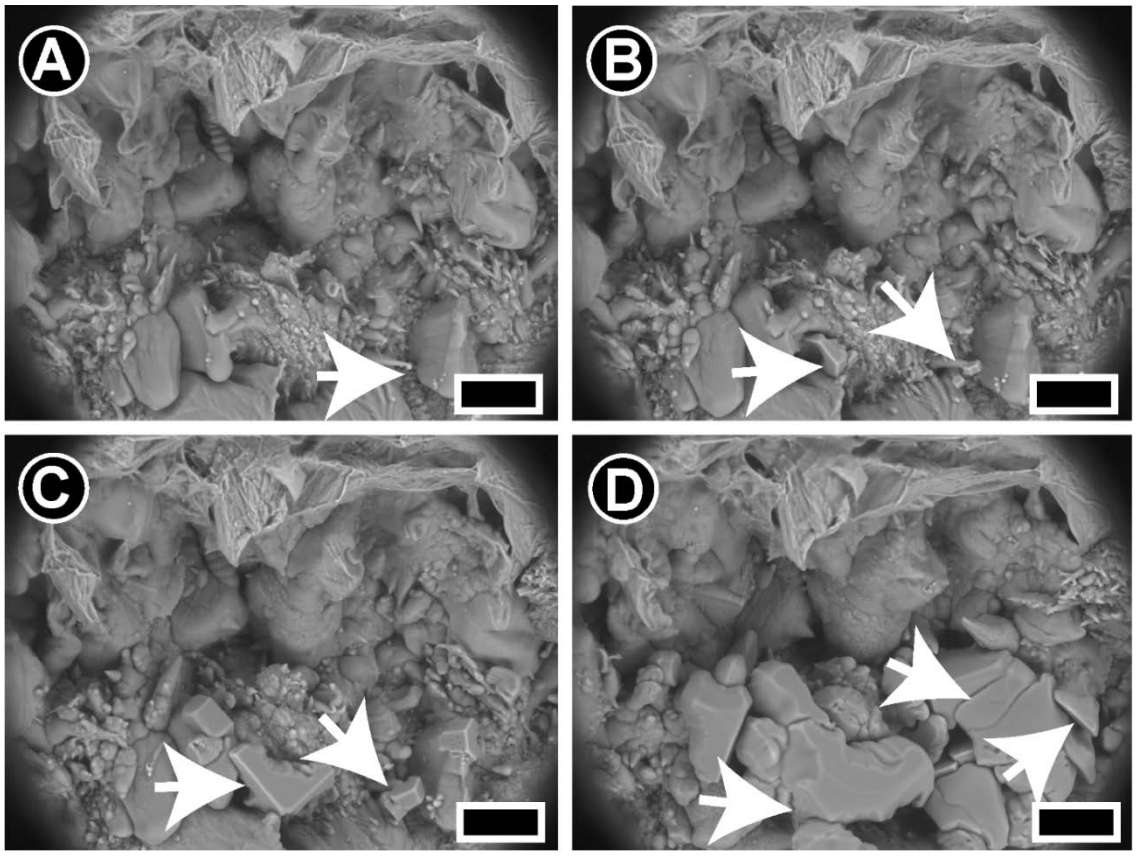

Supplement 1: Selected ESEM images of cross section of an *Equisetum hyemale* var. *robustum* node (temperature: -10°C; pressure: 275 Pa; humidity: ~95%) of continuous recordings. The white arrows highlight the different forms of ice crystals and their growth. A: one of the spirals has another ice crystal on the top: B: A typical ice crystal is growing on top of the spiral and another is developing with sharper edges. C: Both ice crystals grew with sharp edges. D: Some ice crystals are merging and others lost the sharp edges. Scale bars: 100 µm

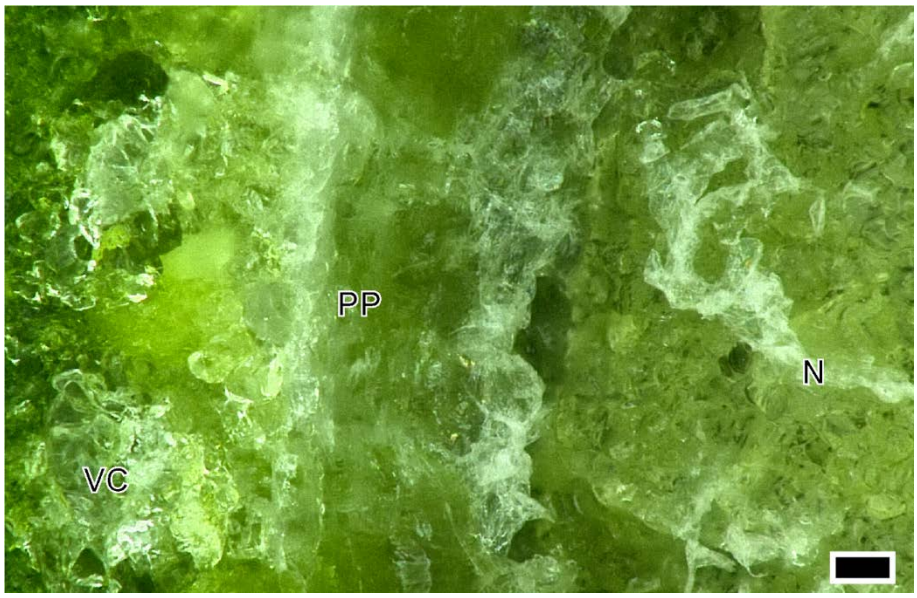

Supplement 2: Part of a cross section of an *Equisetum hyemale* var. *robustum* stem after 18 hours at -15 °C showing ice in the vallecular canals (VC), at the border of the pith cavity on the parenchymatous pith (PP) and on top of the node (N). Scale bar: 100 µm

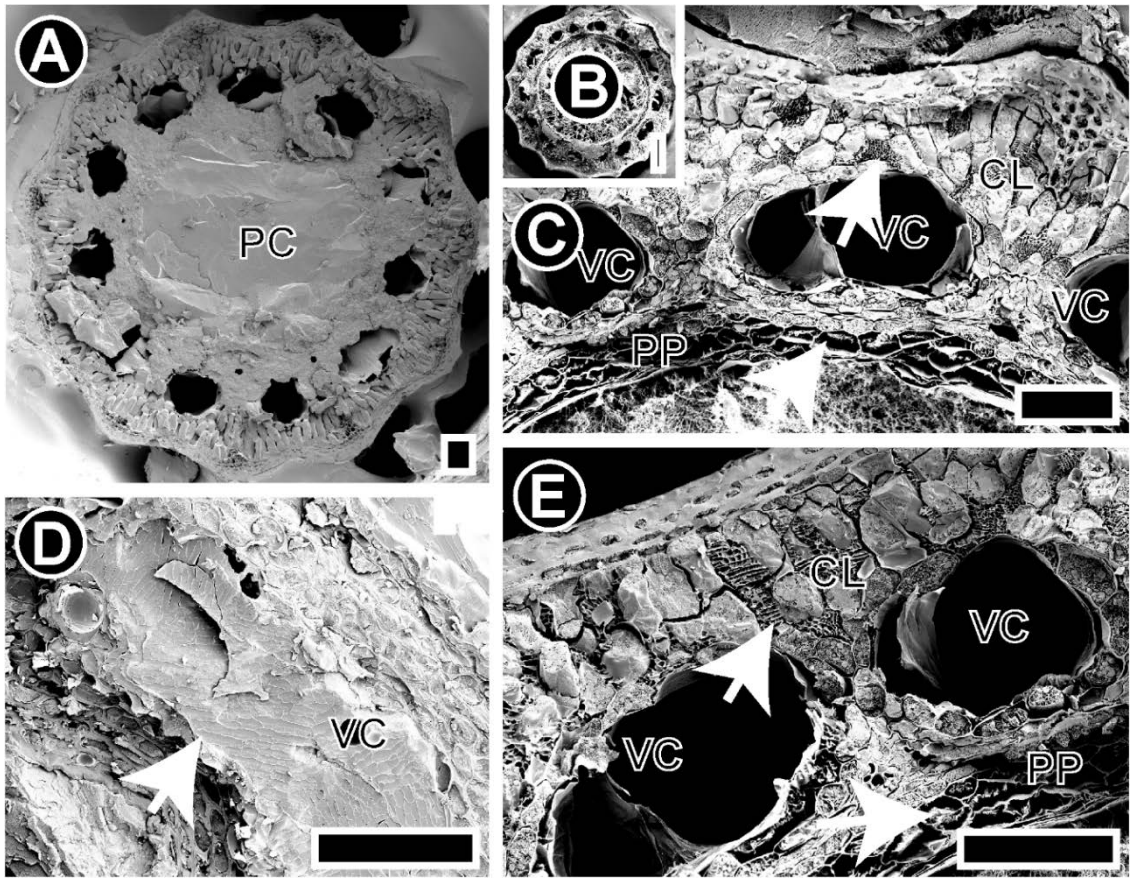

Supplement 3: CryoSEM images of frozen cross sections of current year *Equisetum hyemale* var. *robustum* stems. A: naturally frozen stem has mainly a solid ice block within the pith cavity (PC). B, C, E: stem was frozen at -20 °C for 24 h. Ice as gratings can be seen between the chlorenchyma cells (CL), at the border of the vallecular canals (VC) as well as at the border of the pith cavity (PC). The still enlarged parenchymatous pith (PP) is also containing some ice. C and E are enlargments of B. D: The frozen (72h at -20 °C) part of a cross section showing the deformation and enlargement of the vallecular canals (VC) resulting in a shrinkage of the parenchymatous pith and the chlorenchyma. The surface of the ice within the vallecular canals and the pith cavity (PC) is showing the typical structure of ice and particles departing during the freezing event. White arrows highlight important features. Scale bars: 100 µm

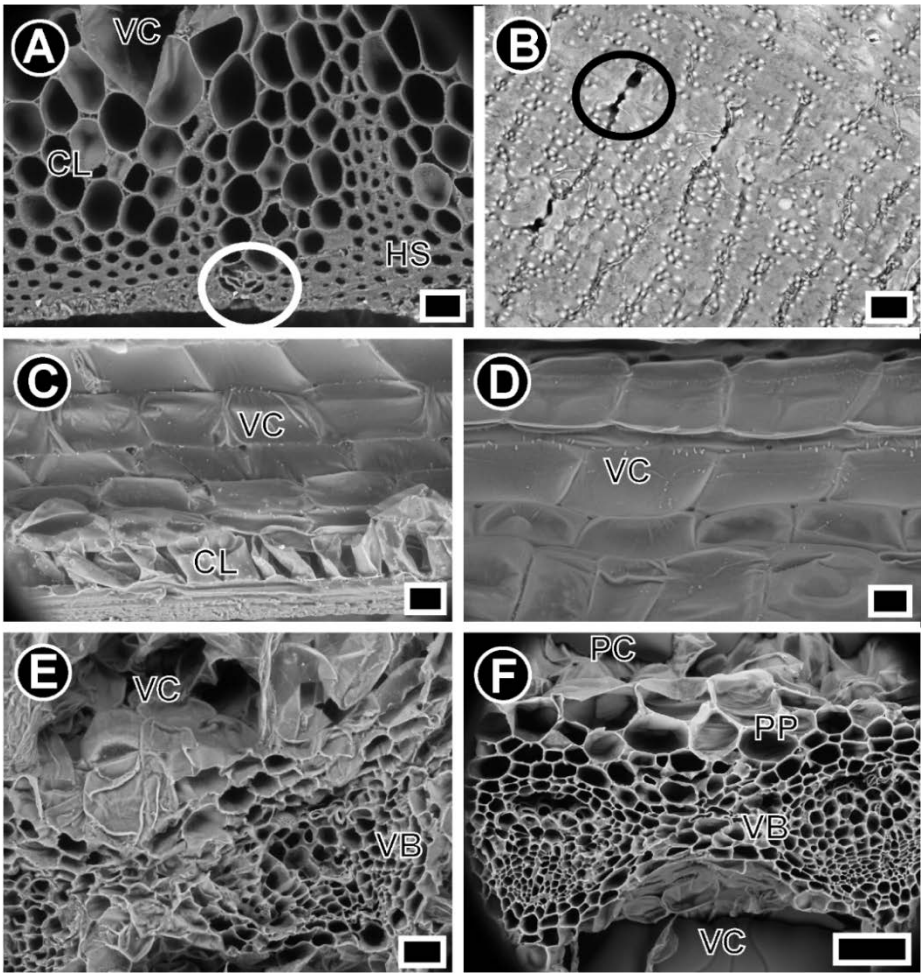

Supplement 4: ESEM images of longitudinal and cross sections of fresh *E. hyemale* stems.The humidity is 75 - 81 % with a pressure of ~ 500 Pa. A: Highlighting the structure of the membranes of the vallecular canal, the chlorenchyma and the hypodermal sterome with a stoma (temperature: 0 °C). B: Showing the surface of a E. hyemale stem with stomata (temperature: -2 °C). C, D: the holes between the cells of the vallecular canal can be spotted (temperature: 1 °). E: showing the different membrans within the vallecular canal and the construction of the vascular bundle (temperature: 1 °C). F: Next to the structure of the vascular bundle the growing ice within the vallecular canal and the pith cavity can be seen (temperature: -10 °C). CL: chlorenchyma; HP: hypodermal sterome; PC: pith cavity; PP: parenchymatous pith; VB: vascular bundle; VC: vallecular canal; in circles are stomata. Scale bars: 50 µm

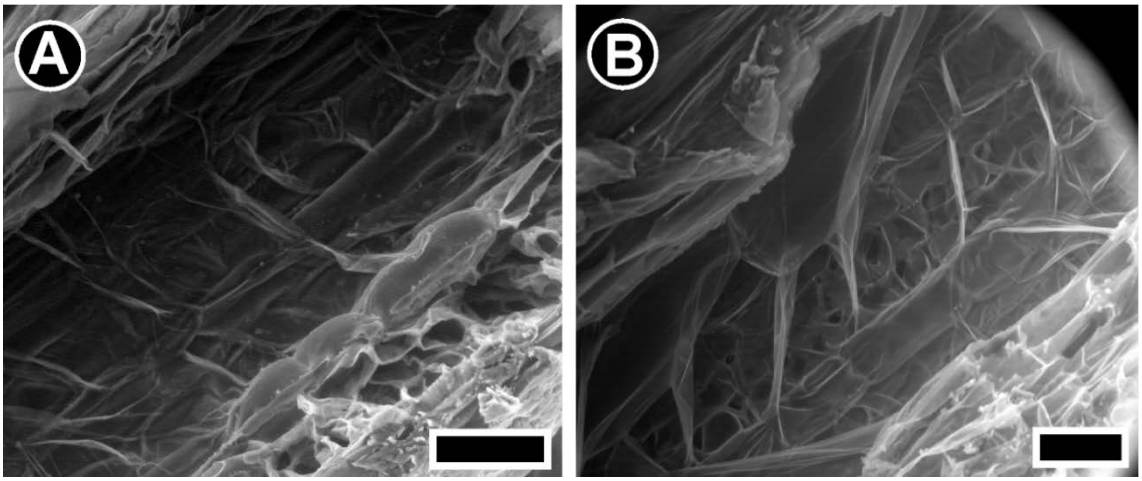

Supplement 5: ESEM images (pressure: 550 Pa; temperature: 1 °C, humidity: ~ 83.5 – 84 %) of longitudinal sections of *Equisetum hyemale* var. *robustum*). A & B: showing more details of the pith cavity including the layers of the parenchymatous pith (PP). Scale bars: 100 µm

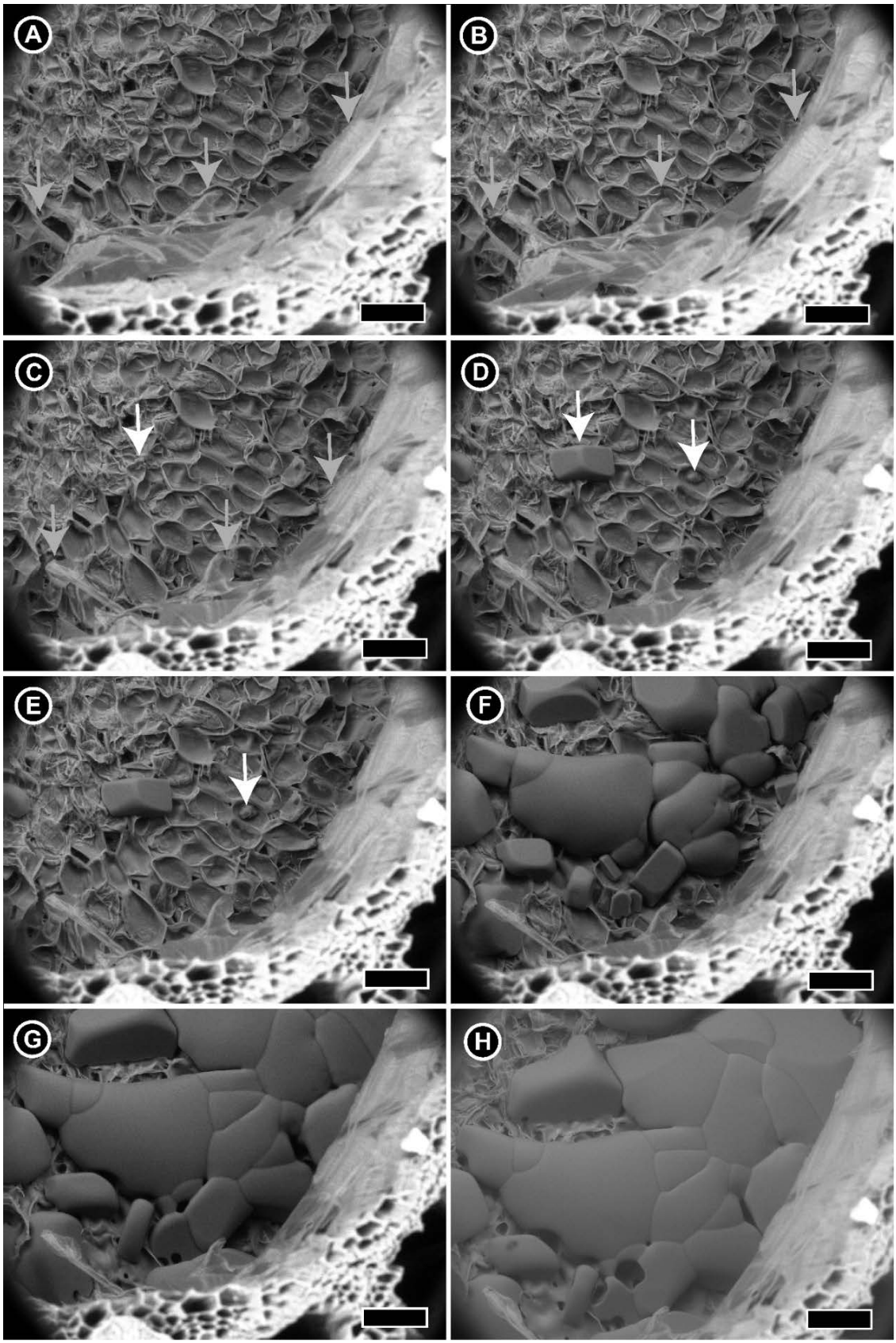

Supplement 6: Selected ESEM images of node top of an *Equisetum hyemale* var. *robustum* stem (temperature: -10 °C; pressure: 275 Pa; humidity: ~95 %) of continuous recordings. A-C: grey arrows show the deformation of the parenchymatous pith. C-E: white arrow highlight the growing ice crystals. F-H: The growing ice crystals and their slow movement to the borders of the pith cavity are shown. Scale bars: 100 µm

Manuscript in preparation 2: Anatomical adaptations of *Stachys byzantina* C. Koch to extracellular ice formation

Schott, Rena T. & Roth-Nebelsick, Anita (**in prep**) Anatomical adaptations of *Stachys byzantina* C. Koch to extracellular ice formation

Anatomical adaptations of *Stachys byzantina* C. Koch to extracellular ice formation

Rena T Schott[a] and Anita Roth-Nebelsick[a]

[a]State Museum of Natural History Stuttgart, Rosenstein 1, 70191 Stuttgart, Germany

Corresponding author: Rena T Schott, State Museum of Natural History Stuttgart, Rosenstein 1, D-70191 Stuttgart, Germany, telephone: +49 (0) 711 8936170, e-mail: rena.schott@smns-bw.de

Abstract:

In this contribution, the sites of extracellular ice formation within leaves and petioles of *Stachys byzantina* C. Koch were identified and anatomically studied by different imaging techniques. Naturally acclimated plant parts were analyzed during the winter season in various formerly naturally acclimated states (fixed, native, before freezing, frozen and after thawing) by using digital microscopy, cryo scanning electron microscopy or via µ-CT. Within the lamina of a *S. byzantina* leaf ice accumulated mainly in the intercellular spaces of the spongy mesophyll. And close to the leaf ribs, ice grew in three to four already existing intercellular spaces separated by steady connection areas underneath the epidermis or the collenchyma (parenchyma). Two intercellular spaces exist on the abaxial half of the leaf and one or two on the adaxial half. This kind of symmetrical distribution could also be seen within the petioles. Together with the ice formation a deformation of the living tissue and the epidermis became visible. Nearly no freezing induced wilting, however, could be detected.

Keywords: leaf, petiole, intercellular spaces, cryoSEM, frosthardiness, freezing

1. Introduction

Frost hardiness requires acclimation and de-acclimation during the seasons, triggered by changing environmental conditions, such as gradual decrease of temperature. The various processes evoked during acclimation and de-acclimation are manifold. One aspect, for example, is the production of antifreeze proteins (AFPs), which are also known as ice restructuring proteins, to prevent the cell content from freezing and the cell membranes from being damaged by growing ice crystals or to modify the ice crystals (Sharma & Deswal 2014). Initiating ice crystal growth in pre-existing and/or expanding intercellular spaces also represents an important strategy to survive frost periods. This process, termed extracellular ice formation, invokes a dehydration process which draws water from adjacent cells. Upon water loss, the solute content of the cells increases which leads to cell shrinkage and further depression of the freezing point resistance (Mazur 1969). This not yet completely understood mechanism of freeze avoidance, which includes all physical processes preventing intercellular freezing (Gusta & Wisniewski 2013), is object of research for several decades. All kinds of plants and organs - leaves (Ball et al. 2002; Ball et al. 2004), flower buds (Ishikawa *et al.* 2015), stems (Schott, Voigt & Roth-Nebelsick 2017), petioles (McCully, Canny & Huang 2004), wood (Schott & Roth-Nebelsick 2018) - were examined with respect to freezing avoidance. One of the first studies was conducted by Prillieux (1869) on different herbaceous plants. He was one of the first to identify special sites for extracellular ice

formation: gaps – narrow intercellular spaces - underneath the epidermis in which extracellular freezing can take place, leading to the accumulation of ice lenses which expand the sub-epidermal intercellular space further. Herbaceous plants which show such a mechanism often show a wilting-like reaction upon freezing as a result of cell dehydration. This process is, however, reversible and cell turgidity is restored after thawing (McCully *et al.* 2004). Other plants or plant parts as, such as snow gum leaves (*E. pauciflora*), remain stiff during freezing and no or nearly no deformation can be detected during freezing and thawing (Ball *et al*. 2004).

Many different methods, such as high-resolution infrared thermography (Wisniewski, Neuner & Gusta 2015) and infrared differential thermal analysis combined with differential imaging chlorophyll fluorescence (Hacker, Spindelböck & Neuner 2008), exist to observe and determine the freezing process and its temporal course. Microscope images of the fresh and the freshly frozen state on the other hand can provide information on the structure of the tissue and the distribution of tissue, water, air and ice, while cryo-scanning electron microscope experiments (cryo-SEM) can reveal further details (Schott et al. 2017). To the authors' knowledge, studies using micro-CT scans for identifying dimensions and distribution of intercellular spaces before and after a freezing event are scarce (*e.g.* Zhao & Takhar 2017). The use of micro-CT allows for detailed reconstructing the three-dimensional architecture of intercellular spaces and its role in extracellular freezing.

In this study, *Stachys byzantina* C. Koch (Fig. 1), a small and rosette-like evergreen herbaceous plant, was analyzed in this study with respect to intercellular space distribution and its dynamics during freezing events. The natural habitats of *S. byzantina* are located in the Near East and Caucasus. The perennial *S. byzantina* has sterile basal rosettes and the height of the flowering stem amounts to about one meter. Basal leaves are mostly around 3-8 x 0.5-3.5 cm with a 2-6 cm long petiole and densely covered with trichomes (Davis 1982). A number of studies focus on the medicinal potential of *S. byzantina* since the plant is used in traditional medicine (for example, Sarikurkcu *et al.* (2016)). Nowadays, *S. byzantina* can be found in many gardens as an ornamental plant or as an important component in older medicine gardens. The presented study focuses on the identification of sites of extracellular ice crystal growth within the tissues of *S. byzantina* leaves and petioles as well as on the shape and distribution of the involved intercellular air spaces.

2. Material and Methods

2.1 Plant Material

Four potted plants purchased from a commercial breeder (Pflanzmich GmbH, Hamburg, Germany) were grown in the inner courtyard of the State Museum of Natural History Stuttgart, Germany (SMNS; 48.793308° latitude, 9.190340° longitude). The potted plants were watered and fertilized as needed. Furthermore, plants growing in the Botanical Garden of the Technical University Dresden, Germany (TU D; 51.040074° latitude, 13.771024° longitude) were included in the study.

Experiments were only conducted with naturally acclimated plants or plant parts during winter. Acclimated plants or plant parts were naturally frozen (outside during natural frost) or artificially frozen, either with a precooled (0 °C) custom-built freezer (CBF) (Fryka, Esslingen, Germany) with a cooling rate of 2 °/h to -10 °C (SMNS) or with a laboratory freezer (LF) showing a constant temperature of -20 °C (Dresden).

2.2 External appearance during freezing

Shape and posture change during artificial freezing in the CBF was evaluated with a GoPro HERO 3. The starting temperature was always +3 °C. During the first experiment with a single potted plant, which was used to get a better focus on the details, the temperature was lowered at -2 °C after 20 minutes and after an hour to -5 °C. After another hour the temperature was again raised to -2 °C. After one and two hours the temperature of +1 °C and +4 °C were reached. During the second experiment with a "whole" pot holding several individuals the temperature was lowered to 0 °C after an hour. After 30 minutes the temperature was lowered to -3 °C and after 75 more minutes to -6 °C. The temperature was raised again (-1 °C) after 80 minutes. After 1 hour the potted plants were in the freezer at +4 °C for two hours. The different freezing and thawing speeds were evaluated.

2.3 Microscopic analysis

2.3.1 Digital microscopy

For a first survey of the tissue structure and ice distribution, cross sections from two of the four potted plants were evaluated for 1) the fresh and unfrozen state and 2) the artificially frozen state (CBF) with a digital microscope (DM), a Keyence VHX-5000 (with VH-ZST; Keyence Corp.).

2.3.2 CryoSEM

Unfrozen plant parts were collected after natural acclimation in the Botanical Garden (TUD). The cut ends were sealed with modelling clay and the material was transported to the lab in a sealed plastic bag. Half of the samples of leaves and petioles were analyzed in the fresh and unfrozen state, while the other half was put into the LF to freeze for 76 hours before analyzing. The frozen samples were stored on dried ice before use. Tissue samples were mounted with Tissue-Tek, O.C.T. (Sakura Finetek Europe B.V., Alphen aanden Rijn, Netherlands) on a sample holder. Then, petioles and leaf parts, both unfrozen and pre-frozen material, were put into liquid nitrogen and freeze-fractured within an EMITECH K250X cryo-preparation unit (Quorum TechnologiesLtd., Ashford, Kent, United Kingdom) at -140 °C before sputter coated with platinum (layer thickness ca. 6 nm). All samples were neither etched nor sublimed. The samples were then analyzed with a cryo-SEM SUPRA 40VP-31-79 (Carl Zeiss SMT Ltd., Oberkochen, Germany) and the software Smart SEM 05.03.05 (CarlZeiss SMT Ltd., Oberkochen, Germany) at -100 °C and 5 kV accelerating voltage.

The cells are cut during fractioning which leads to the special freezing patterns of vacuole and the other cell content visible in the cryo-SEM while the ice in the intercellular spaces show a structure similar to flaky pastry.

2.4 Micro-CT

For a better understanding of the three-dimensional structure of the intercellular spaces, µCT scans were produced from a naturally acclimated and formerly naturally frozen leaf (from the material grown in the courtyard of the SMNS) whose petiole was cut into three parts (Fig. 2). The first part contained the upper part of the leaf, including the leaf tip. The second part consisted mainly of the lower half of the leaf lamina and a small piece of the

petiole. The third part consisted of the rest of the petiole. All sample parts were dehydrated after cutting for 10 minutes in pure methanol. The solution was exchanged with pure ethanol again after 30 minutes (Talbot & White 2013). The samples were then critically point dried (CPD; Leica EM CPD300 (Leica Microsystems GmbH, Wetzlar, Germany)). Additionally, a complete plant was freeze dried with a sublimator (Zirbus Sublimator 2x3x3/5, serial no. 2840 (Zirbus Technology GmbH, Bad Grund, Germany)) at the Institute of Applied Mineralogy in the Department of Geosciences at the Eberhard Karls University of Tübingen, Germany.

The CPD samples as well as the completely freeze-dried plant were scanned (Skyscan 1272; Bruker), the micro-CT files reconstructed (NRecon) and analyzed with Amira 6.2 and 6.5 and Avizo 9.4. The CPD samples were scanned with an image pixel size of 5.9 µm and a resolution of 4032x2688. The freeze dried plant was scanned with an image pixel size of 12.5 µm and a resolution of 2016x1344.

At this point it is emphasized that the different preparation methods of the imaging techniques (DM, cryo-SEM and µCT) mostly showed similar results with respect to anatomy. With respect to the methanol/ethanol protocol described by Talbot and White (2013), the tissue becomes minimally shrunken and deformed, revealing three-dimensional images of the tissue architecture without serious artifacts.

Table 1: growing sites and use of naturally acclimated *S. byzantina* petioles and leaves in winter

Growing site	Used for
Inner courtyard of SMNS	DM, µCT
Botanical Garden (TUD)	CryoSEM

3. Results

3.1 Structure of intercellular spaces and corresponding connection zones

Intercellular spaces could be found on the upper and lower side of the leaves and petioles, as visible in the freeze dried, scanned and segmented *S. byzantina* plant which was frozen and then thawed (Fig. 1B and Fig. 2). As described in a later section, intercellular spaces running along the lower side of the veins and vascular bundle of the petiole are the main sites for ice accumulation (Fig. 2B). The distribution of the intercellular spaces through the petiole and the veins of the leaf are nearly symmetrical, with the vascular bundle of the petiole and primary and secondary veins as axes of symmetry (Fig. 2B and C). Figure 2B also reveals that the intercellular spaces, from the petioles to the leaf veins, are connected. The lower left side (yellow), however, is separated with a connection zone between the epidermis/chollenchyma and the parenchyma with the lower right side displayed in blue (Fig. 2B), which is further described in the following. The position of the gaps, between epidermis and parenchyma, are similar in the leaf veins and petioles and probably the stem (Fig. 2C). Intercellular spaces of the upper side of the petiole and the leaf are hardly visible and separate by connection zones on the left and right side.

3.2 Structure of fresh and acclimated leaves and petioles of *S. byzantina* in winter

The DM images show the tissue arrangement within the petiole which has one main vascular bundle and sometimes two sub vascular bundles which are surrounded by parenchyma and 3-4 layers of collenchyma (Fig. 3) (Salmaki *et al.* 2011). Gaps between the epidermis and the collenchyma can be seen in plants being in the acclimated and

not yet frozen state during winter (Fig. 3A). Close to the gaps, three to four continuous connections between the left and right side of the petiole, the middle of the lower side and sometimes the middle of the upper side can be found always in the same places (Fig. 3, 4). These continuous connections might support the development of the three to four gaps, each one on both lower sides and one long or two shorter ones on the upper side, by ensuring the connection and associated the supply of all cells. Within the left and right side and the middle of the lower part of the petiole cell connections are quite tight (Fig. 4A and B). There are various intercellular spaces between the first and second row of collenchyma cells which allow formation and growth of ice crystals (Fig. 4). Further small intercellular spaces within the parenchyma can be detected (Fig. 4D).

Fresh cross sections of leaves of *S. byzantina* show the typical dense hair cover with the spongy and palisade parenchyma as well as the parenchyma surrounding the primary and secondary veins (Fig. 5). A one-layered collenchyma below the lower and upper epidermis along the major vein (Salmaki et al. 2011) reveals natural gaps underneath the epidermis or the collenchyma (Fig. 5, 6). In the acclimated and unfrozen state, two gaps are visible on the abaxial side, along the midvein as well as along other veins (Fig. 5C). CryoSEM images are shown in Fig. 6. Underneath the epidermis and above the veins already existing short gaps can be detected (Fig. 6).

3.3 Petioles and leaves of *S. byzantina* during freezing and after thawing in winter

During the freezing process especially the intercellular spaces on the lower side of the petioles expanded due to accumulating ice and accompanied by tissue shrinkage (Fig. 7A). Thawed petioles still show the two long gaps on the lower side of the petiole (Fig. 7B). Petioles prepared directly from the frozen state additionally show considerable gaps between epidermis and collenchyma on the upper side, with the epidermis bulging outwards (Fig. 7A, C-E). On the upper side, the two ice filled intercellular spaces remain, however, more narrow. Both ice filled spaces are separated in the middle by a connection zone in which epidermis and parenchyma remain connected to each other, with deformation and shrinkage of the living tissue being apparent. Figs. 7D and E display cryoSEM pictures of frozen petioles (pre-frozen before cryoSEM) which also show large intercellular spaces partly filled with ice at the left and right side. CryoSEM images reveal that the extended gaps along the lower and upper side of the petiole consist next to the large compartments of some smaller compartments also containing ice (Fig. 8). Furthermore, steady and probably ice impermeable cell connections within the left and right side of the petiole can be identified containing some small intercellular spaces as places for ice crystal growth for the adjacent cells (Fig. 9). These connection zones seem to be steady throughout the whole petiole. Along the long and continuous gaps, the seemingly, naturally teared first row of collenchyma cells also shows some already existing gaps within the frozen sample (Fig. 8C, D, F). Fig. 9 shows that the gaps between the first and second row of collenchyma cells can be filled with ice even as main places for ice crystal storage (Fig. 8). The contact zone on the lower side remains intact, while the one in the middle of the upper part of the petiole seems to loosen during the freezing process with ice accumulation (Fig. 8E).

During the freezing process the ice crystallization within the leaves occurs within the already mentioned gaps at the midvein and veins right underneath the epidermis or between tissue rows close to the epidermis (collenchyma) (Fig. 11 A-C). The strongest ice accumulation occurs within the two intercellular spaces on the abaxial half of the leaf (Fig. 10). The connection zone for the veins is in the middle of the abaxial part and the

left and right side exist as connection zones to the rest of the leaf tissue, despite ice filling the enlarged intercellular spaces between the cells completely (Fig. 11).

3.4 External appearance

The single plant showed nearly no response to the decreasing temperatures during the artificial freezing experiment (Supp. 1). The potted plants, for proving the results of the single plant, showed the same slight freezing reactions with a small backwards movement during the longer thawing process (pictures not included), which indicated a more time consuming mechanism. The few, slight movements were only detectable through the continuous monitoring.

3.5 Comparison of the different methods

Different preparation methods and imaging techniques were used and displayed in this study. It was shown that the results of the fresh, frozen and thawed tissues captured and evaluated with different imaging techniques (DM, cryoSEM, µCT) were comparable. For the pure anatomical adaptation, the difference in freezing speed was not essential, but more ice accumulated over time. The methanol/ethanol protocol seem to have only an acceptable amount of shrinkage and less deformation. The freeze dried sample highlighted the maximum growth of the intercellular spaces within the expected sides.

4. Discussion

This study aimed at obtaining information on extracellular freezing and distribution of intercellular air spaces in *Stachys byzantina*, together with dehydration during the freezing process. Caused by the rosette-like order of this densely growing plant the petioles seem to be better protected (Fig. 1B) and the space available for structure deformation is bigger on the lower half especially for younger and smaller petioles (Fig. 1). Inspection of the external appearance (Supp. 1) of *S. byzantina* during a freezing event revealed almost no wilting during the actual freezing process, in contrast to taller and/or more slender herbaceous species, such as *T. repens* and *E. californica* (McCully *et al.* 2004). The behavior of *S. byzantina* leaves during freezing is similar to that of the leaves of *E. pauciflora* (Ball *et al.* 2004). Probably wilting is prevented by the internal structure despite the strong dehydration and deformation of the living tissue. The collenchyma and the massive midvein may function as supporting tissues during wilting. In *Equisetum hyemale* var. *robustum*, for example, a supporting structure, consisting of the hypodermal sterome on the outside and the two layered endodermis on the inside exists, which prevents the stems completely from wilting (Schott *et al*. 2017). When comparing the frozen and unfrozen state, the vascular bundles seem to be the most unaffected tissues during the freezing process. The left and right sides of the petioles or leaf veins also show nearly no deformation during the freezing process. Maybe under natural conditions the densely growing plant is also slightly supported by the carpet of older leaves and its small height compared with taller *T. repens* and *E. californica* might also be an advantage with respect to mechanical stabilization.

The analysis of DM and cryo-SEM images (Fig. 3-11) of the acclimated *S. byzantina* petioles in unfrozen and frozen state indicates both a separation of the intact epidermal layer from the collenchyma or of the outermost collenchyma cell row from the next internal cell layer. The separation of the shrunken tissue layers from each other during the freezing event with extracellular ice formation was already observed by Prillieux

(1869) for petioles of some herbaceous species. The separation was mostly between the epidermal layer and the collenchyma but occasionally the first parenchyma layer separated completely, partly or even broke, probably in a natural way. Prillieux (1869) also observed such differences within a species and between species. McCully *et al.* (2004) described for poppy (*E. californica*) that the gap occurred after a single epidermal row and within clover (*T.repens*) after two rows tightly sticking close to each other. The gap within the edge of the leaf vein in figure 6C highlights the difference in cell form and dimensions on both side of the gap. It is the same for the petiole (Fig. 4). The epidermis and collenchyma cells separating from the rest of the living tissue are smaller with a square like form and straight radial walls compared with bigger and rounder or oval shaped parenchyma cells. Straight walls allow for a large contact area between adjacent cells and therefore for a probably strong connection (Fig. 4, 6C).

The normal three to four connection zones (anchorages), which are the still intact connection areas of the shrunken internal tissue with the outer layers during the ice crystallization, could be identified within the petioles and the leaf veins for *S. byzantina*. There is one in each side of the petiole and the leaf veins, one on the lower side and sometimes one on the upper side. “The fault, which was defined as a particular region of compact tissue arranged so that by expansion it can accommodate large masses of extracellular ice, and by contraction on thawing can restore its form with no apparent damage” by McCully *et al*. (2004) and can already be seen in Prillieux (1869) is an important part of the freezing process as it includes the living tissue. In *S. byzantina*, the gaps are continuous throughout the plant (Fig. 1A). This was also indicated in some previous studies (*e.g.* Wisniewski *et al.* 2015; Hacker *et al.* 2008), were the ice growth throughout a whole plant or plant part was captured and analyzed. Possibly, a continuous intercellular space is important as it allows for unhindered ice accumulation along the plant. The same positions of intercellular spaces within the petioles and veins of the leaves could be a result of the overall similar structure and arrangement of the vascular bundle (Salmaki *et al.* 2011).

Ice accumulates close to living cells which “feed” the growing ice body, as shown by ice crystallization within internal leaf tissue especially between the spongy parenchyma cells (Fig. 11D) as well as within the small ice lakes within the left and right side of the petiole (Fig. 9). In general, it is the same for the big ice lakes within the leaf veins (Fig. 10, 11) and the petiole (Fig. 7). Both, leaf veins and petioles, have in this case similar preconditions and needs. They have outer layers (epidermis and collenchyma) and vascular bundles surrounded by cells with higher water content (parenchyma), which should protect the vascular bundles by external ice crystal growth. So far extracellular ice was mainly detected within the few major regions of petioles and leaves (Ball *et al.* 2004). The occurrence of big and tiny ice lakes together could be observed in other plants, too. *E. hyemale* has already existing and empty spaces – pith cavity and vallecular canals – for the ice crystal growth but ice also accumulated in the intercellular spaces of the chlorenchyma despite the close distance to the vallecular canals (Schott *et al.* 2017). This highlights the need of big and small places for the ice crystal growth. It seems that in general stiffer tissues as some leaves (Ball *et al.* 2004) and wood (Kishimoto *et al.* 2014; Schott & Roth-Nebelsick 2018) would prefer smaller places for ice crystallization and slender tissues as most herbaceous plants (McCully et al. 2004; Prillieux 1869) would prefer bigger storage places for the ice during the colder season. So there may be species using both versions as *E. hyemale* or *S. byzantina*, which might

be a necessity for the occurrence of the big ice lakes. The ice accumulating between the leaf mesophyll cells (Fig. 11D) would also be an example.

Analyses of the architecture of intercellular spaces of with respect to freezing processes by using µCT scans are - to the authors' knowledge – not widespread (*e.g*. Zhao *et al.* 2017). Comparison with other methods showed that the different preparation methods that were used (methanol/ethanol dehydrated and critical point dried (Fig. 2B, C)) provided comparable results. By combining these methods, the complete 3D structure of the intercellular spaces from the petiole through the leaf veins can be displayed easily and it confirms the symmetric design of the left (yellow) and right lower part (blue) with an axis of symmetry through the vascular bundle in the midvein of the leaf or the middle of the petiole (Fig. 2B). The intercellular spaces along the upper part of the petiole and midvein of the leaf (red) has no visible connection with the other gaps which proves the existence of the necessary anchorage point in the left and right side. This results in the assumption of the left and right edges of the petiole and midvein are being ice impermeable connection zones. They are continuous connection zones from the leaf tip to the stem including small ice lakes but no holes or connections between the big intercellular spaces on the upper and lower side of the petioles and leaf midveins. The anchorage points on the left and right side of the petioles are big enough to connect the important tissues which results in the already mentioned small ice lakes within them. The upper one or two intercellular spaces of the petiole and veins of the leaf were not as easily recognized as the two on the lower sides of this acclimated and formerly frozen leaf and petiole. It was the same for the other fresh samples during summer and winter. The slower continuous accumulation of ice within the intercellular spaces also takes place within the upper two gaps. It seems that over time the connection zone in the middle is separated (7B, C, 8E), which has to be investigated further. The plant parts especially the petiole might have more space available for deformations on the lower side than on the upper one close to the stem. A possible role might play the gravity with the lower form of the veins and the bigger number of parenchyma rows on the lower side of petioles and veins. The faster recovery of the deformation of the epidermis on the upper side with the 3-4 collenchyma rows (Salmaki *et al.* 2011) and the possible slower freezing might be a part of the stiffness during the freezing process. The veins with the vascular bundles require a fast and safe protection from ice crystallization.

Investigation of fully acclimated plants is necessary to exclude freezing injuries and to observe processes, such as rehydration after thawing, which do not occur readily in unacclimated plants (Ball *et al.* 2004). The chosen methods – microscope and cryo-SEM studies as well as X-ray micro-CT scans – helped to identify places of ice crystallization. In further studies the ice crystal growth itself should be investigated closer to address more detailed questions. How fast does the tissue itself cool down during the dropping temperatures at night? Where do the ice crystals start growing and do they grow along the intercellular spaces? Are the small intercellular spaces originally transport canals for the water or do they exist for the prevention of the freezing of the cells within the anchorages? – for future studies.

Acknowledgements:

This work has been funded by the German Research Foundation (DFG) as part of the Transregional Collaborative Research Centre (SFB/Transregio) 141 'Biological Design and Integrative Structures'/A01. The authors would like to thank Dr. Barbara Ditsch

(Botanical Garden, Dresden, Germany) for providing fresh samples. Furthermore, we are grateful to Markus Günther, Dr. Dagmar Voigt and Prof. Dr. Christoph Neinhuis (Institute for Botany at the Technical University of Dresden, Germany) for allowing us to use the cryo-SEM, fruitful discussions, and excellent and friendly technical support. The authors would like to thank Gerald Buck and Prof. Dr. Klaus Nickel (Institute of Applied Mineralogy in the Department of Geosciences at the Eberhard Karls University of Tübingen, Germany) for the opportunity of using the sublimator and the technical support.

References

Ball M.C., Canny M.J., Huang C.X. & Heady R.D. (2004) Structural changes in acclimated and unacclimated leaves during freezing and thawing. *Functional Plant Biology,* 29–40.

Ball M.C., Wolfe J., Canny M., Hofmann M., Nicotra A.B. & Hughes D. (2002) Space and time dependence of temperature and freezing in evergreen leaves. *Functional Plant Biology* **29,** 1259.

Davis, P.H., ed. (1982) Flora of Turkey and the East Aegean Islands. Edinburgh Univ. Press, Edinburgh.

Gusta L.V. & Wisniewski M. (2013) Understanding plant cold hardiness: an opinion. *Physiologia plantarum* **147,** 4–14.

Hacker J., Spindelböck J.P. & Neuner G. (2008) Mesophyll freezing and effects of freeze dehydration visualized by simultaneous measurement of IDTA and differential imaging chlorophyll fluorescence. *Plant, cell & environment* **31,** 1725–1733.

Ishikawa M., Ishikawa M., Toyomasu T., Aoki T. & Price W.S. (2015) Ice nucleation activity in various tissues of Rhododendron flower buds: their relevance to extraorgan freezing. *Frontiers in plant science* **6,** 149.

Kishimoto T., Yamazaki H., Saruwatari A., Murakawa H., Sekozawa Y., Kuchitsu K., Price W.S. & Ishikawa M. (2014) High ice nucleation activity located in blueberry stem bark is linked to primary freeze initiation and adaptive freezing behaviour of the bark. *AoB PLANTS* **6**.

Mazur P. (1969) Freezing Injury in Plants. *Annu. Rev. Plant. Physiol.,* 419–448.

McCully M.E., Canny M.J. & Huang C.X. (2004) The management of extracellular ice by petioles of frost-resistant herbaceous plants. *Annals of botany* **94,** 665–674.

Prillieux M.é. (1869) Effet De La Gelée Sur Les Plantes. Formation De Glaçons Dans Les Tissus Des Plantes. *Bulletin de la Société Botanique de France* **16,** 140–152.

Salmaki Y., Zarre S., Lindqvist C., Heubl G. & Bräuchler C. (2011) Comparative leaf anatomy of Stachys (Lamiaceae Lamioideae) in Iran with a discussion on its subgeneric classification. *Plant Systematics and Evolution* **294,** 109–125.

Sarikurkcu C., Kocak M.S., Uren M.C., Calapoglu M. & Sihoglu Tepe A. (2016) Potential sources for the management global health problems and oxidative stress. Stachys byzantina and S. iberica subsp. iberica var. densipilosa. *European Journal of Integrative Medicine* **8,** 631–637.

Schott R.T. & Roth-Nebelsick A. (2018) Ice nucleation in stems of trees and shrubs with different frost resistance. *IAWA Journal* **39,** 177–190.

Schott R.T., Voigt D. & Roth-Nebelsick A. (2017) Extracellular ice management in the frost hardy horsetail Equisetum hyemale L. *Flora* **234,** 207–214.

Sharma B. & Deswal R. (2014) Antifreeze proteins in plants: an overview with an insight into the detection techniques including nanbiotechnology. *Journal of proteins and proteomics* **5,** 89–107.

Talbot M.J. & White R.G. (2013) Methanol fixation of plant tissue for Scanning Electron Microscopy improves preservation of tissue morphology and dimensions. *Plant methods* **9,** 36.

Wisniewski M., Neuner G. & Gusta L.V. (2015) The use of high-resolution infrared thermography (HRIT) for the study of ice nucleation and ice propagation in plants. *Journal of visualized experiments: JoVE,* e52703.

Zhao Y. & Takhar P.S. (2017) Micro X-ray computed tomography and image analysis of frozen potatoes subjected to freeze-thaw cycles. *LWT - Food Science and Technology* **79,** 278–286.

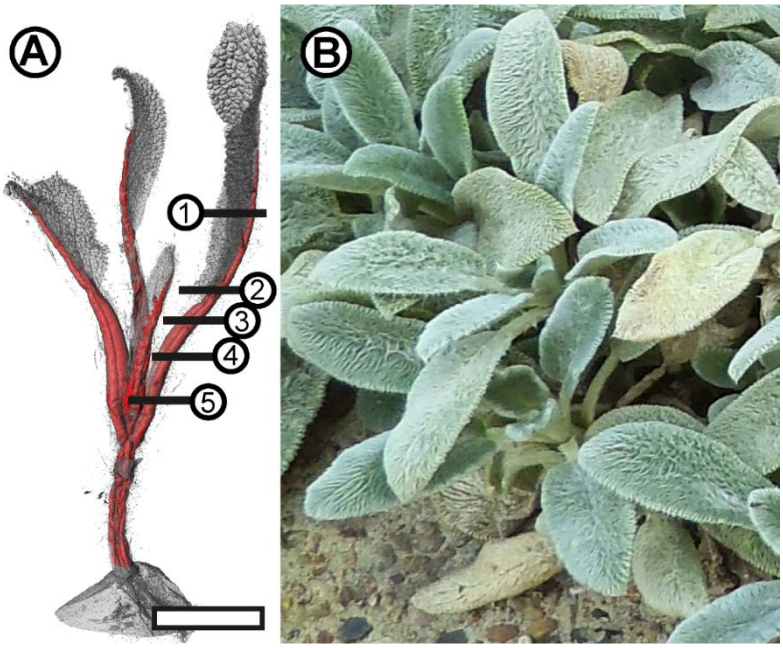

Figure 1: A: Isosurface (grey) and segmented intercellular spaces (red) of a freeze dried *S. byzantina* plant. Numbers indicate approximately the origination of the samples in the following figures. Scale bar: 1 cm. B: Fresh and living *S. byzantina* plants displaying the dense growth.

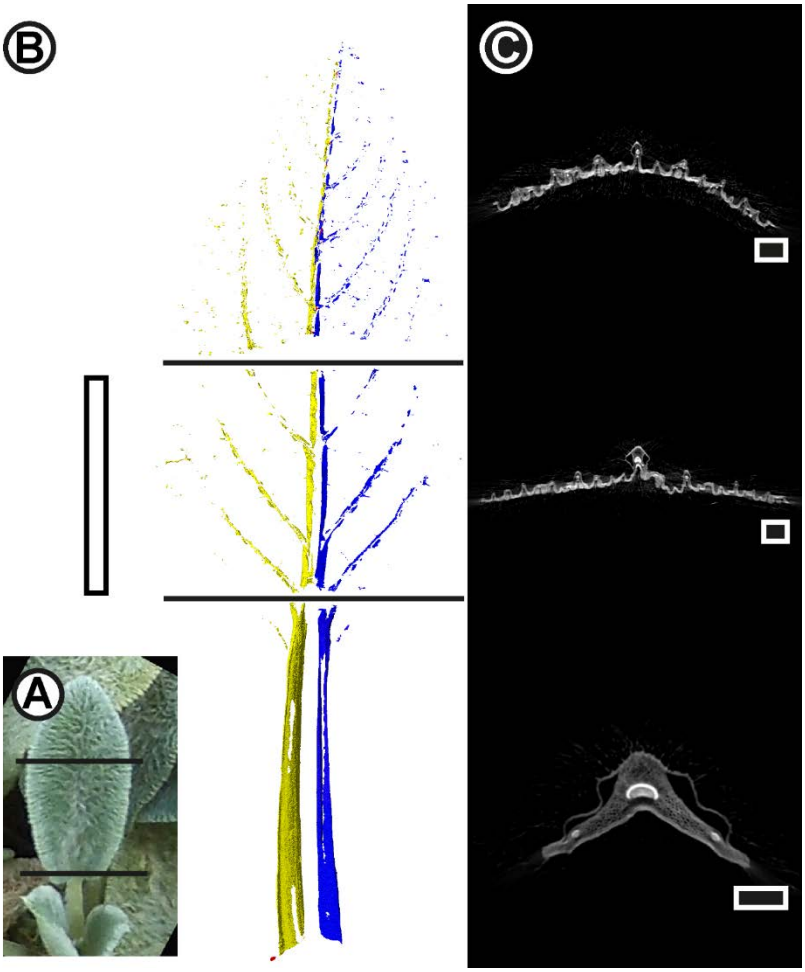

Figure 2: A: Image of the upper part of a fresh *S. byzantina* leaf with petiole showing the orientation of the segmented parts and the cuts. B: Segmentation of µCT scans of methanol/ethanol dehydrated and CPD dried fresh *S. byzantina* leaf with petiole cut in 3 parts. The intercellular spaces on the left side of the lower part of the leaf and petiole are colored yellow and on the right side blue. The small red areas are the intercellular spaces of the upper part. Scale bars: 1 cm. C: one cross section of each part as an example. Scale bars: B: 1 cm; C: 0.1 cm

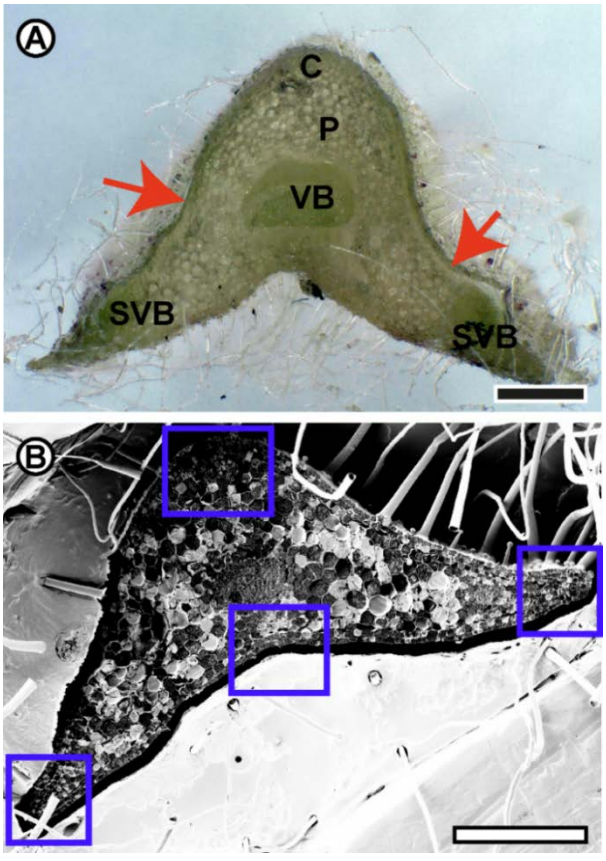

Figure 3: Cross section of a fresh *S. byzantina* petioles in winter A: DM image showing the natural and already visible gaps under the epidermis (red arrows). B: cryoSEM image displaying the enlargements in figure 4 of four different parts of the petiole (blue squares). Position in figure 1: 4. C: collenchyma; P: parenchyma; SVB: sub vascular bundle; VB: vascular bundle. Scale bars: 500 µm

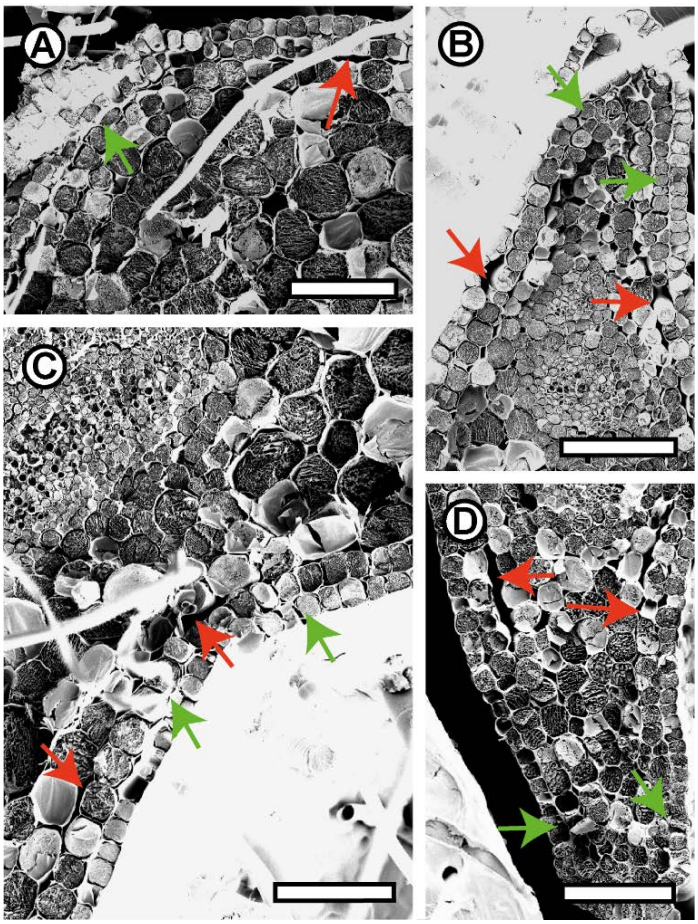

Figure 4: Detailed cryoSEM images of *S. byzantina* petioles in winter highlighting the natural gaps under the epidermis (red arrows) and connection zones (green arrows). A: abaxial side of the petiole containing one connection zone and a gap further away. B, D: left and right side of a petiole showing the big connection zone in the edges and further away some gaps on the abaxial and adaxial side.C: adaxial side of a petiole containing some natural gaps and connection zone in the middle. Position in figure 1: 4. Scale bars: 100 µm.

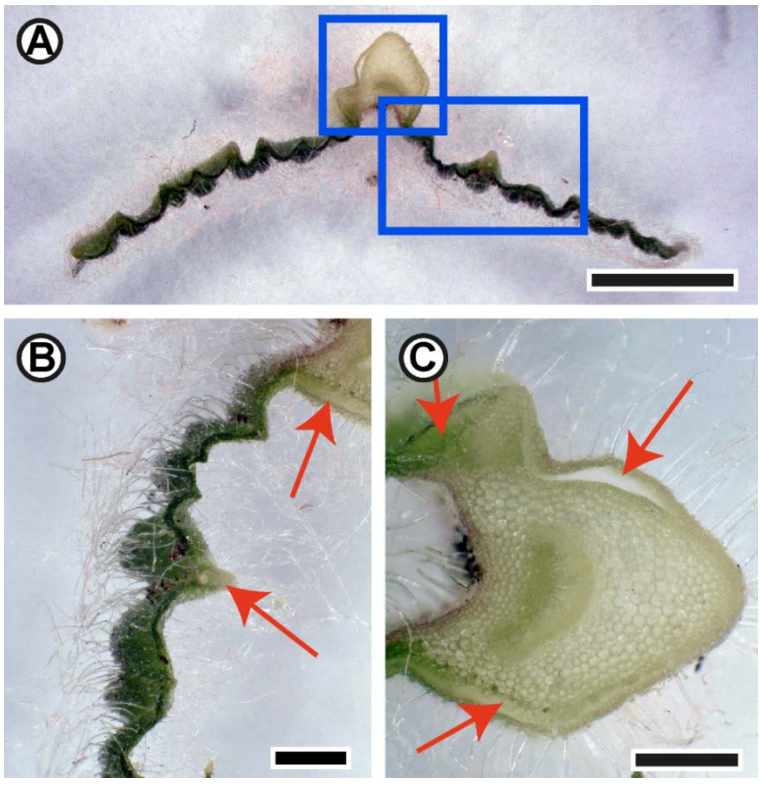

Figure 5: Cross sections of a fresh and unfrozen *S. byzantina* leaf in winter showing natural gaps under the epidermis (red arrows). A: cross section of a whole leaf as an overview with two blue boxes highlighting the sites shown in B and C at higher magnification. B: Leaf, detail with veins. C: Detailed view of major vein. Position in figure 1: 1. Scale bars: 500 µm.

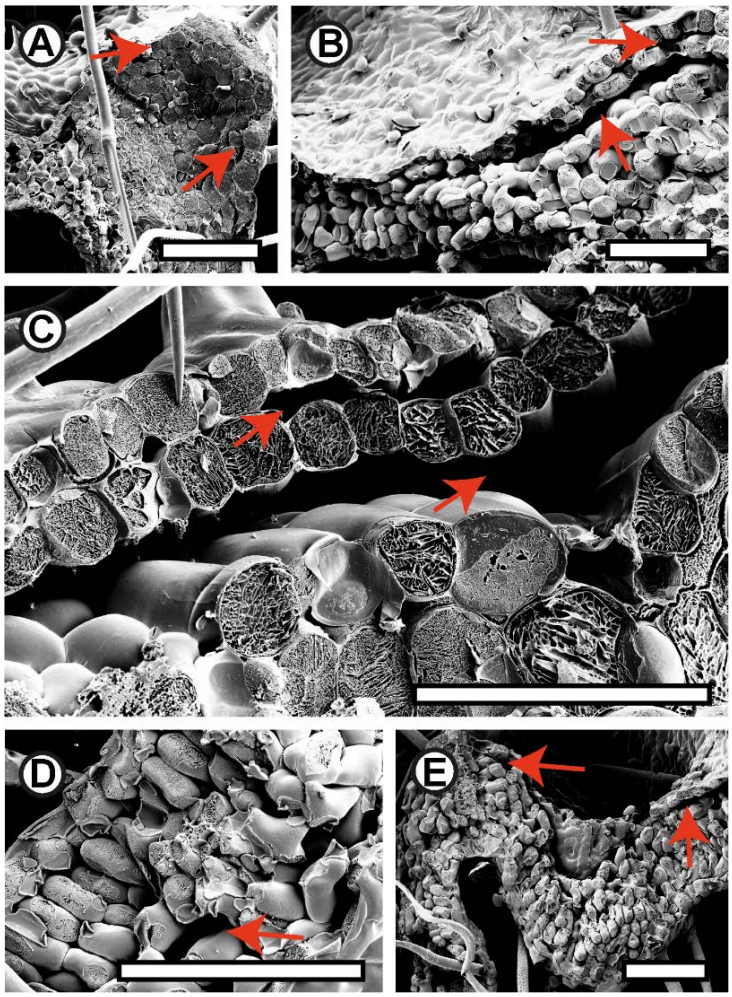

Figure 6: Detailed cryoSEM images of *S. byzantina* leaves acclimated and unfrozen in winter showing the natural gaps underneath the epidermis (= intercellular spaces = red arrows) and contact sides. A-C showing veins with gaps near the epidermis. D-E showing the leaf with the palisade and spongy parenchyma. Position in figure 1: 1. Scale bars: 100 µm.

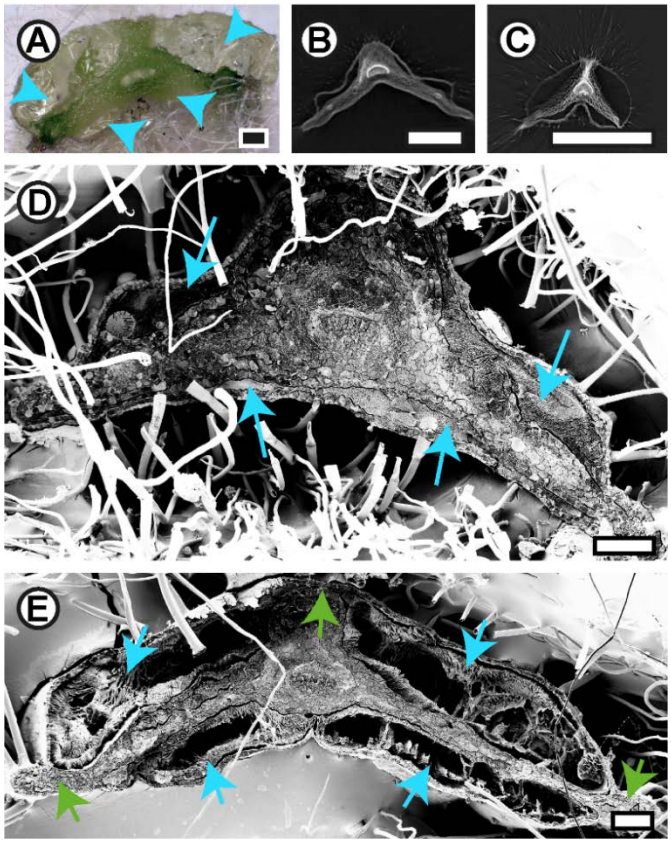

Figure 7: Cross sections of acclimated and frozen or thawed *S. byzantina* petioles in winter. A: Enlarged intercellular spaces partly filled with ice in a frozen petiole. B: Fresh and naturally in the morning thawed petiole in methanol/ethanol dehydrated and critical point dried (microCT-scan). C: displaying the formerly frozen petiole in methanol/ethanol dehydrated and critical point dried (microCT-scan). D: a frozen petiole showing ice in the intercellular spaces on the abaxial and adaxial side and connection zones at the left and right side. E: a frozen petiole highlighting the dimensions of the intercellular spaces still with ice at the borders and some contact sides at the left and right side of the petiole and at the abaxial and adaxial half. Blue arrows indicate some places of ice crystal growth and green ones indicate contact sides. Positions in figure 1: 2-5. Scale bars: 200 µm.

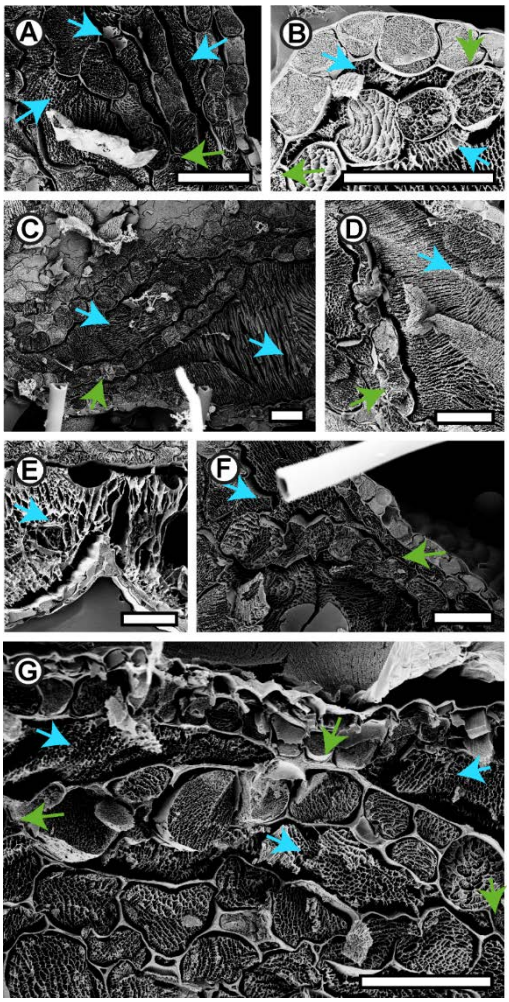

Figure 8: CryoSEM images of cross sections of frozen *S. byzantina* petioles in winter. The ice has a flaky pastry like structure. A – D, F: showing sites near the epidermis on the lower side where the natural gap right underneath the epidermis is not the main place for ice crystal growth or/and where the parts of the first row of the parenchyma cells loosened. E: showing the middle of the upper side loosened at a later point during ice crystal growth which results in the typical form. G: indicates the connection zone at the middle of the lower part where ice crystal growth in smaller intercellular spaces between the first and second row of parenchyma cells is possible, too. Blue arrows indicate the ice and green ones indicate connection zones. Position in figure 1: 4. Scale bars: 50 µm.

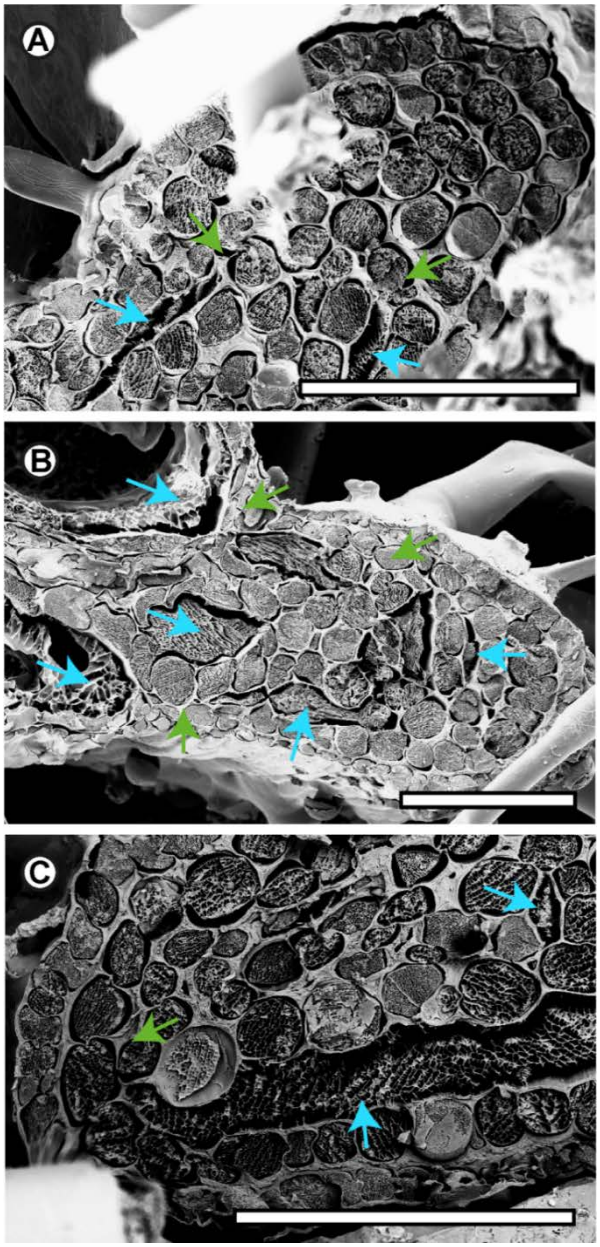

Figure 9: CryoSEM images of cross sections of *S. byzantina* petioles in winter which were pre-frozen before CryoSEM analysis. The ice has a flaky pastry like structure. A - C: Showing the left and right side of frozen petioles with ice at particular places and intact connection zones. Blue arrows indicate some places of ice crystal growth and green ones indicate connection zones. Position in figure 1: 4. Scale bars: 100 µm.

Figure 10: Cross sections of an acclimated and frozen *S. byzantina* leaf in winter showing the enlarged intercellular spaces partly filled with ice (blue arrows). Position in figure 1: 1. Scale bars: 200 µm.

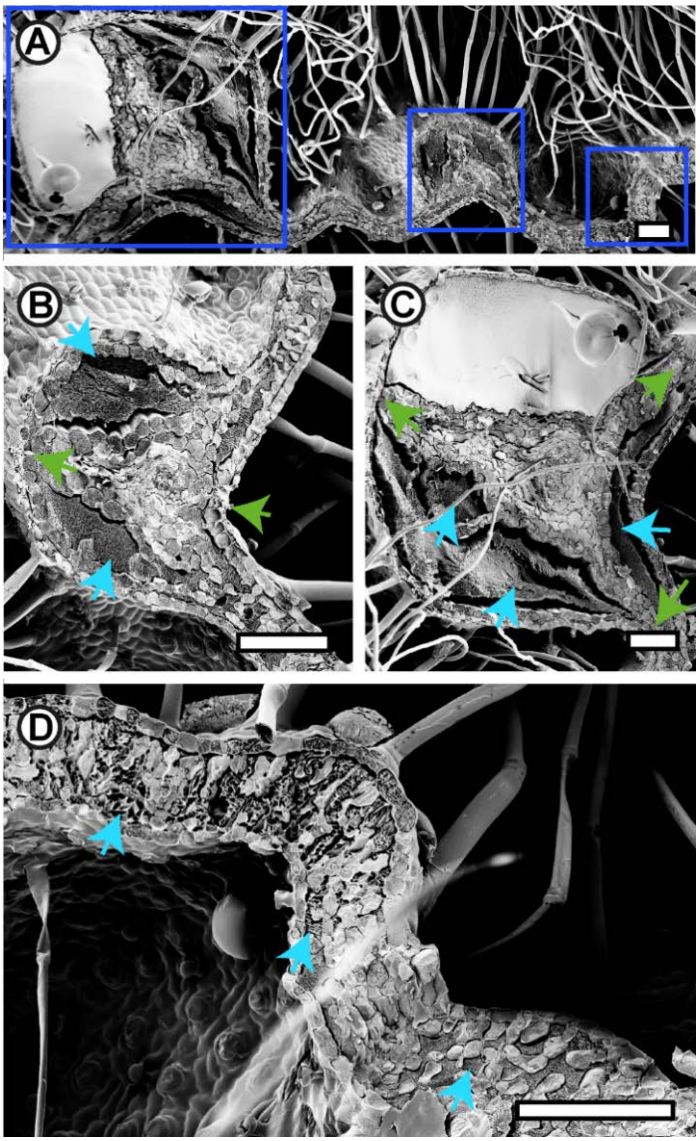

Figure 11: Frozen CryoSEM images of cross sections of a *S. byzantina* leaf in winter. The ice has a flaky pastry like structure. The white area is tissue tec. A: Showing a larger part of the leaf with mostly ice in the enlarged intercellular spaces. Blue boxes highlight the enlarge parts in B-D. B: Detailed image of the midvein with mostly ice in the expanded intercellular spaces. C: Detailed image of a vein with ice at similar places than the midvein. D: Detailed part of the leaf showing ice between the cells in the leaves. Blue arrows indicate the ice and green ones indicate connection zones. Position in figure 1: 1. Scale bars: 100 µm.

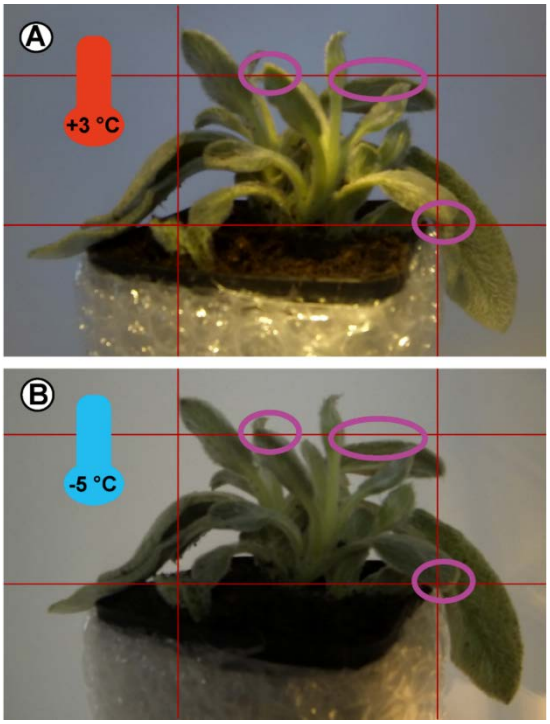

Supplement 1: Chosen images from serial recordings of a freezing experiment with a potted *S. byzantina* plant. A-B: Only very few slight movements can be detected in the continuous photographing of the freezing of a single plant.